Influence of Tectonic Inversion and Salt Mobility on Structural Styles and Reservoir Quality in the Norwegian Central Trough

Steven R. F. Sawyer M.EarthSc. (Oxon.)

Volume II (Figures)

Thesis submitted for the degree of Doctor of Philosophy

October 2010

List of Figures

6 Tectonic Inversion, Halokinesis and Reservoir Quality

7 Supplementary Results from Onshore Field Observations

8 Discussion

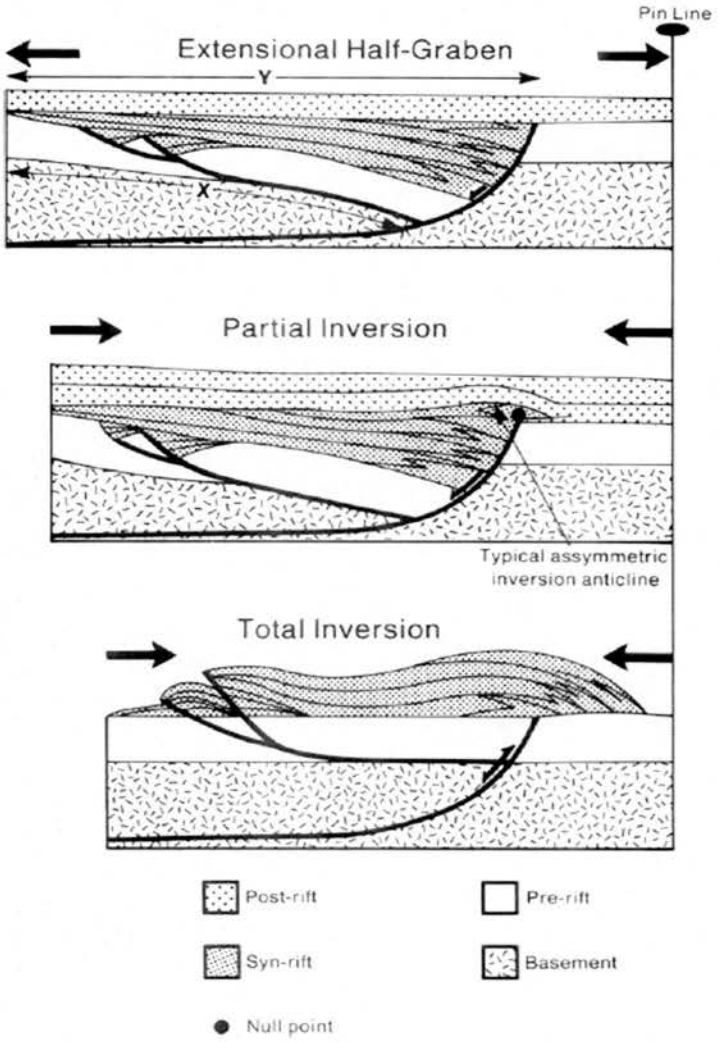

Figure 2.1: Schematic diagram showing the development of a tectonic inversion structure. The pre-rift, syn-rift and post-rift stratigraphic sequences are shaded differently. Inversion is identified through recognition of an uplifted synrift. Onlaps within the post-rift (if preserved) can be used to date the inversion. The post-rift can then be subdivided into pre-inversion, syn-inversion and post-inversion sequences. *(From Cooper et al., 1989)*

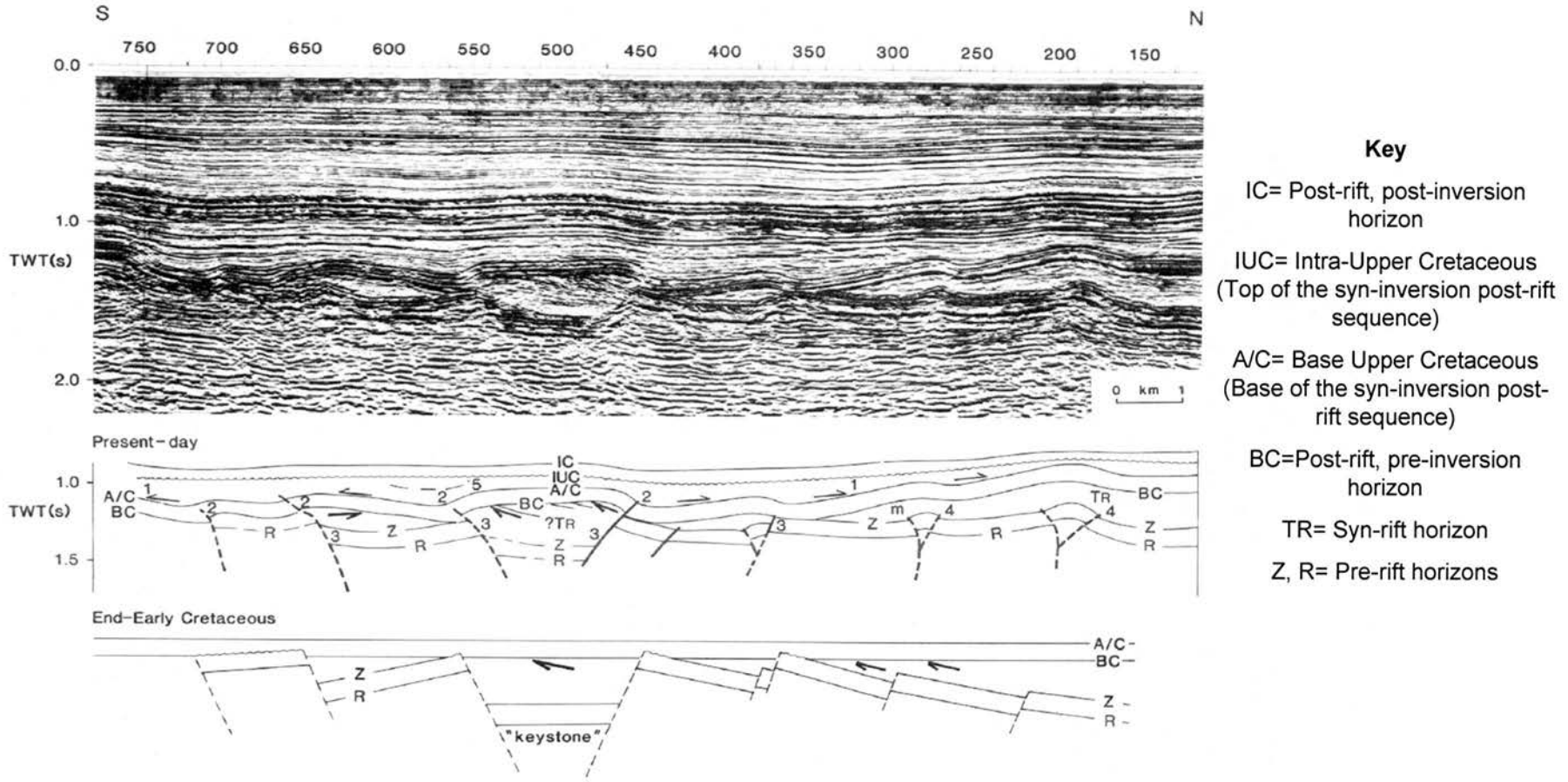

Figure 2.2: Example of tectonic inversion structures identified from seismic reflection data. Location is the South Hewett area of the Southern North Sea (UKCS Quadrant 53). Compression caused reversal of movement on pre-existing normal faults. Timing of inversion is Upper Cretaceous (the syn-inversion post-rift sequence is defined by seismic onlaps between the IUC and A/C). The Lower Cretaceous and parts of the Upper Cretaceous were thrown into forced asymmetric (harpoon shaped) folds above the reversed faults. In some cases the faults propagated into the cover (2). The magnitude of shortening is less than the magnitude of earlier (Triassic-Jurassic) extension and reverse movement on many of the faults was insufficient to cancel the original normal throw (3). Reflection terminations beneath the intra-Upper Cretaceous unconformity (IUC) date the cessation of uplift. *(From Badley et al., 1989)*

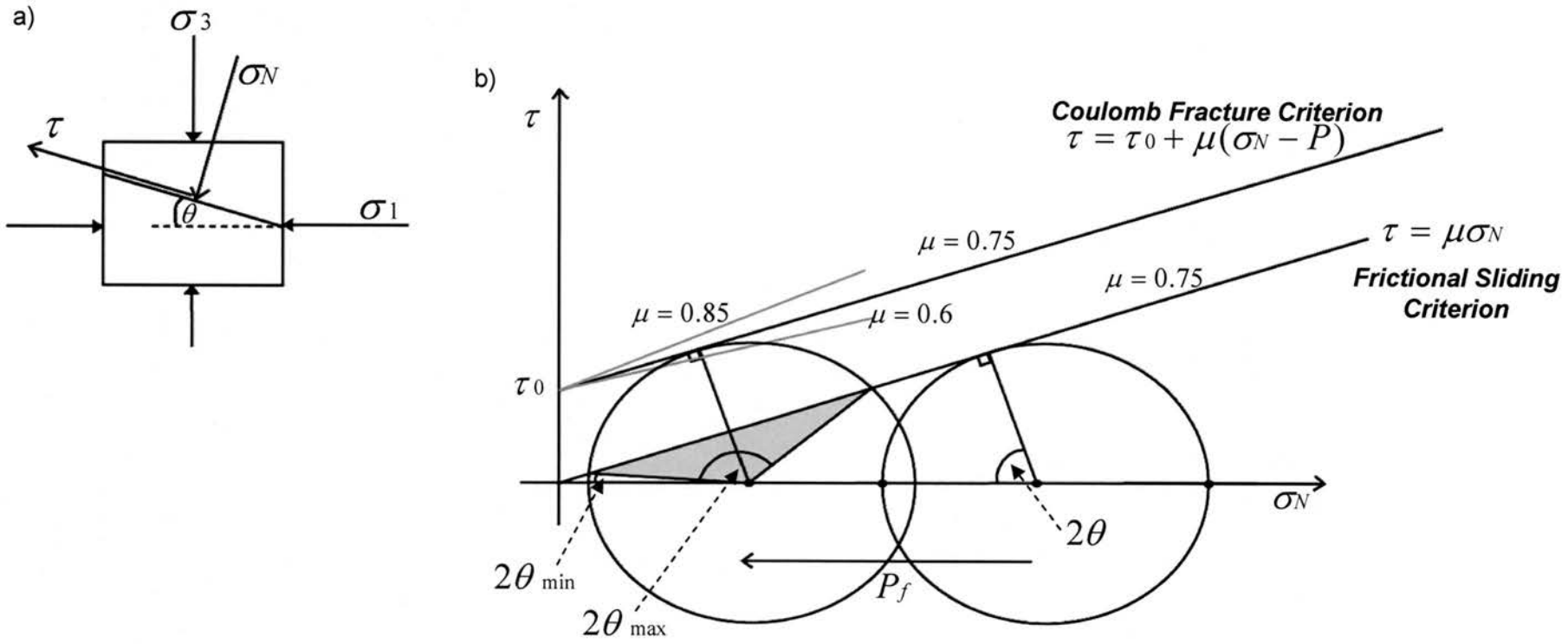

Figure 2.3: Illustration of the mechanical criteria for fault initiation and reactivation. Whether a new fault forms or an old fault reactivates depends on the cohesive strength of the intact rock (ζ_0), the coefficient of internal friction (μ) and the pore fluid pressure (P). **a)** Force diagram, defining θ as the angle between the fault plane and the principal stress direction, σ_1. **b)** Mohr diagram for the scenario in a). In this schematic example, where μ=0.75 and P=0 the rock may fail in accordance with the frictional sliding criterion (through reactivation of the pre-existing fault). Where P>0 the effective stress is reduced and brittle failure can occur more easily. Where μ=0.75 and $P=P_f$, a new shear fracture may nucleate, or else reactivation may occur for any pre-existing faults within the shaded orientation range ($\theta_{min}<\theta<\theta_{max}$). *(After Etheridge, 1986; Twiss and Moores, 1992)*

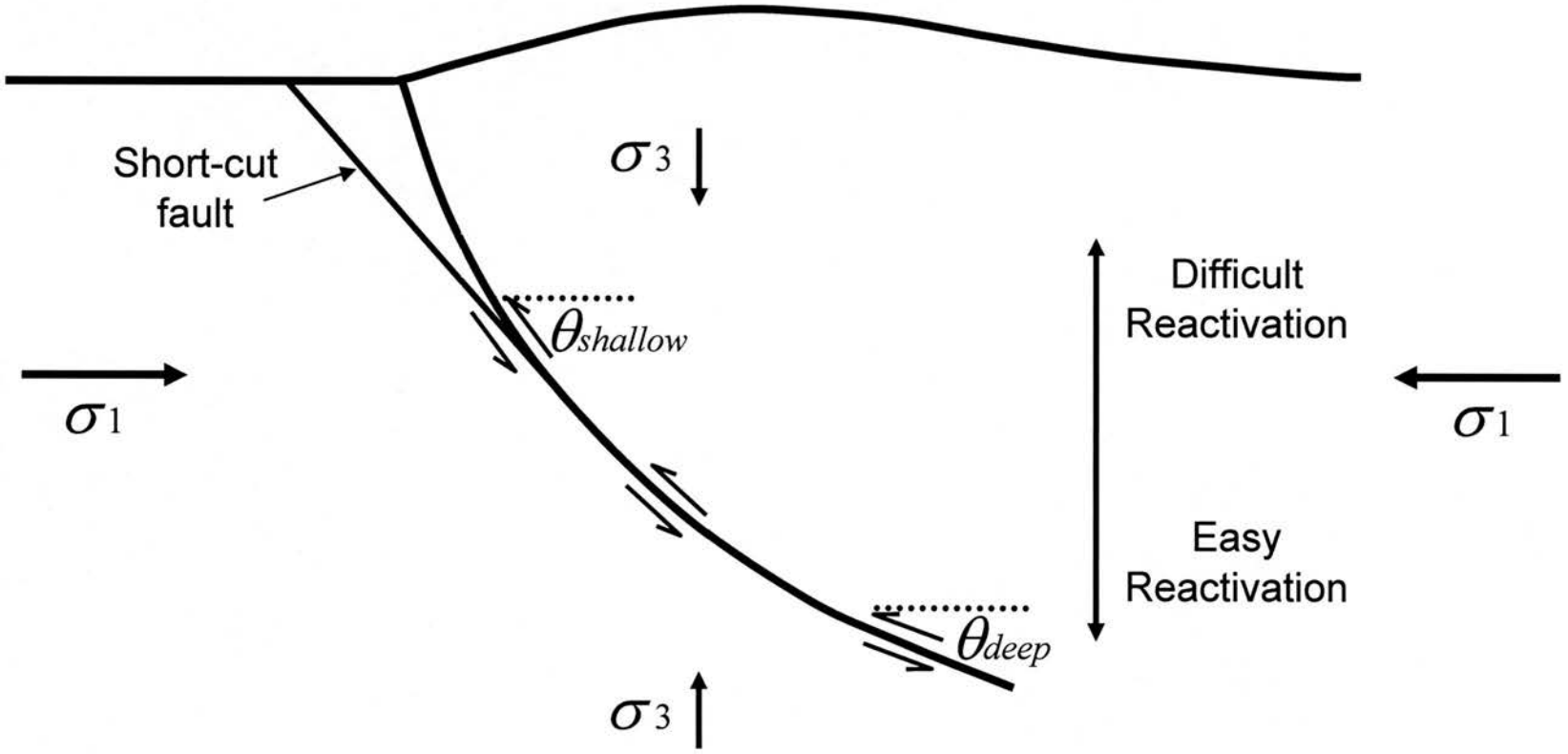

Figure 2.4: Schematic illustration of a listric normal fault: the depth-variable dip affects the response to compression. The angle between the principal stress direction and the fault plane is lower at depth ($\theta_{deep} < \theta_{shallow}$) and closer to the minimum critical stress angle for compressional reactivation. *(After Sibson, 1995)*

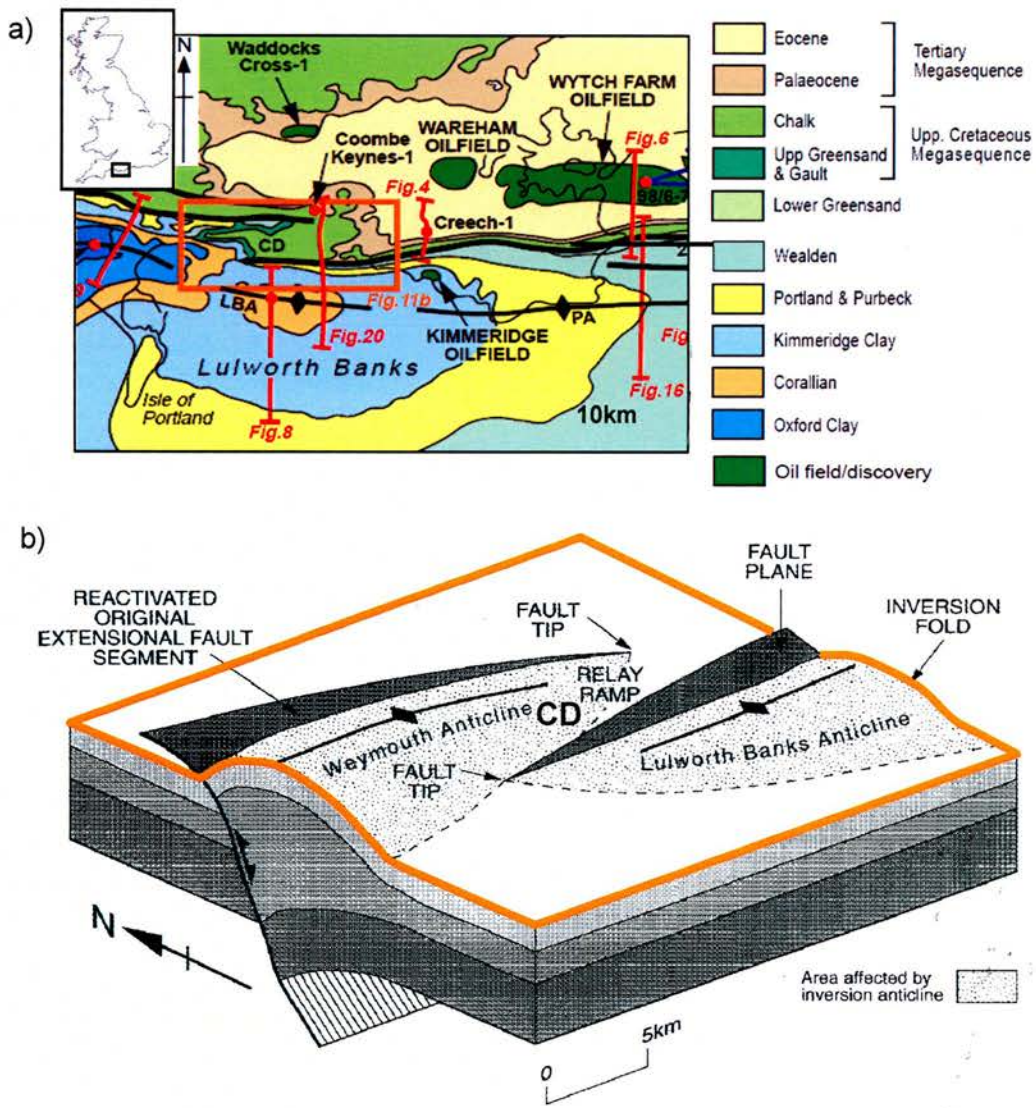

Figure 2.5: Example of an inverted relay ramp setting: Chaldon Down in South Dorset. **a)** Location map. Orange box corresponds to figure in b). The line labelled figure 20 corresponds to figure 2.6b. CD= Chaldon Down. (*After Underhill and Paterson, 1998)* **b)** Schematic block diagram depicts Chaldon Down as the site of an original relay ramp between two normal fault segments that experienced only a limited amount of extensional movement and only a limited amount of contractional deformation. *(From Underhill, 2002)*

a)

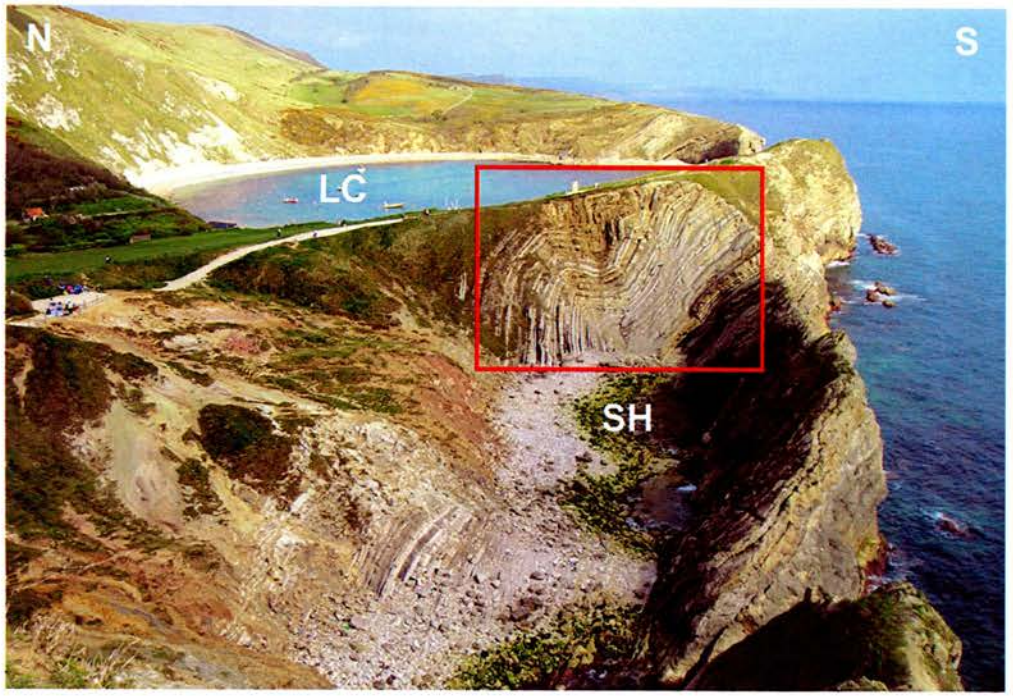

b)

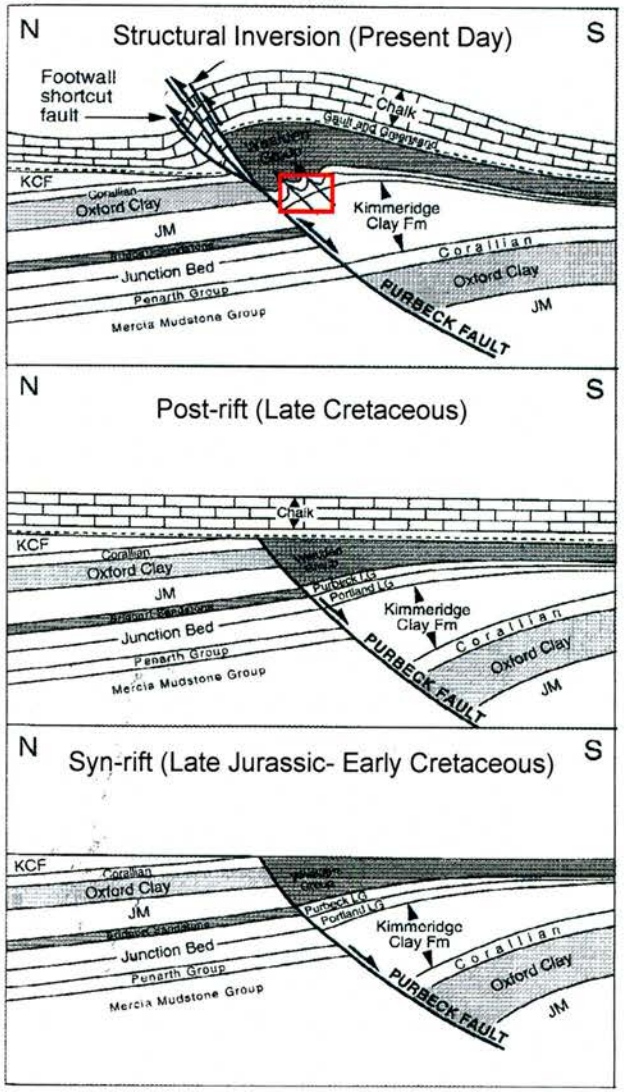

Figure 2.6: Tectonic inversion can generate complex deformation structures within the uplifted hangingwall. The 'Lulworth Crumple' is a classic outcrop example from the Wessex Basin in Dorset. **a)** Field photograph shows the North-verging Lulworth Crumple (boxed). LC= Lulworth Cove, SH=Stair Hole. Note people for scale. **b)** Schematic illustration of the tectonic history of the Lulworth area. Formation of the Lulworth Crumple is attributed to disharmonic movements during hangingwall uplift. See figure 2.5a for location. *(From Underhill, 2002)*

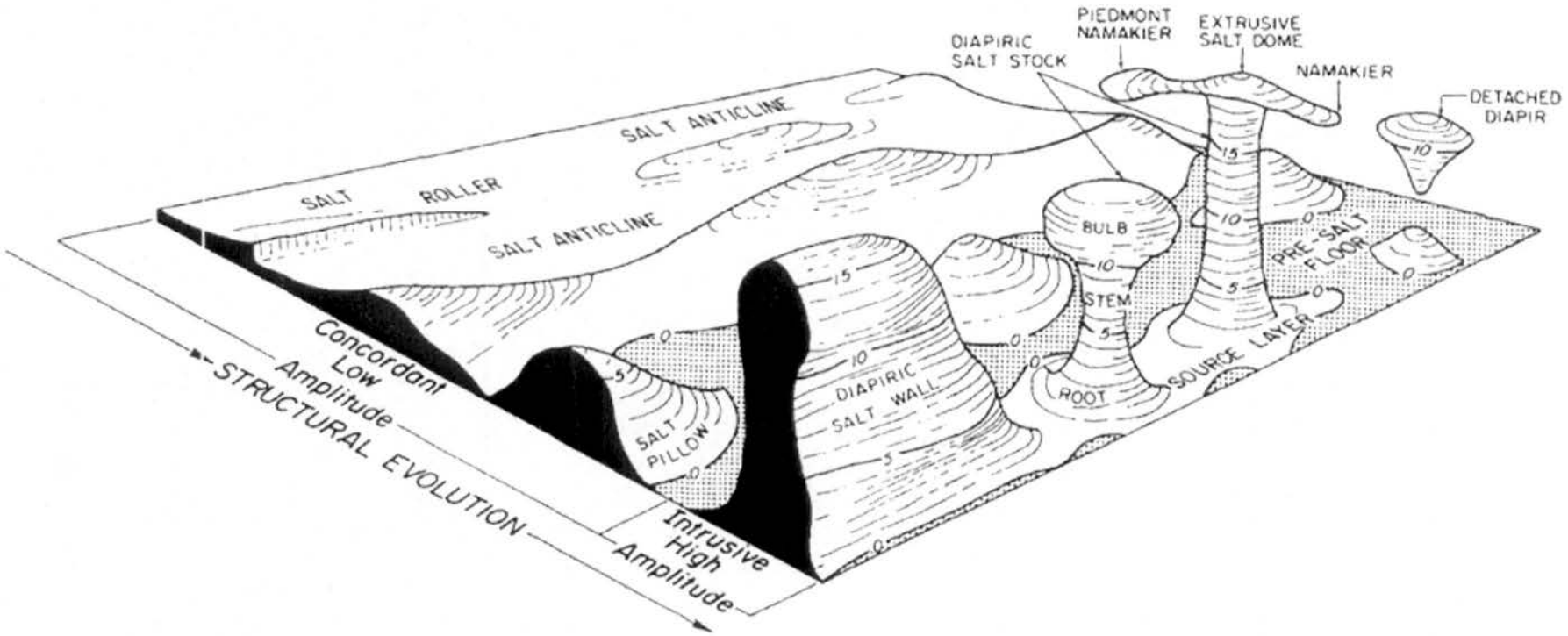

Figure 2. 7: Sketch illustrating the nomenclature for different salt structure styles. *(From Jackson and Talbot, 1986)*

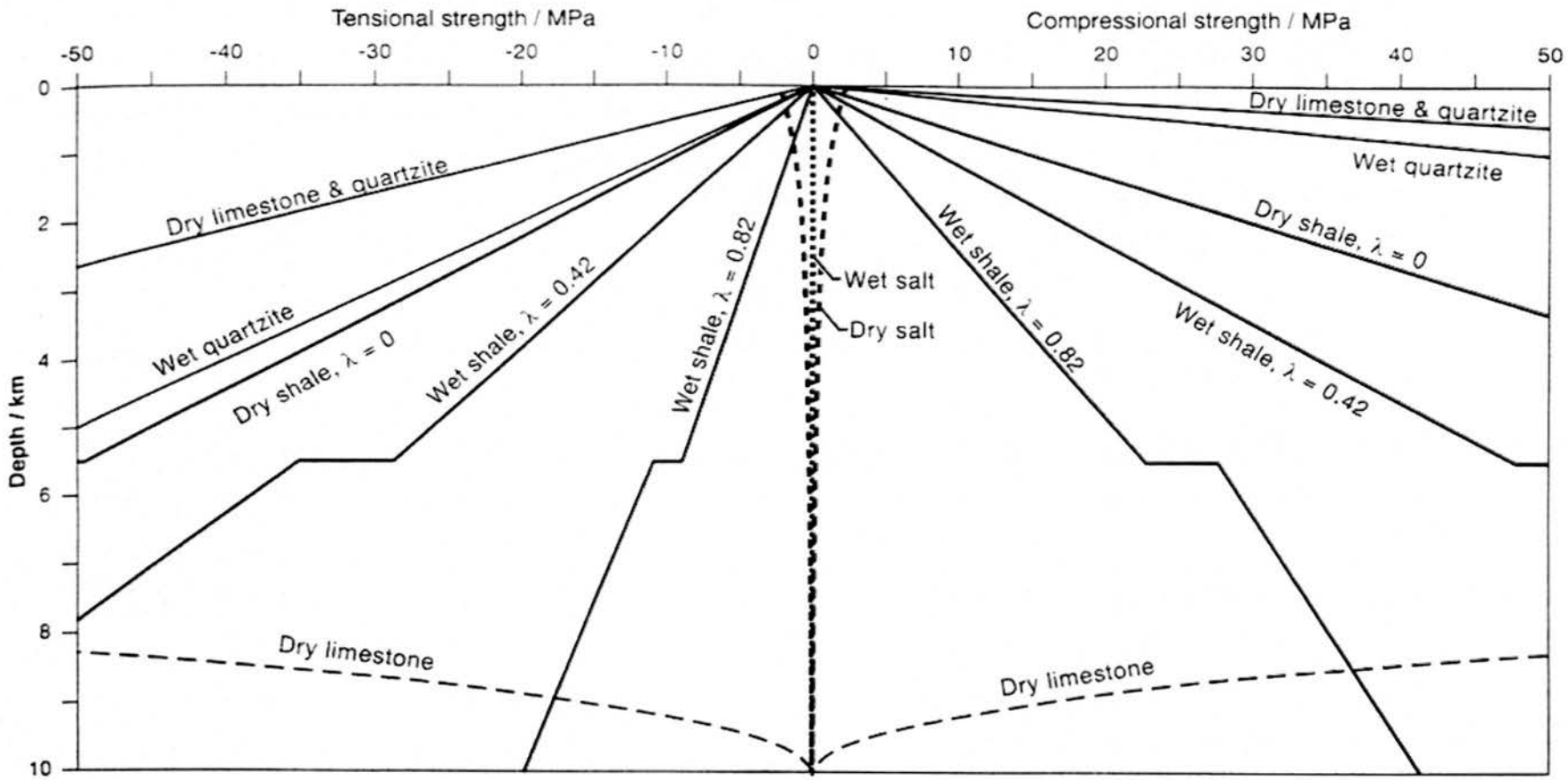

Figure 2. 8: Plot illustrating how the strength of salt and certain other lithologies varies with burial. Salt strength is relatively low and decreases with depth. Salt strength is strain-rate dependent; the plotted values correspond to a (geologically feasible) strain rate of 10^{-14} s^{-1}. λ is the pore pressure coefficient. *(From Jackson and Venderville, 1994)*

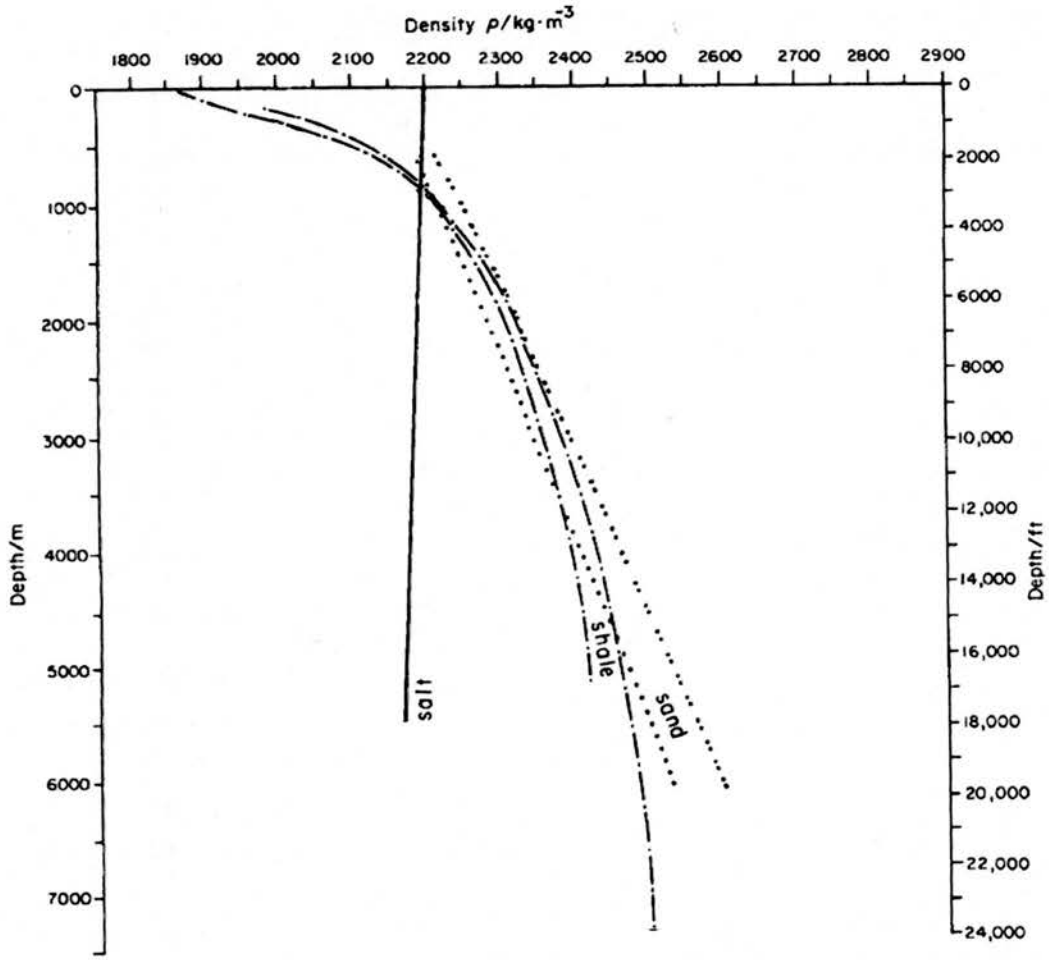

Figure 2.9: Plot illustrating the density change with depth for salt compared to that of sand and shale. (*From Jackson and Talbot, 1986*)

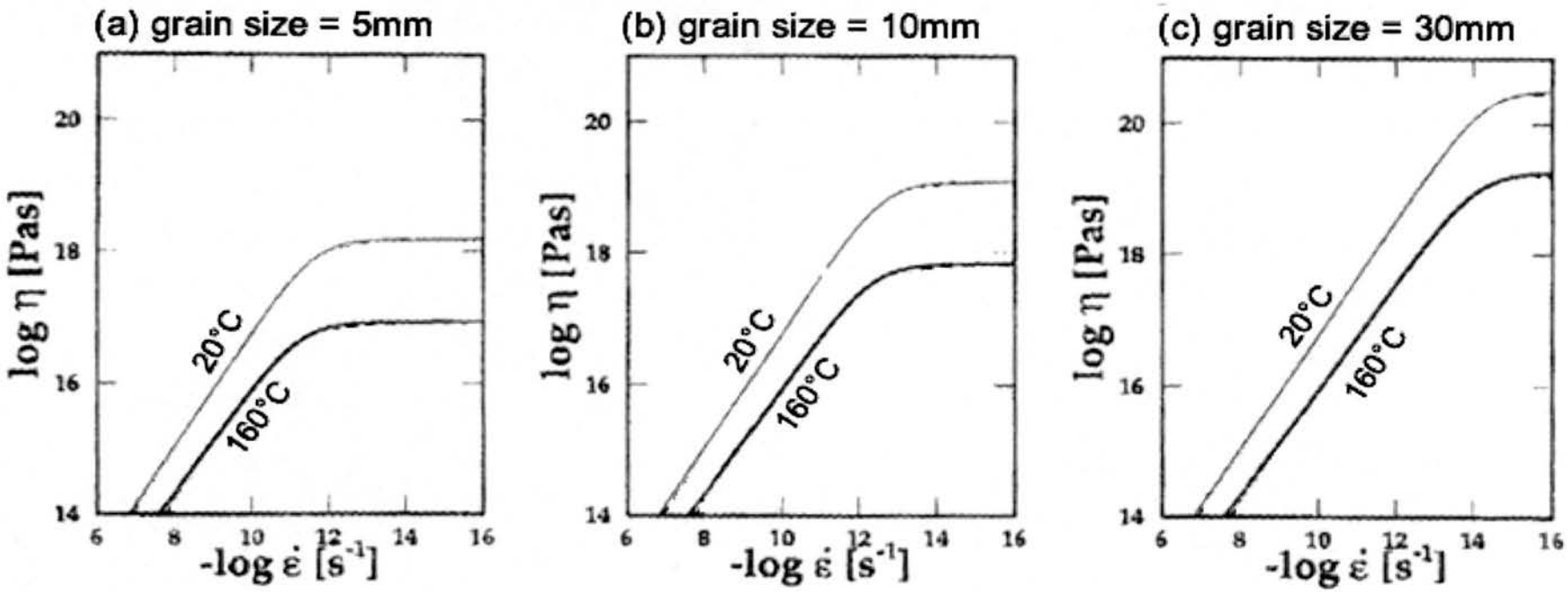

Figure 2.10: Log-log plots of effective viscosity (η) against strain rate (ε) for three different grain sizes of salt deforming by combined dislocation and diffusion creep. Note how the decrease in grain size from 10mm (b) to 5mm (a) results in an effective viscosity decrease of approximately one order of magnitude at (geologically feasible) strain rates of ~10^{-14} s^{-1}. Similarly, an increase in temperature of 140°C results in a decrease in viscosity of one order of magnitude. (*From Van Keken et al., 1993)*

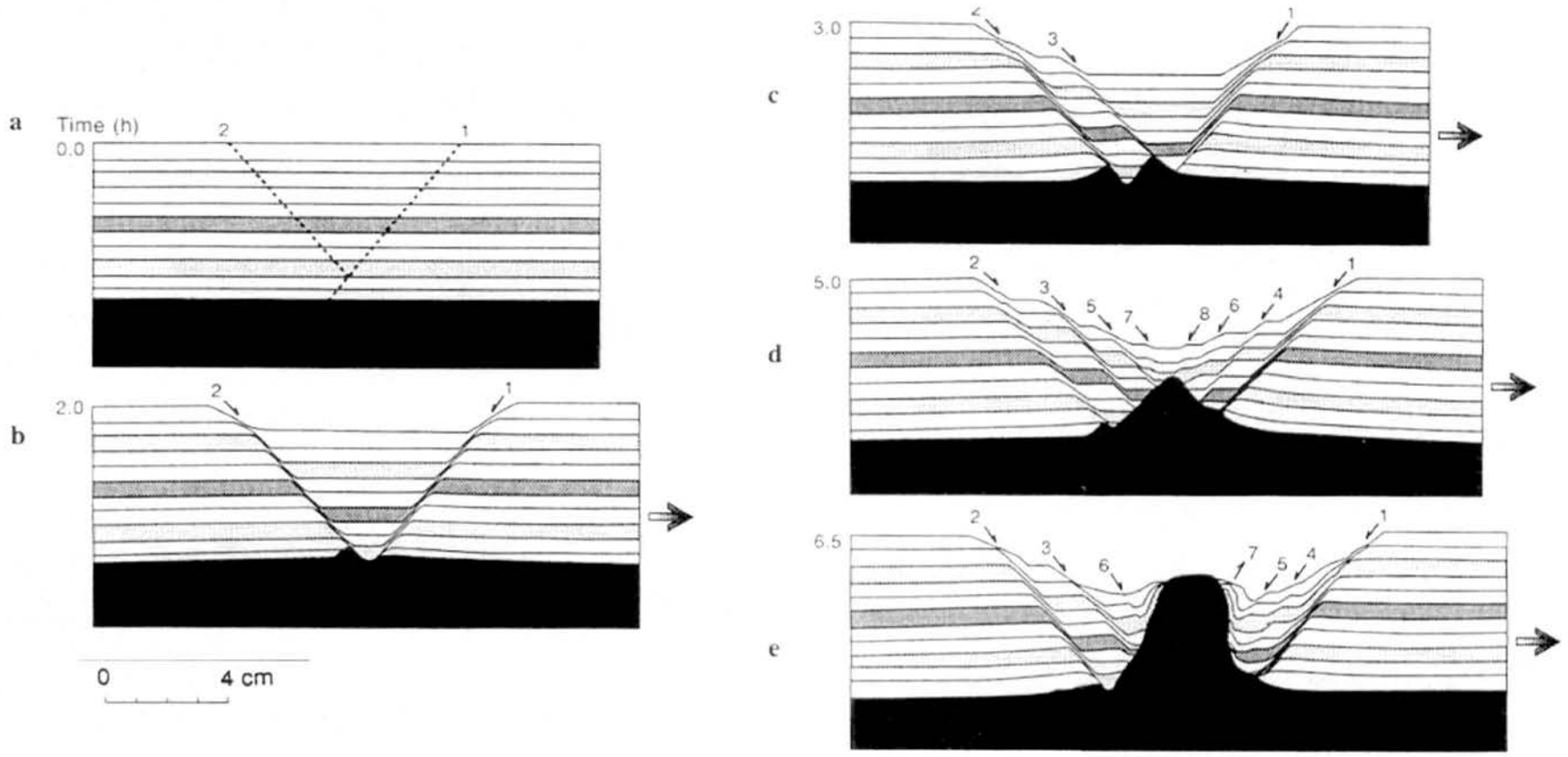

Figure 2.11: Cross sections through an analogue model of the brittle overburden to a salt layer. The different stages represent progressive extension. A reactive diapir forms below the developing graben system. *(From Jackson and Venderville, 1994)*

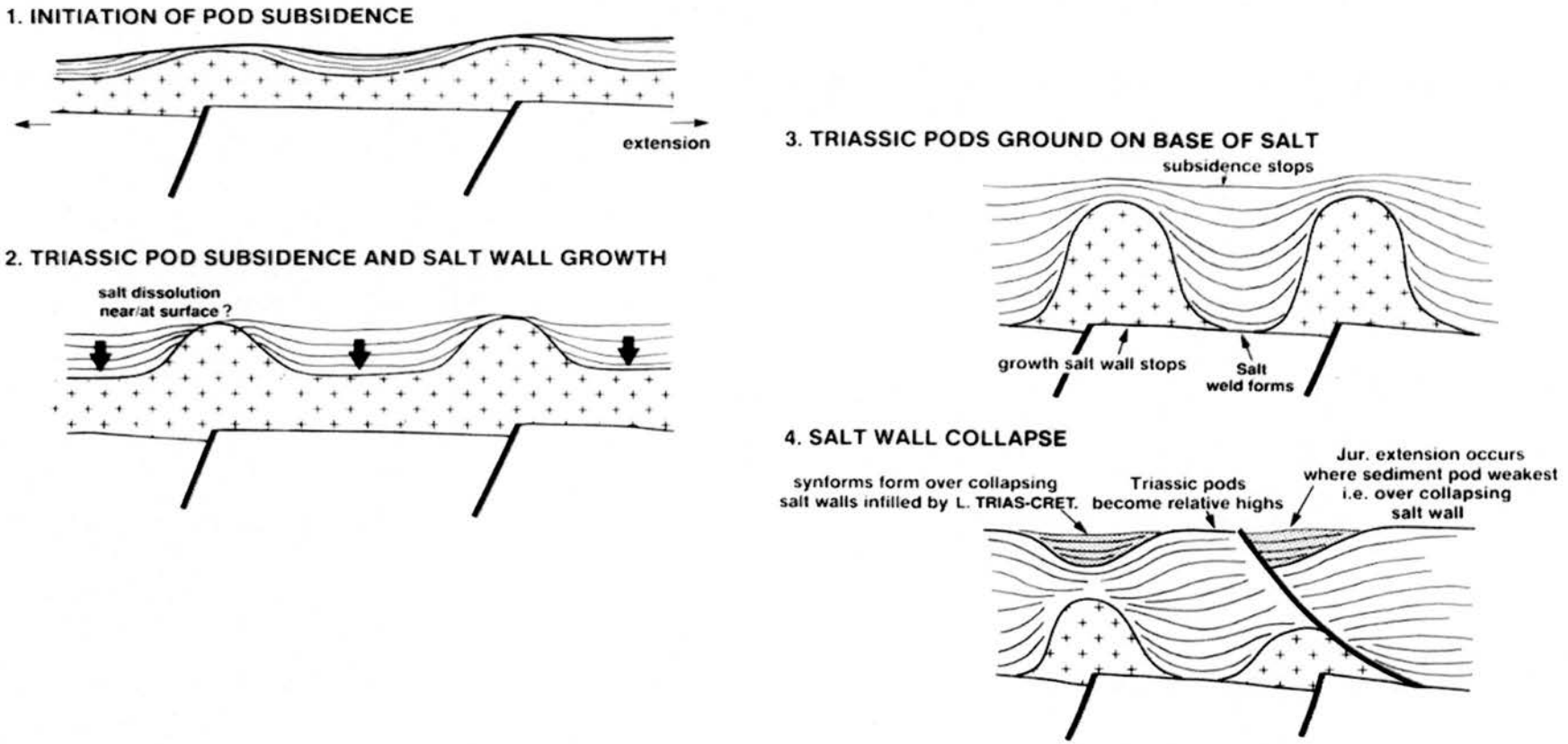

Figure 2.12: Cartoon diagram illustrating minibasin (pod) and salt wall development in the Central North Sea. This figure is specific to Triassic sedimentation in the Central North Sea, but the concepts of salt wall growth, pod grounding and subsequent salt wall collapse are more widely applicable. *(From Hodgson et al., 1993)*

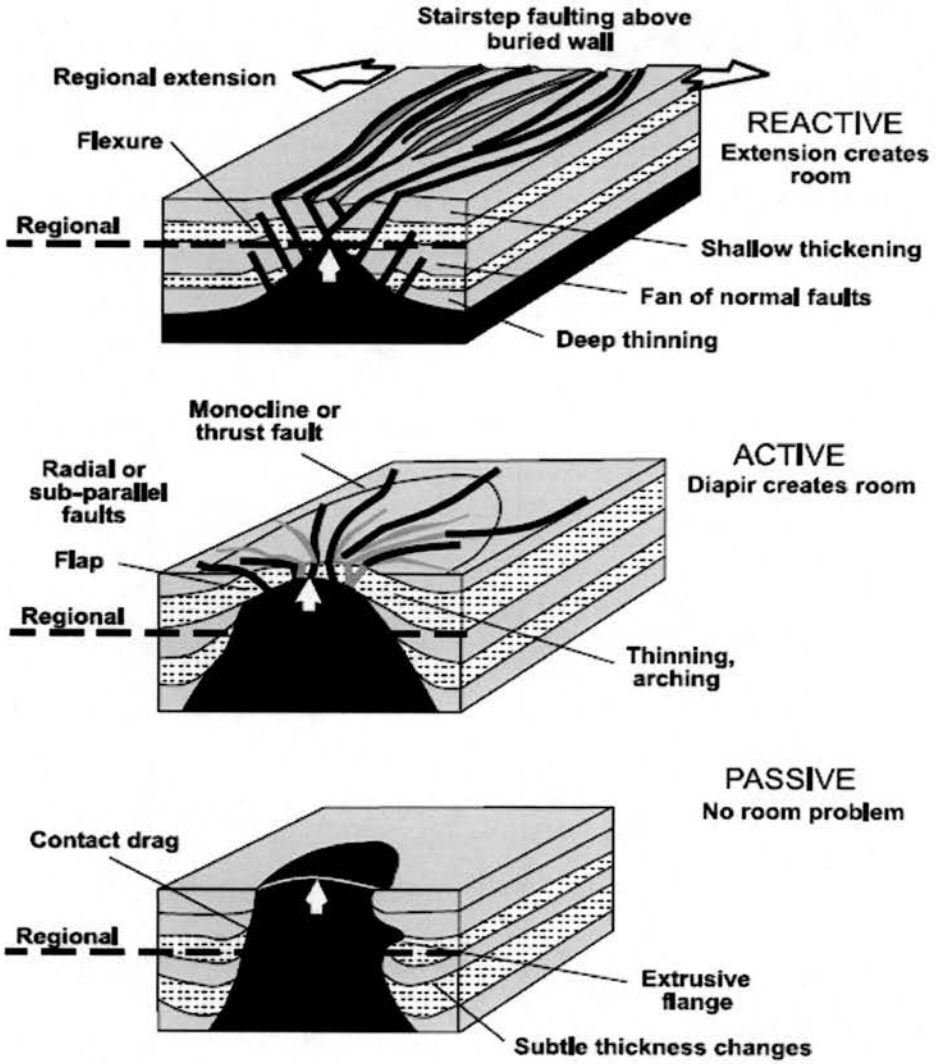

Figure 2.13: Cartoon diagram illustrating the three main modes of diapirism; reactive, active and passive. *(From Dooley et al., 2005)*

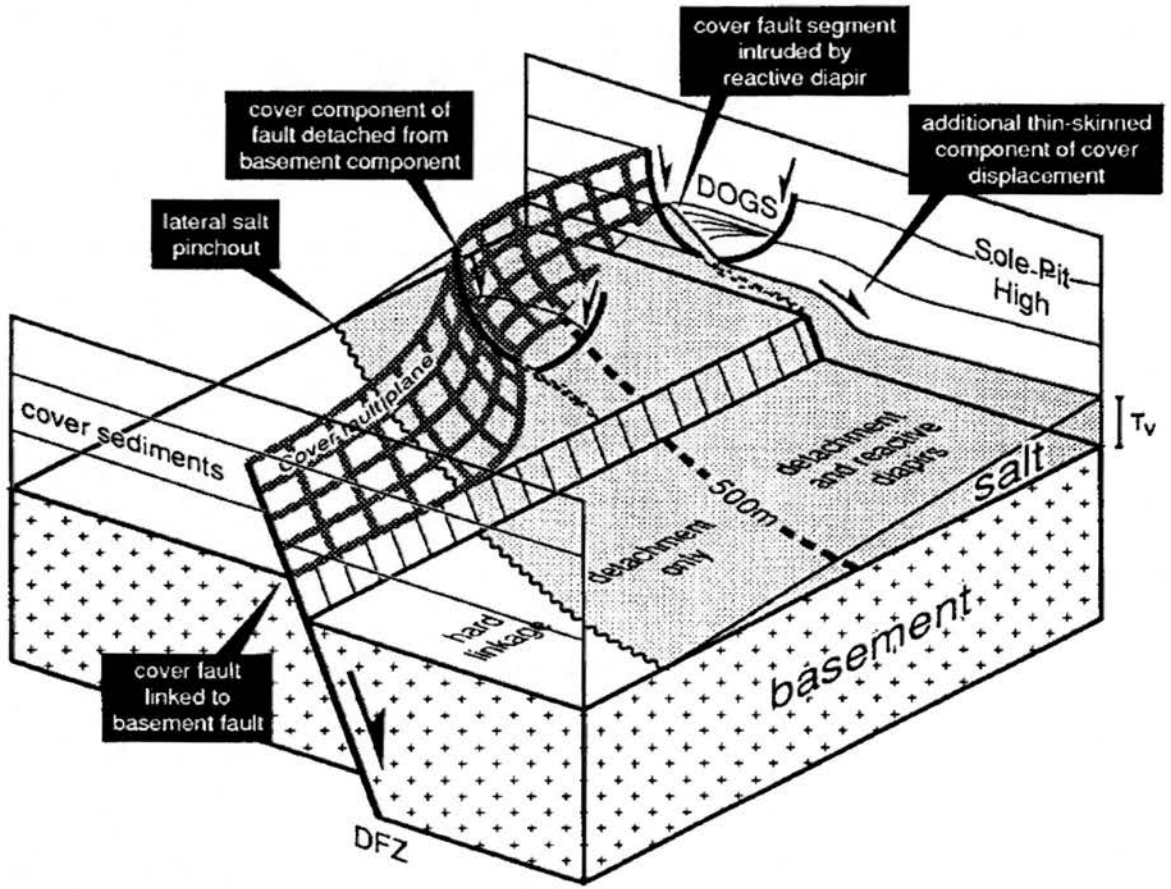

Figure 2.14: Schematic diagram illustrating how basement-cover relationships may vary along a fault strand due to spatial variation in salt layer thickness. The diagram is based on the Dowsing Fault Zone in the Southern North Sea. DFZ= Dowsing Fault Zone, DOGS= Dowsing Graben System. *(From Stewart et al., 1996)*

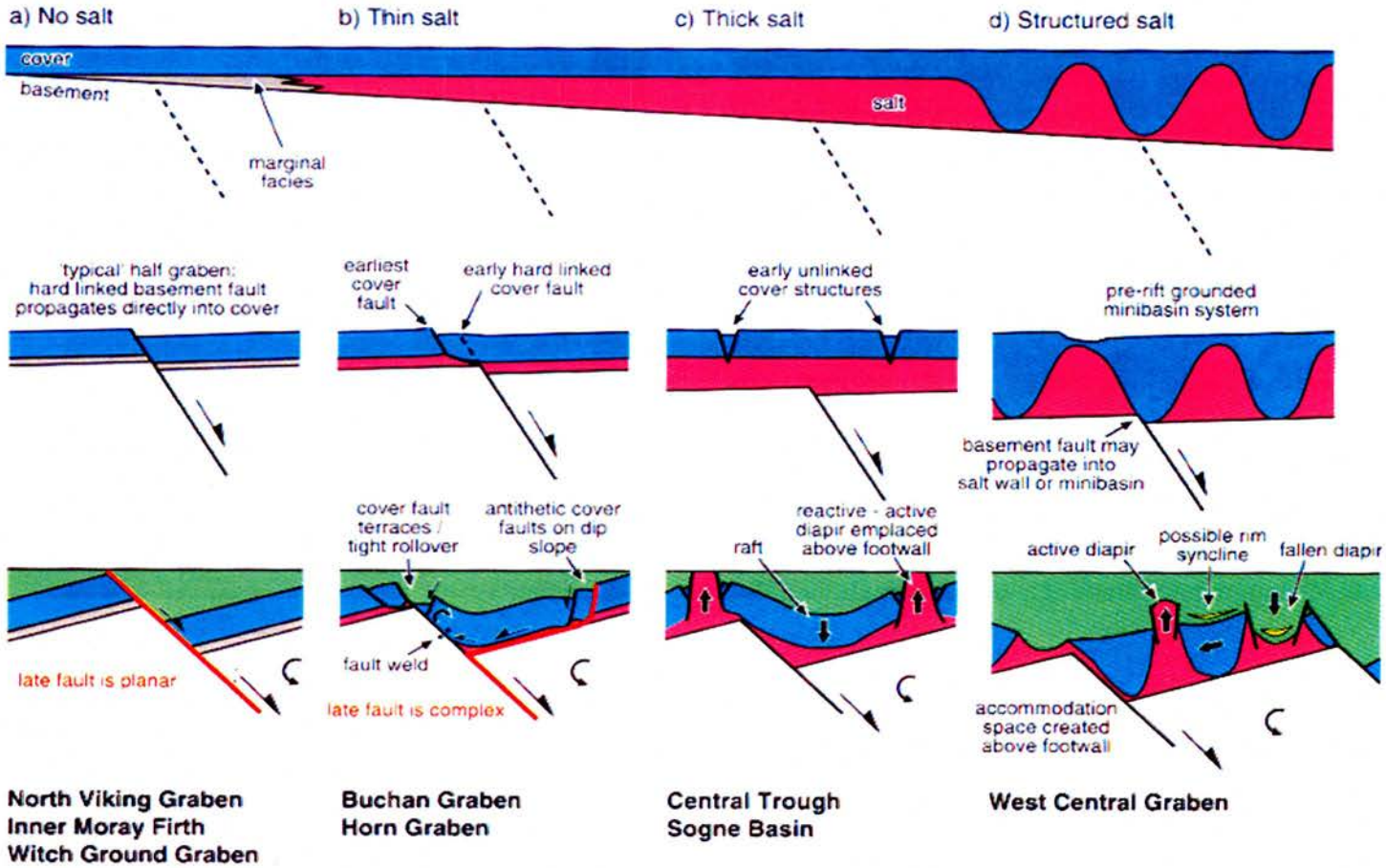

Figure 2.15: Schematic diagram illustrating how structural styles in the supra-salt sequence vary in accordance with salt thickness during Late Jurassic rift development in the Central North Sea area. **a)** Where salt is absent (e.g. Zechstein marginal facies) 'classic' half graben geometries evolve. **b)** Where salt is thin (<~30m) a complex array of cover faults develop over the basement fault scarp. **c)** Where a thick salt layer is present, early cover rafts separated by salt diapirs are draped across the evolving basement topography. **d)** More commonly in the Central North Sea, the salt is already structured due to the Triassic phase of minibasin subsidence (figure 2.12). Rotation of the fault blocks will give rise to further movements of these salt structures; whether they actively rise or fall will primarily depend on their position on the slope. *(From Stewart and Clark, 1999)*

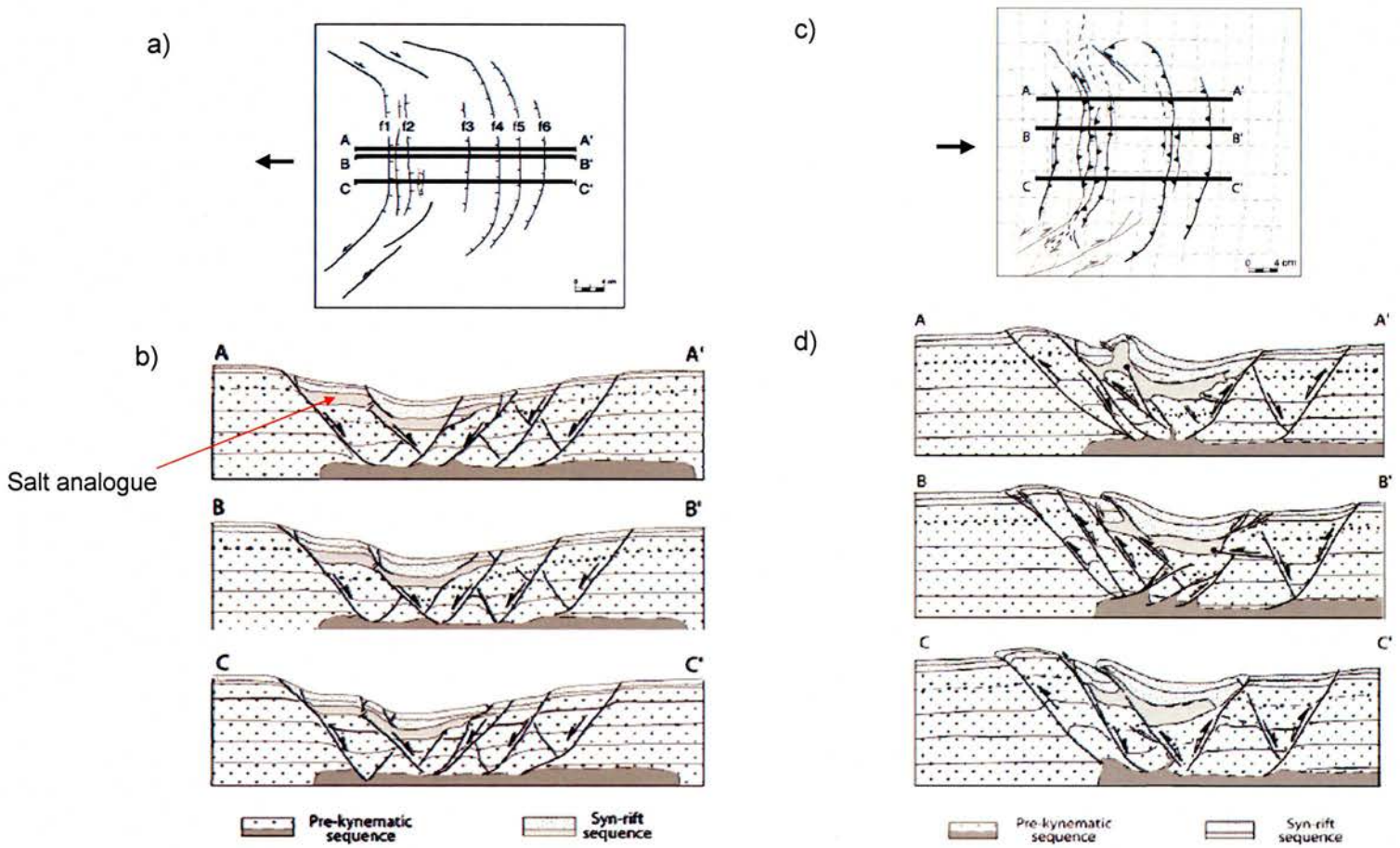

Figure 2.16: Analogue experiments model salt behaviour in response to compression. **a)** Plan view of the model at maximum extension prior to compression. **b)** Serial sections demonstrate structural styles under extension. **c)** Plan view of the model after compression. **d)** Serial sections demonstrate structural styles of inversion and the role of salt. *(From Del Ventisette et al., 2006)*

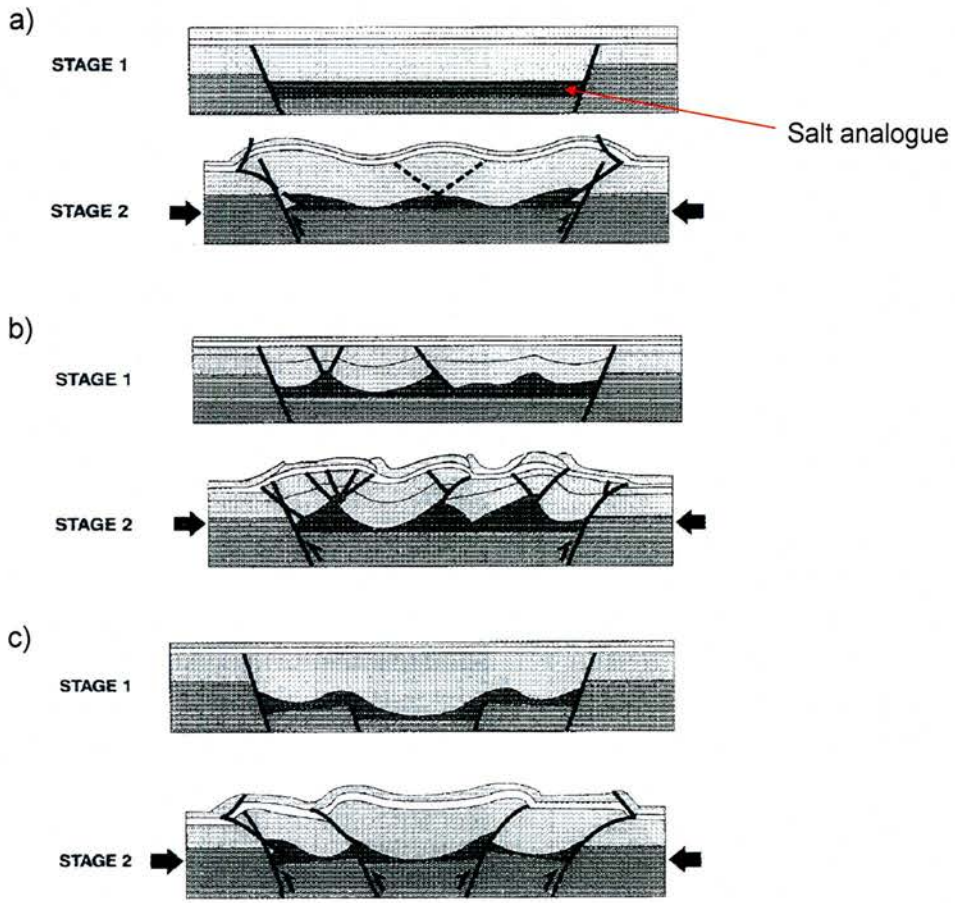

Figure 2.17: Schematic illustration of inversion tectonics in a graben containing salt. Stage 1 is the pre-inversion setting, Stage 2 is post-inversion. **a)** Folds and short-cut faults develop in homogeneous strata above the inverted basement faults. **b)** Thrusts and folds are localized by pre-existing salt structures. **c)** Thrust and folds are localized by reactivation of basement faults. *(From Letouzey et al., 1995)*

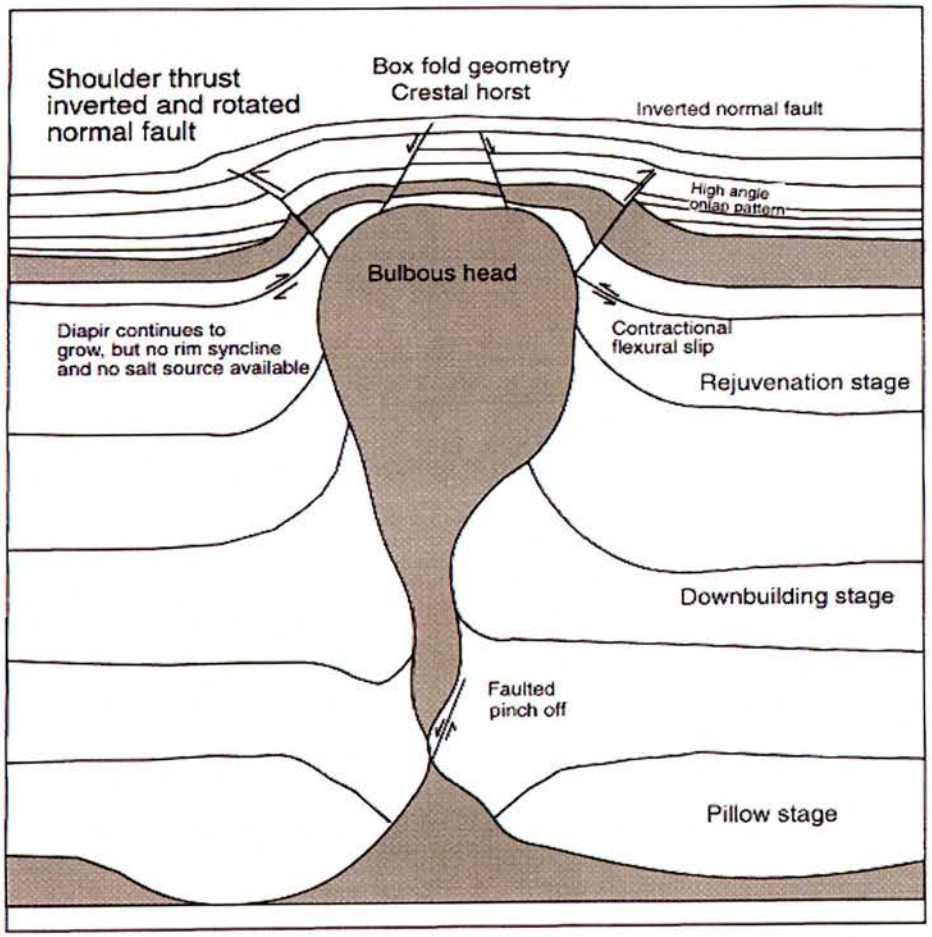

Figure 2.18: Cartoon illustrating the geometric features of a salt diapir modified by compression. Features include an unusually thick lid of overburden strata up-domed above the diapir, evidence for continued upward movement of the diapir even when pinched-off from source, and concentric thrust faults localised at the diapir shoulders. *(From Davison et al., 2000)*

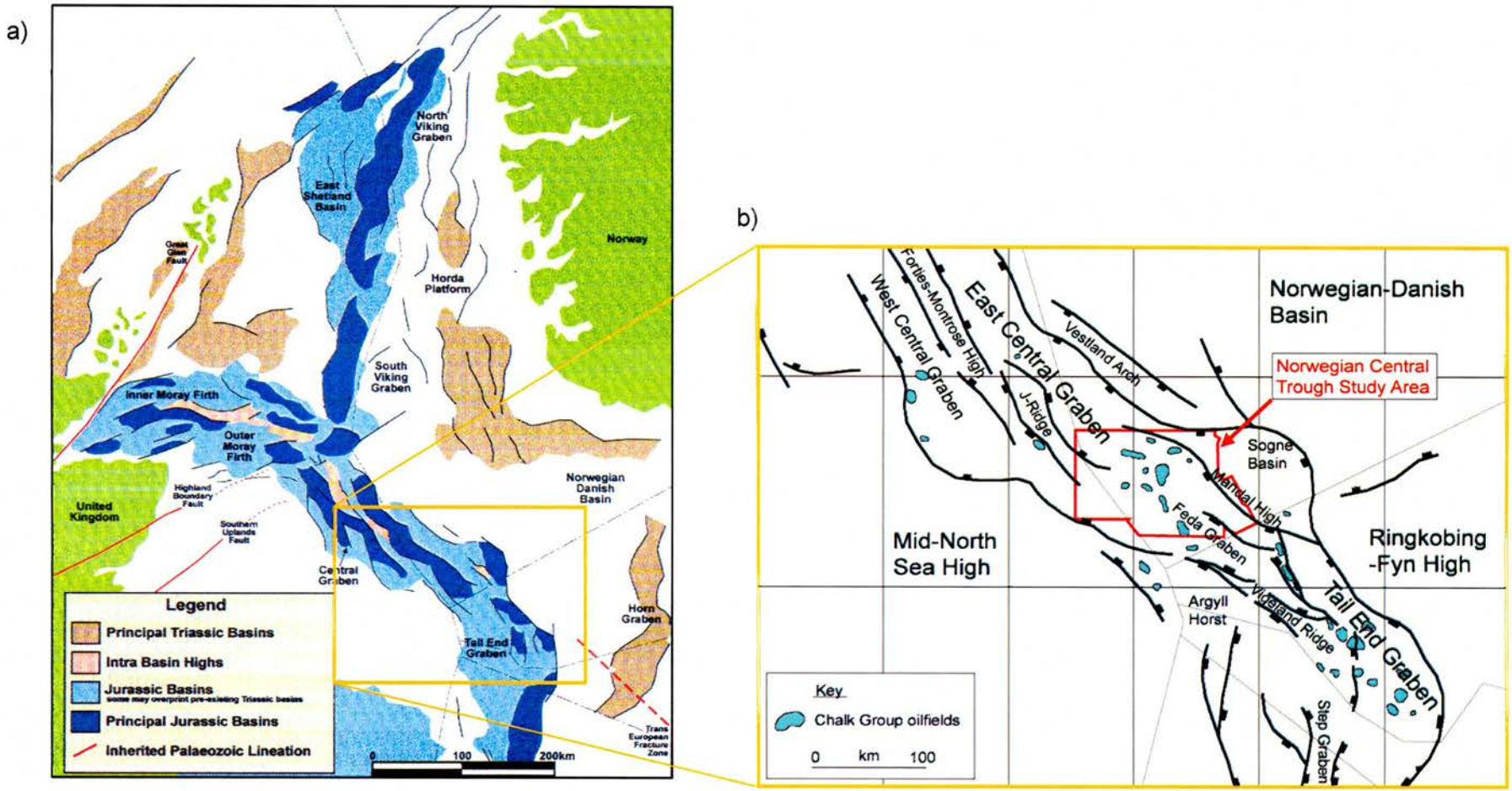

Figure 2.19: Location of the Norwegian Central Trough study area. **a)** Principal structural elements of the North Sea Permian-Cretaceous graben system *(From Erratt et al., 1999)*. **b)** The study area is defined by the spatial extent of seismic data available to this project *(After Megson and Tygesen, 2005; Petroleum Exploration Society of Great Britain, 2007)*

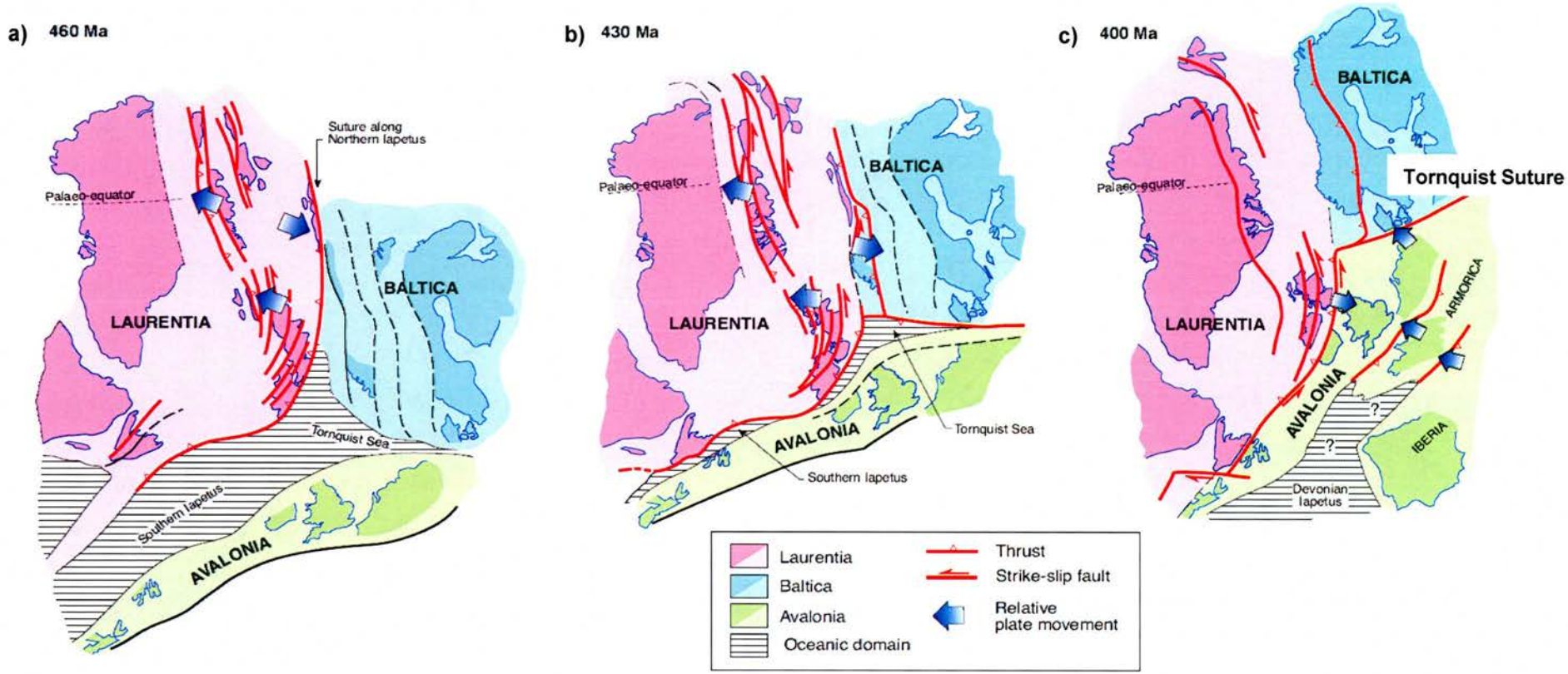

Figure 2.20: Caledonian Orogeny in NW Europe. The Caledonian Orogeny is associated with closure of the Iapetus Ocean and the Tornquist Sea and involved three-way convergence between Laurentia, Baltica and Avalonia. *(From Coward et al., 2003)*

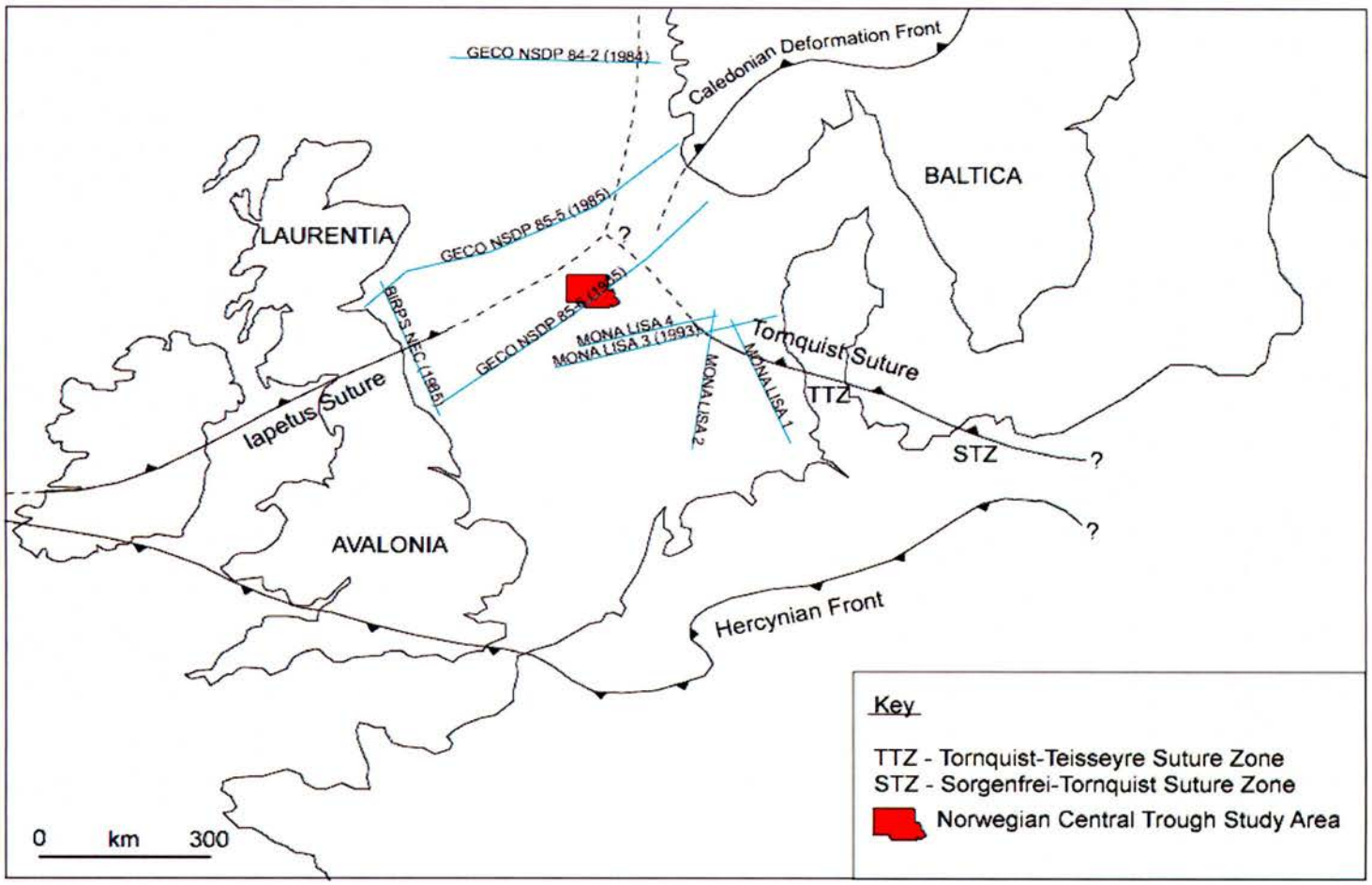

Figure 2.21: Caledonian and Variscan basement in NW Europe. Deep seismic reflection surveys have been shot in attempt to constrain the sub-sea locations of the Caledonian sutures. *(After Glennie and Underhill, 1998; Coward et al., 2003)*

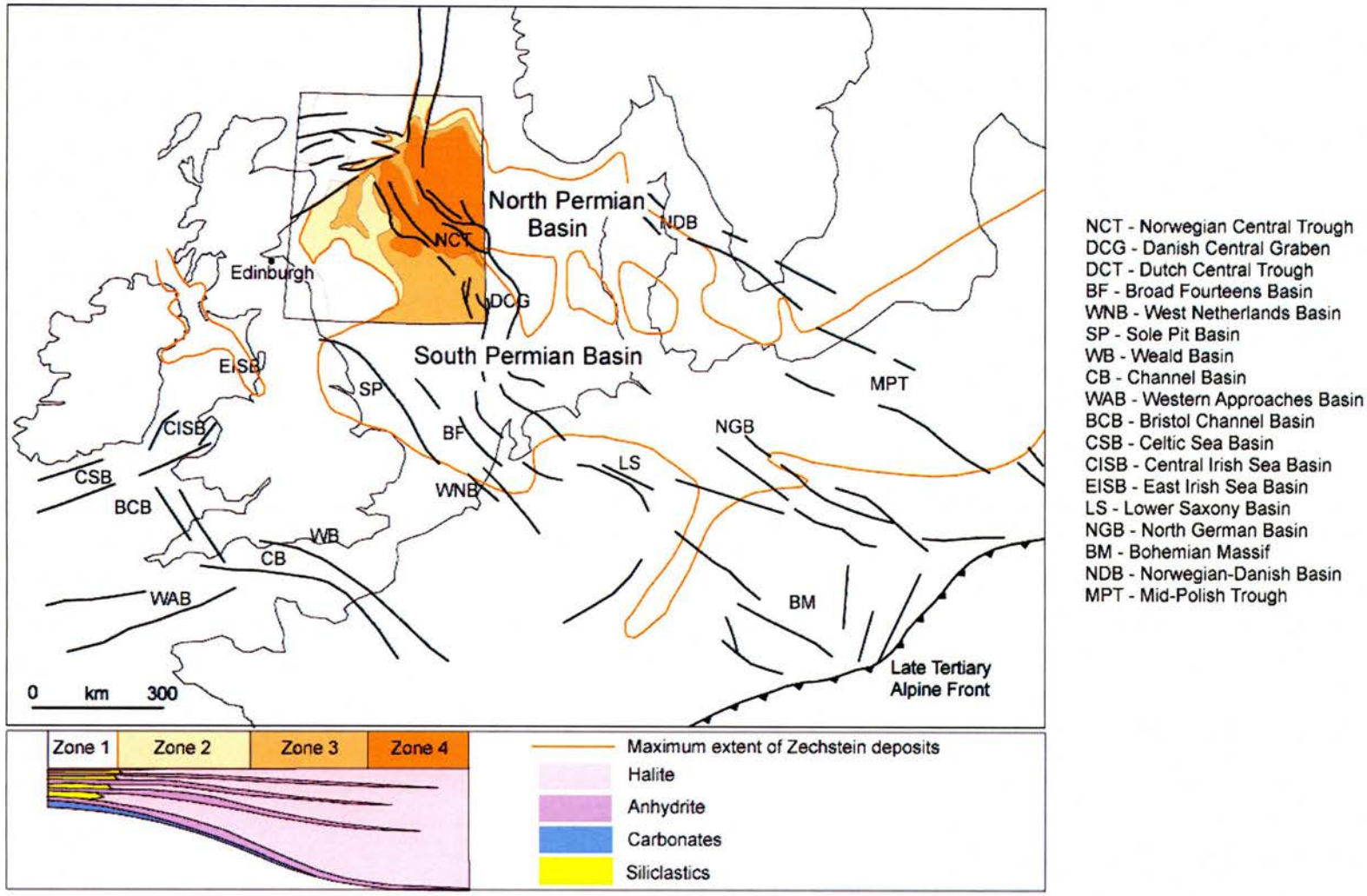

Figure 2.22: Location of Permian Sedimentary basins in NW Europe *(After Stewart and Clark, 1999; Coward et al., 2003)*

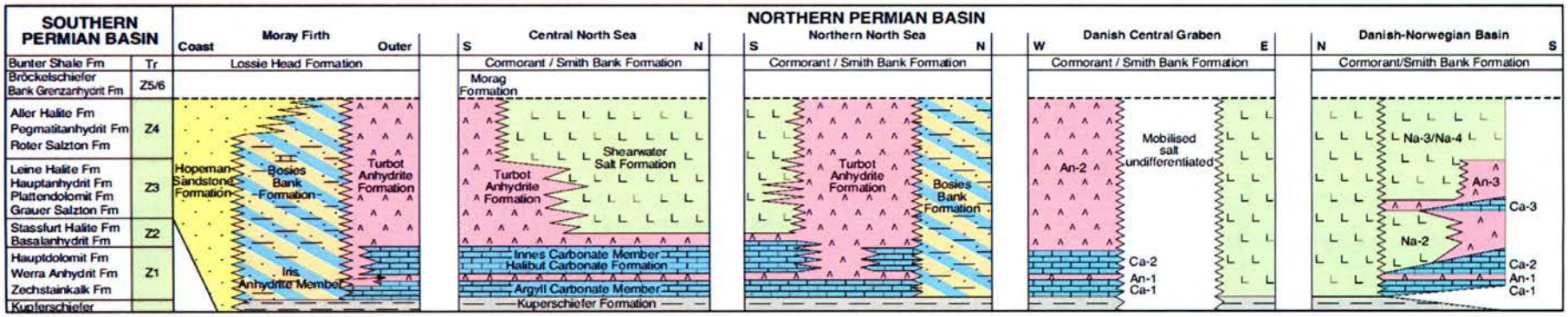

Figure 2.23: Comparison of the Late Permian Zechstein development of the Northern and Southern Permian Basins. Halite and Anhydrite are the two most abundant salts within the Zechstein Group. Anhydrite is relatively immobile compared with halite, and the latter is the primary component of the Shearwater Salt Formation. *(From Glennie et al., 2003)*

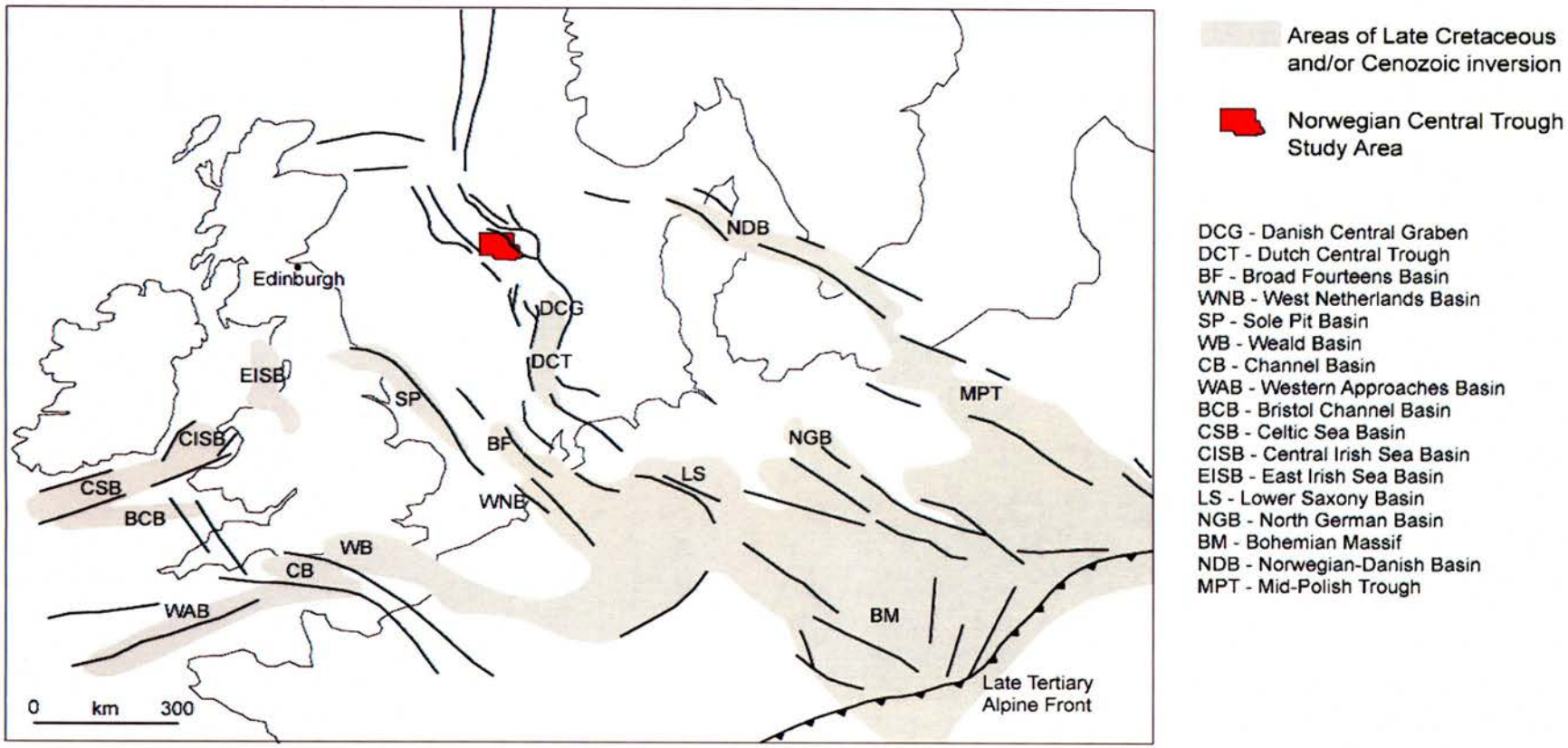

Figure 2.24: The tectonically inverted basins of Western Europe. *(After Ziegler, 1990; Nielsen and Hansen, 2000)*

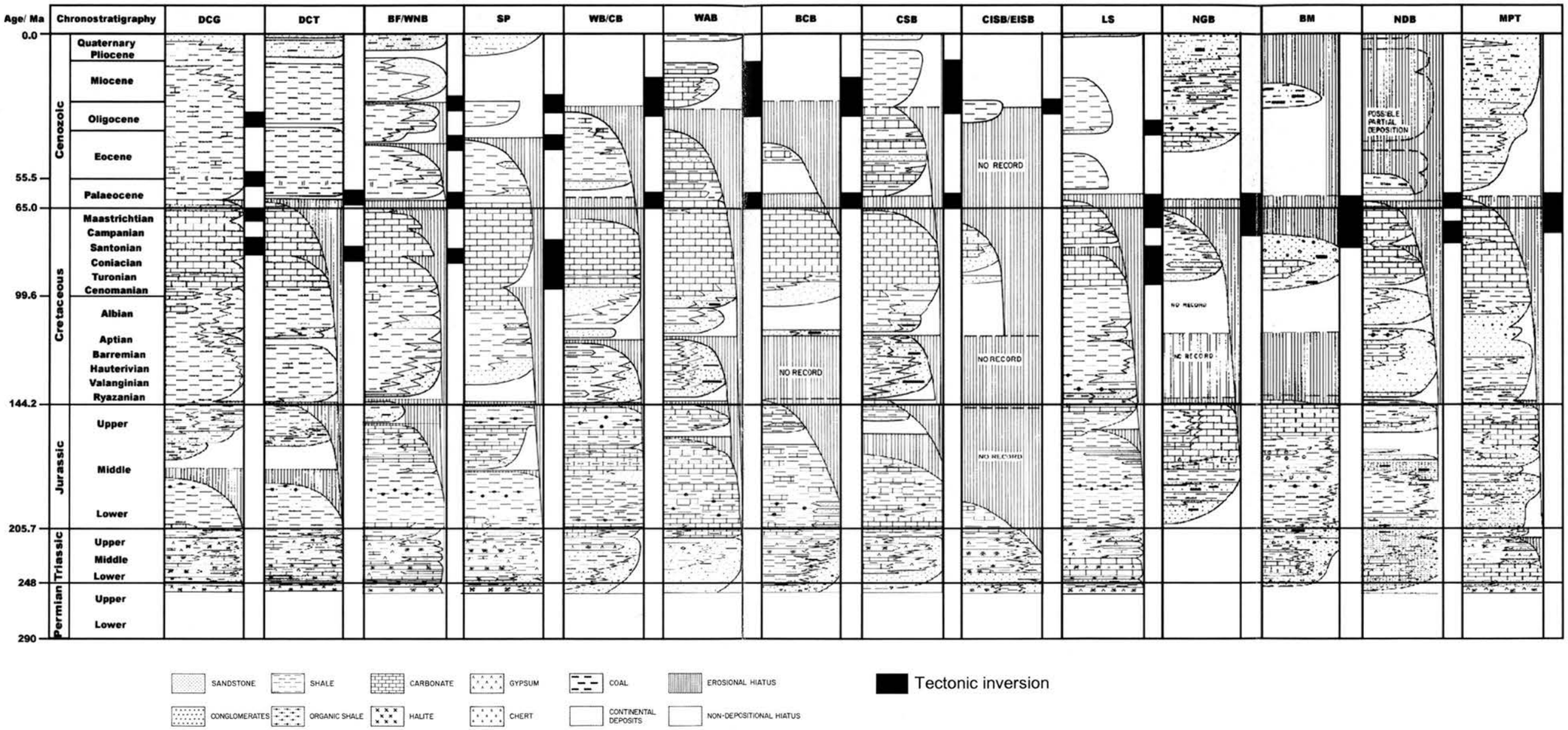

Figure 2.25: Summary diagram of the timings of tectonic inversion identified within the European Plate. *(Stratigraphic columns modified from Ziegler et al., 1987)*
DCG (Danish Central Graben) ages from *Cartwright, 1989; Vejbæk and Andersen, 2002* . DCT (Dutch Central Trough) ages from *De Lugt et al., 2003.* BF/WNB (Broad Fourteens and West Netherlands Basins) ages from *Haywood et al., 1989; Nalpas et al., 1995; Worum and Michon, 2005.* SP (Sole Pit Basin) ages from *Walker and Cooper, 1987.* WB/CB (Weald and Channel Basins) ages from *Underhill and Stoneley, 1998; Blundell, 2002.* WAB (Western Approaches Basin) ages from *Holford et al., 2005.* BCB (Bristol Channel Basin) ages from *Holford et al., 2005.* CSB (Celtic Sea Basin) ages from *Holford et al., 2005.* CISB/ EISB (Central and Eastern Irish Sea Basins) ages from *Green et al., 2001; Holford et al., 2005.* LS (Lower Saxony Basin) ages from *Ziegler, 1990.* NGB (North German Basin) ages from *Ziegler, 1990.* BM (Bohemian Massif) ages from *Malkovsky, 1987.* NDB (Norwegian-Danish Basin) ages from *Hansen et al., 2000.* MPT (Mid-Polish Trough) ages from *Dadlez et al., 1995; Lamarche, 2003.*

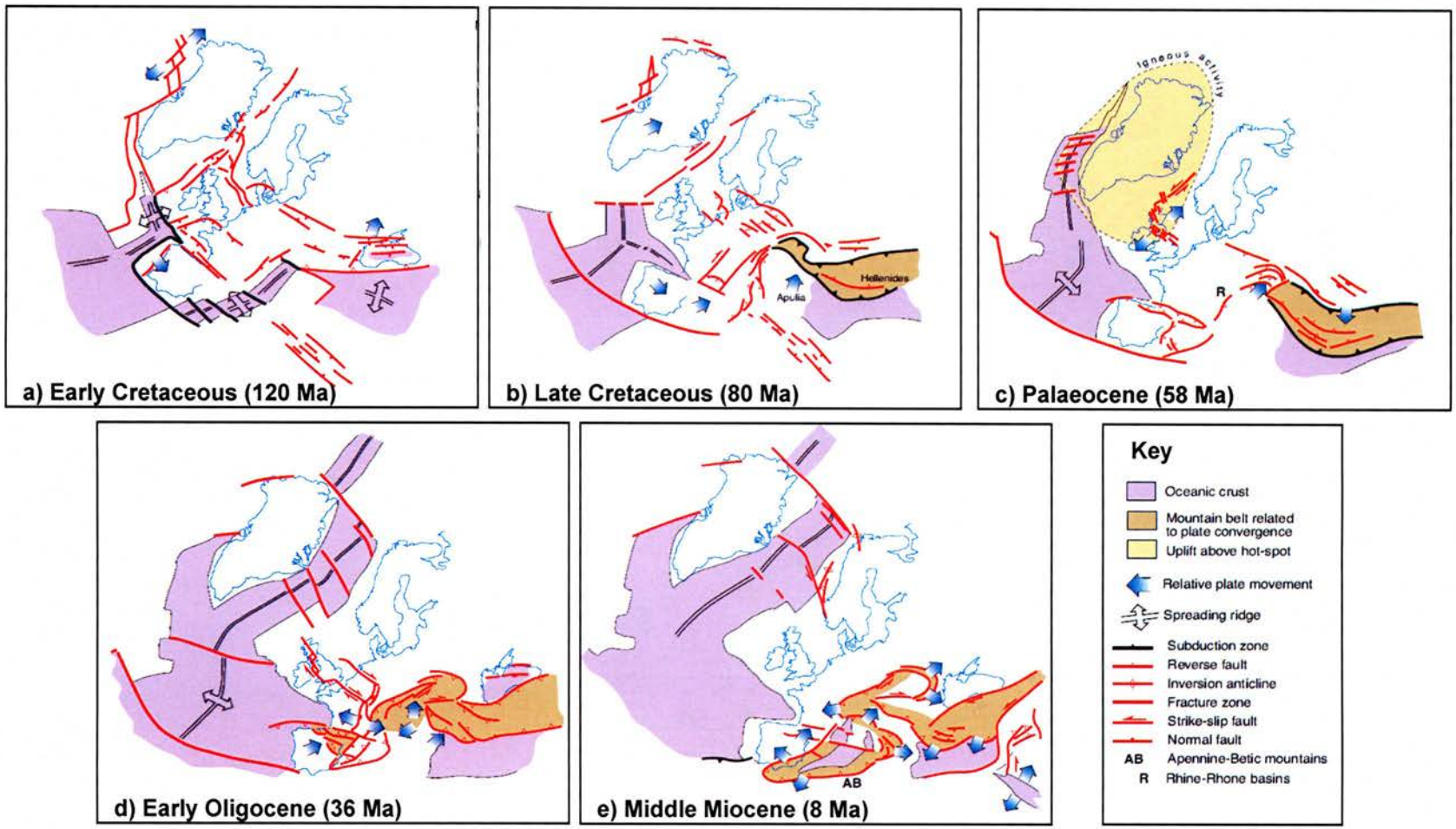

Figure 2.26: Palaeotectonic reconstructions of NW Europe *(From Coward et al., 2003)*

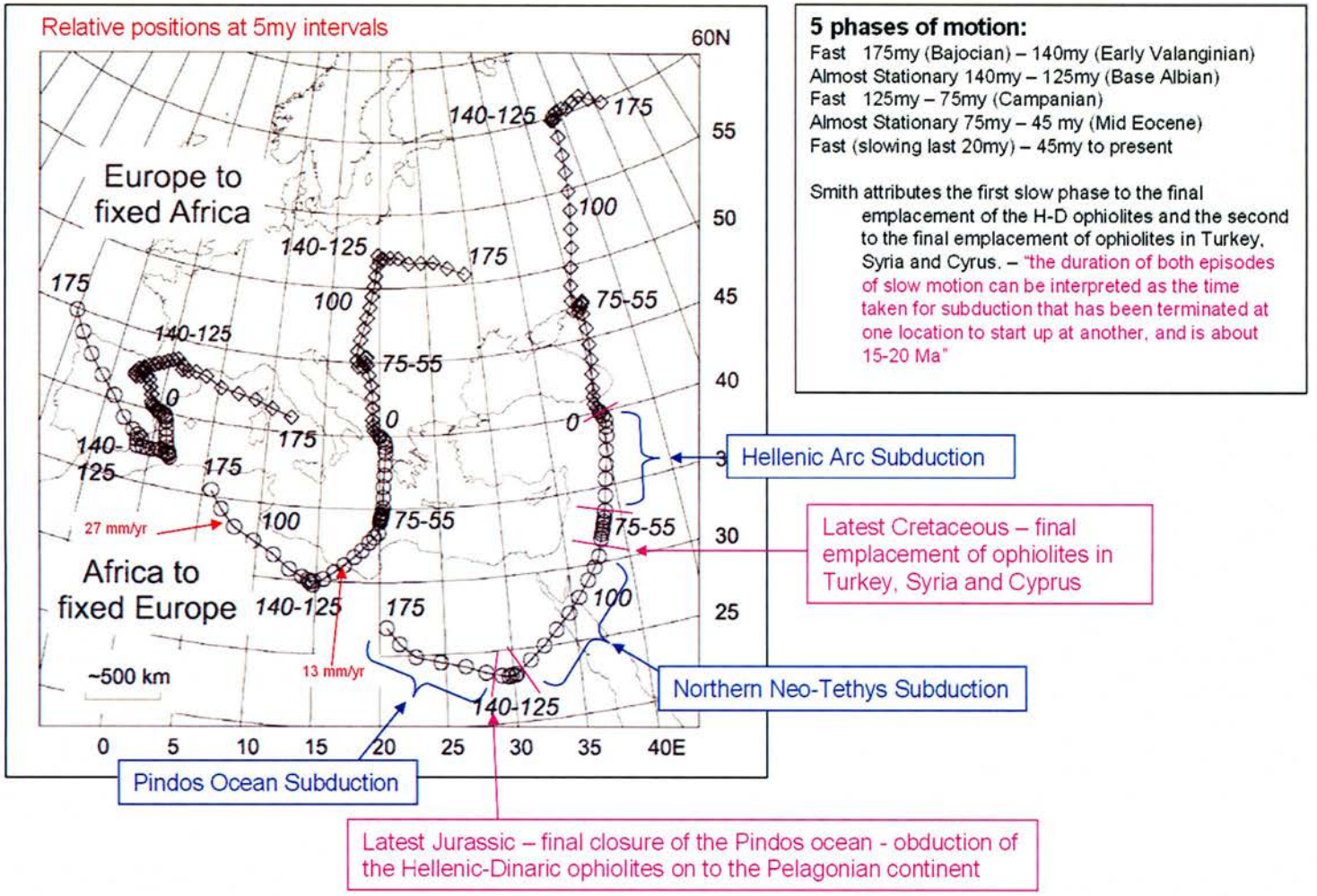

Figure 2.27: Motions of Africa relative to Eurasia (circles) and motions of Eurasia relative to Africa (diamonds) from 175 to 0 Ma *(After Smith, 2006)*

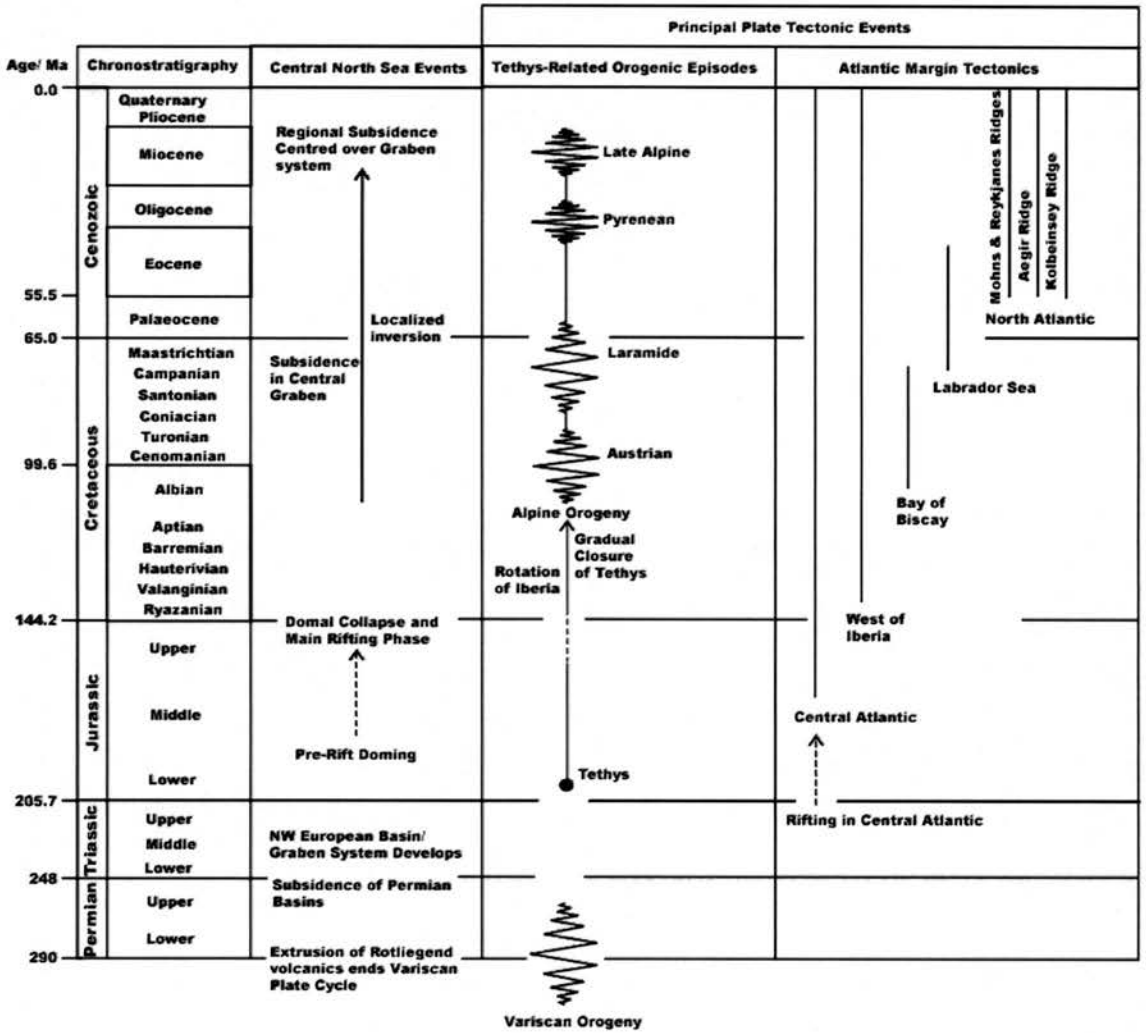

Figure 2.28: Summary illustration of the major Permian to Recent tectonic events affecting Western Europe. (*After Ziegler, 1990; Glennie and Underhill, 1998)*

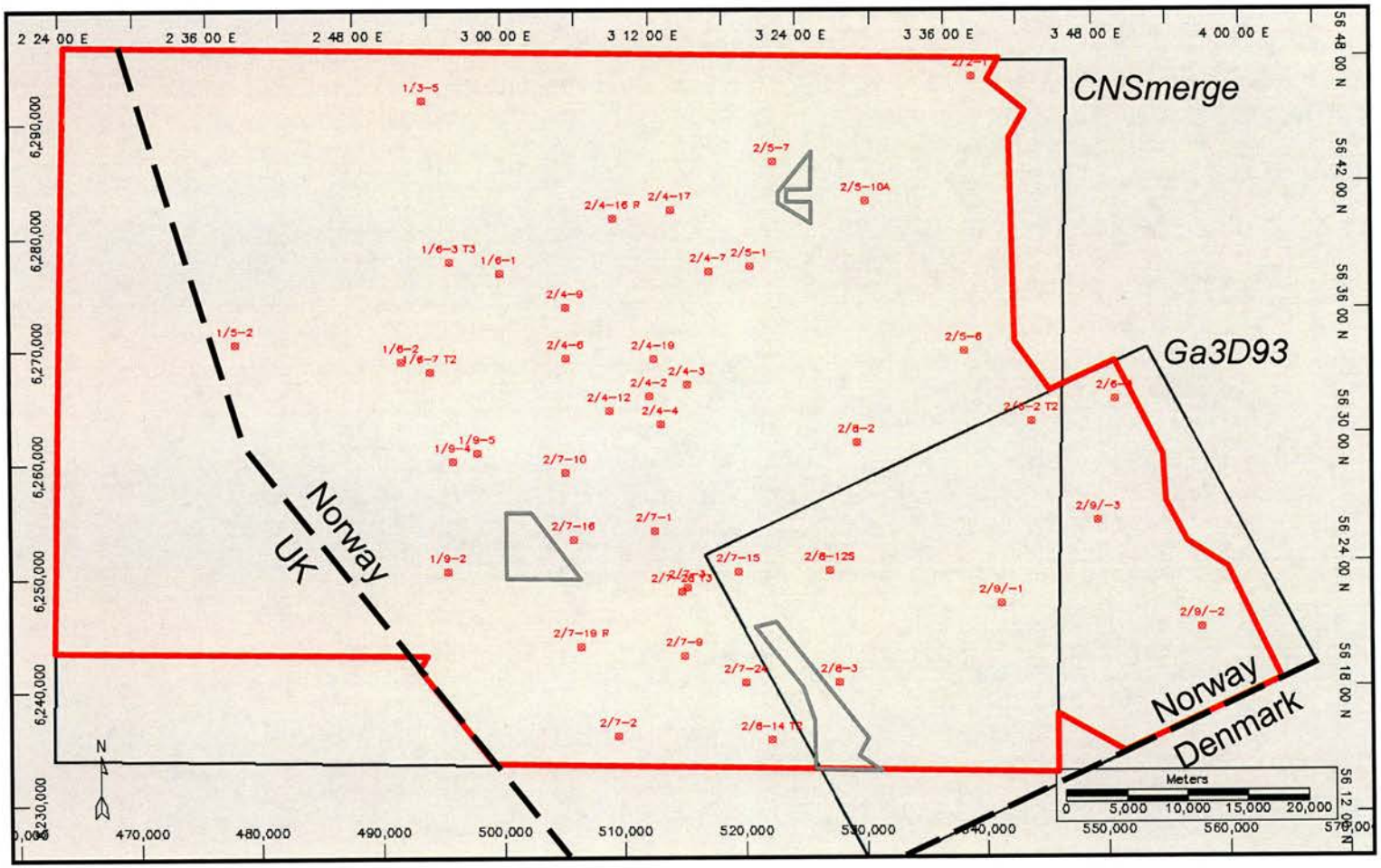

Figure 3.1: Spatial extent of seismic reflection data used in this study. The data comprise two partially overlapping surveys (black rectangles). Red outline shows the actual area of seismic coverage. Small grey boxes are regions with no seismic coverage within the studied area; interpretation across these areas was by interpolation. Dotted black lines are international boundary lines. There are 43 wells in the project database.

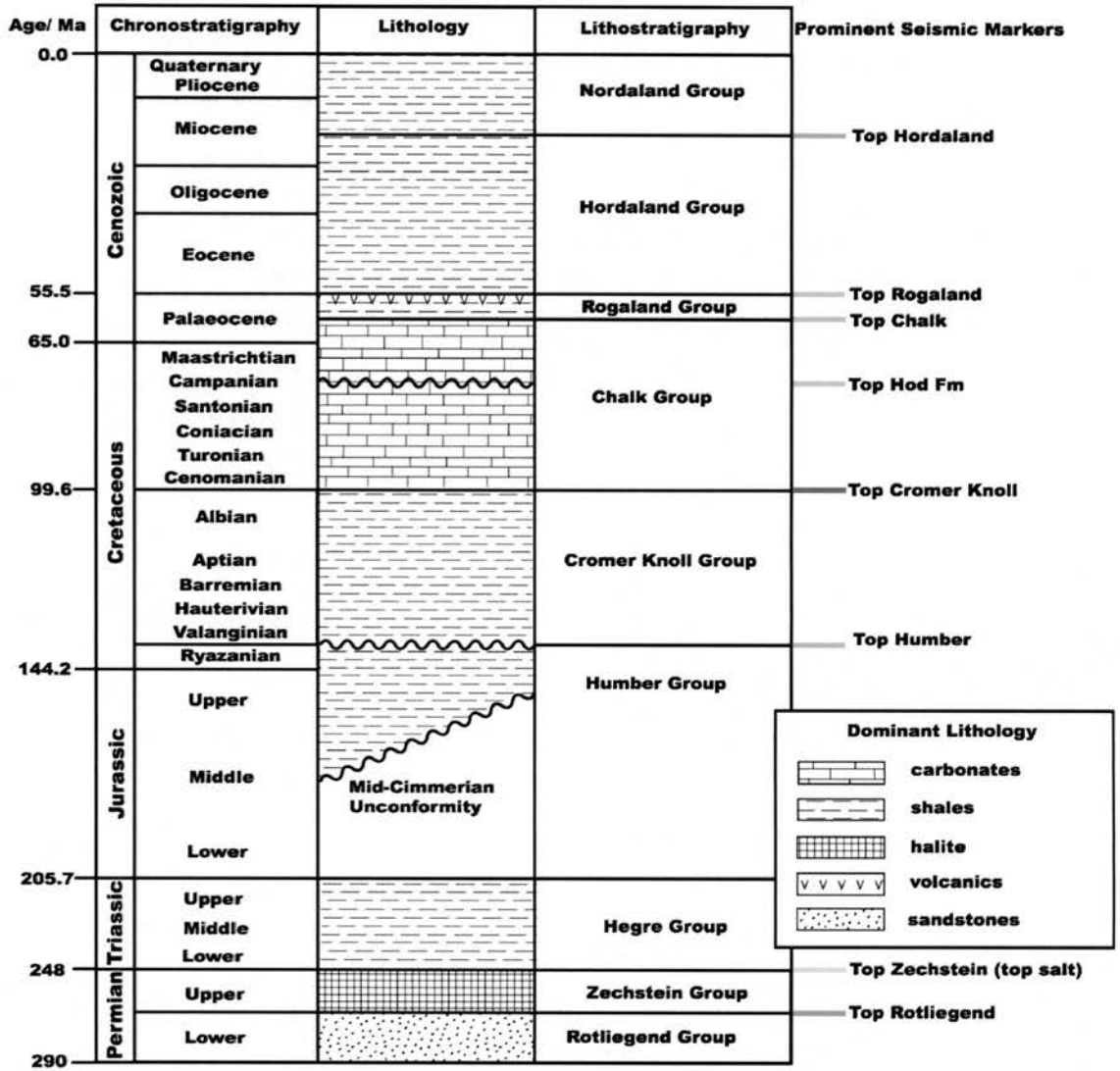

Figure 3.2: Generalised stratigraphic column for sediments of the Norwegian Central Trough *(after Erratt et al., 1999)*

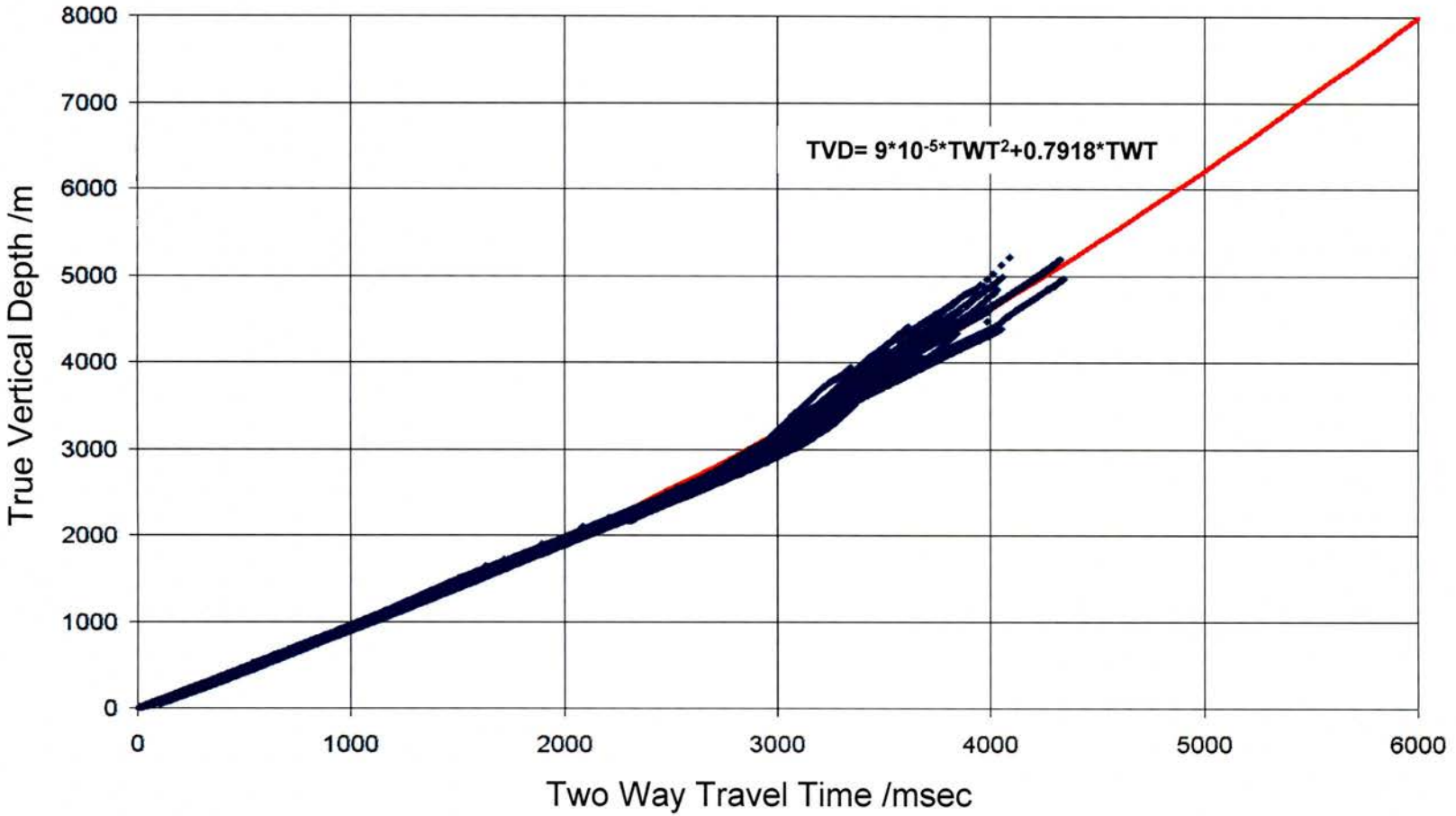

Figure 3.3: Time-Depth data for 43 wells in the Norwegian Central Trough (blue). The well data extend to ~4300 msec (5200m) but have been extrapolated to 6000 msec for depth conversion. See text for discussion.

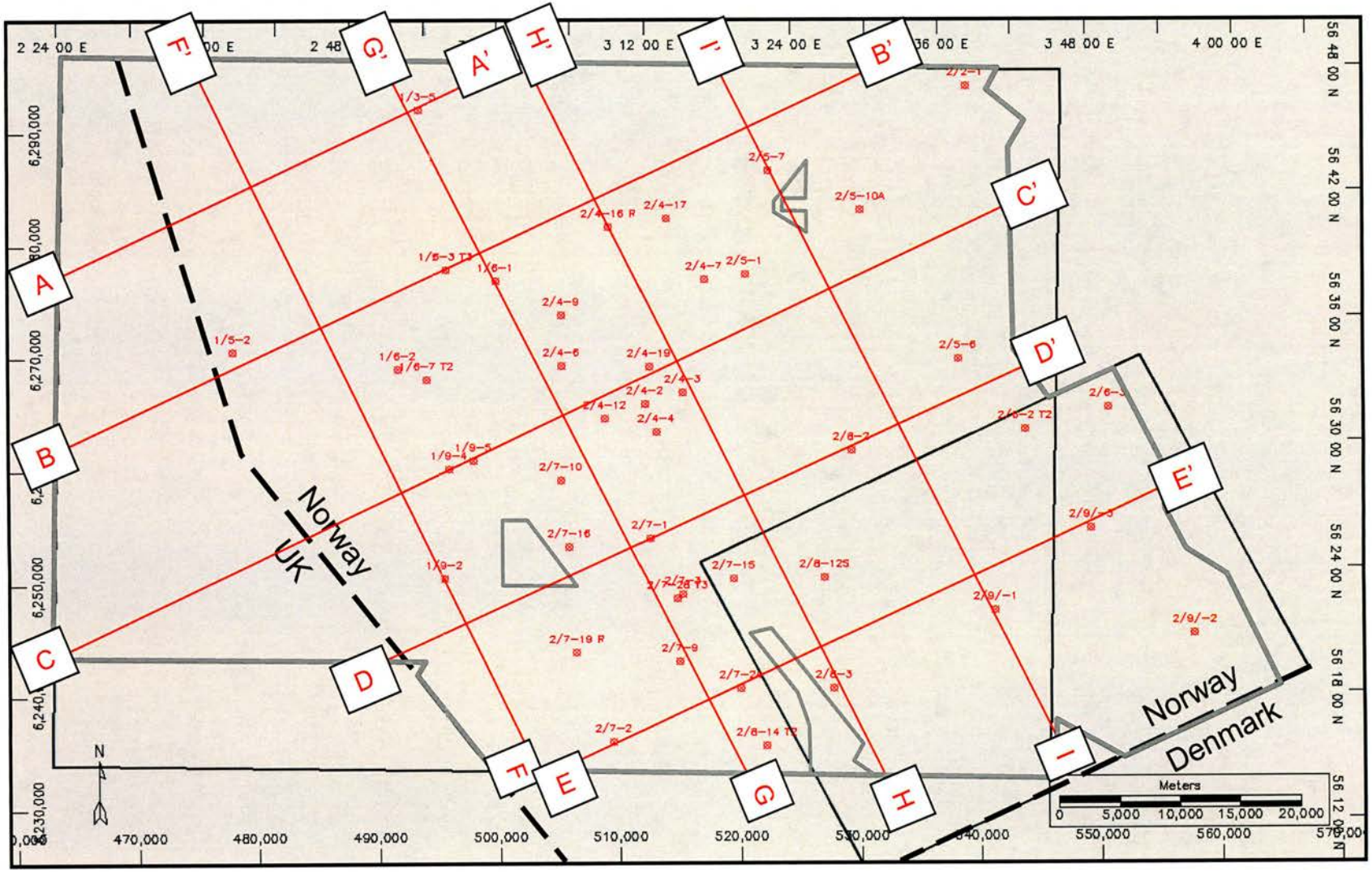

Figure 4.1: Key to sections displayed in chapter 4

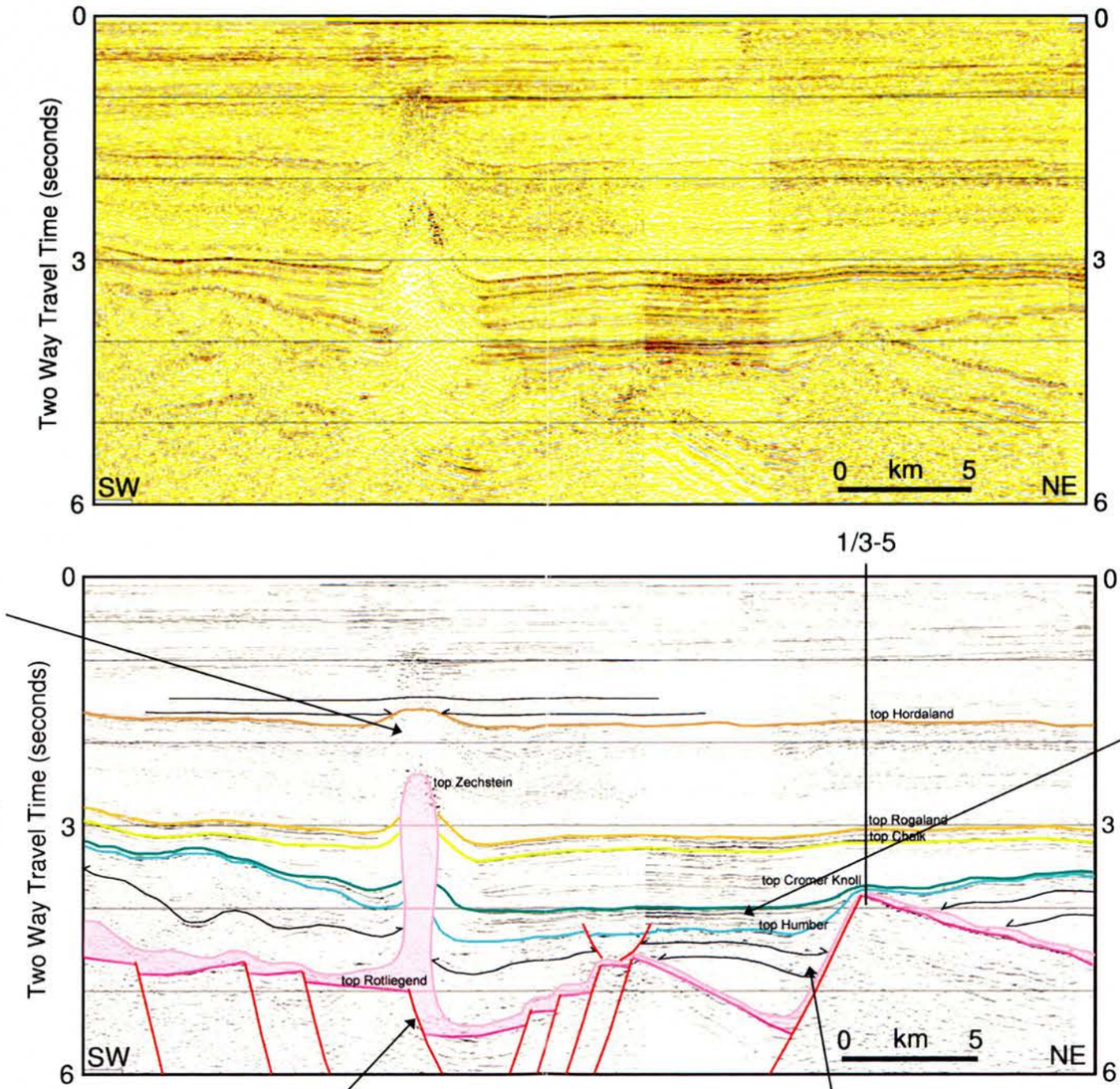

Relief over crest of Zechstein salt diapir may be attributed to: either salt uplift (e.g. due to Cenozoic compressional squeezing); to differential compaction effects; or to both processes. The contribution from differential compaction has been modelled in Ch5 (see figure 5.2).

There is a thick lid of locally elevated strata above the diapir, capped by pronounced onlap onto the top Hordaland surface, rather than a gradual upward reduction in fold amplitude. There is also the suggestion of thinning in the neck of the salt diapir, with upward-rotated onlaps of adjacent sediments. These observations suggest Cenozoic compressional squeezing has occurred (see figure 2.18).

Reflections above top Humber are less asymmetric. They are typically concordant and indicative of passive infill not a thermally subsiding basin.

Figure 4.2a: Seismic cross section A-A'. Vertical scale is in TWTT but approximates to a two times vertical exaggeration.

The Zechstein diapir (Breiflabb South) is situated above a sub-salt extensional fault. From this single line interpretation it is not possible to determine whether the diapir's location is controlled by this fault, nor the extent to which the interpreted fault offset is real as opposed to being an artefact of velocity differences between the salt and non-salt layers. 3D interpretation has enabled the fault-salt relationship to be examined more thoroughly (see section 4.3.3 for discussion).

Asymmetric infill between top Zechstein and top Humber, with sediment thickness in the hangingwall increasing towards the fault. This is a syn-rift geometry that dates extensional growth on the fault to the post-Zechstein, pre-Cromer Knoll (i.e. Triassic and Jurassic) interval.

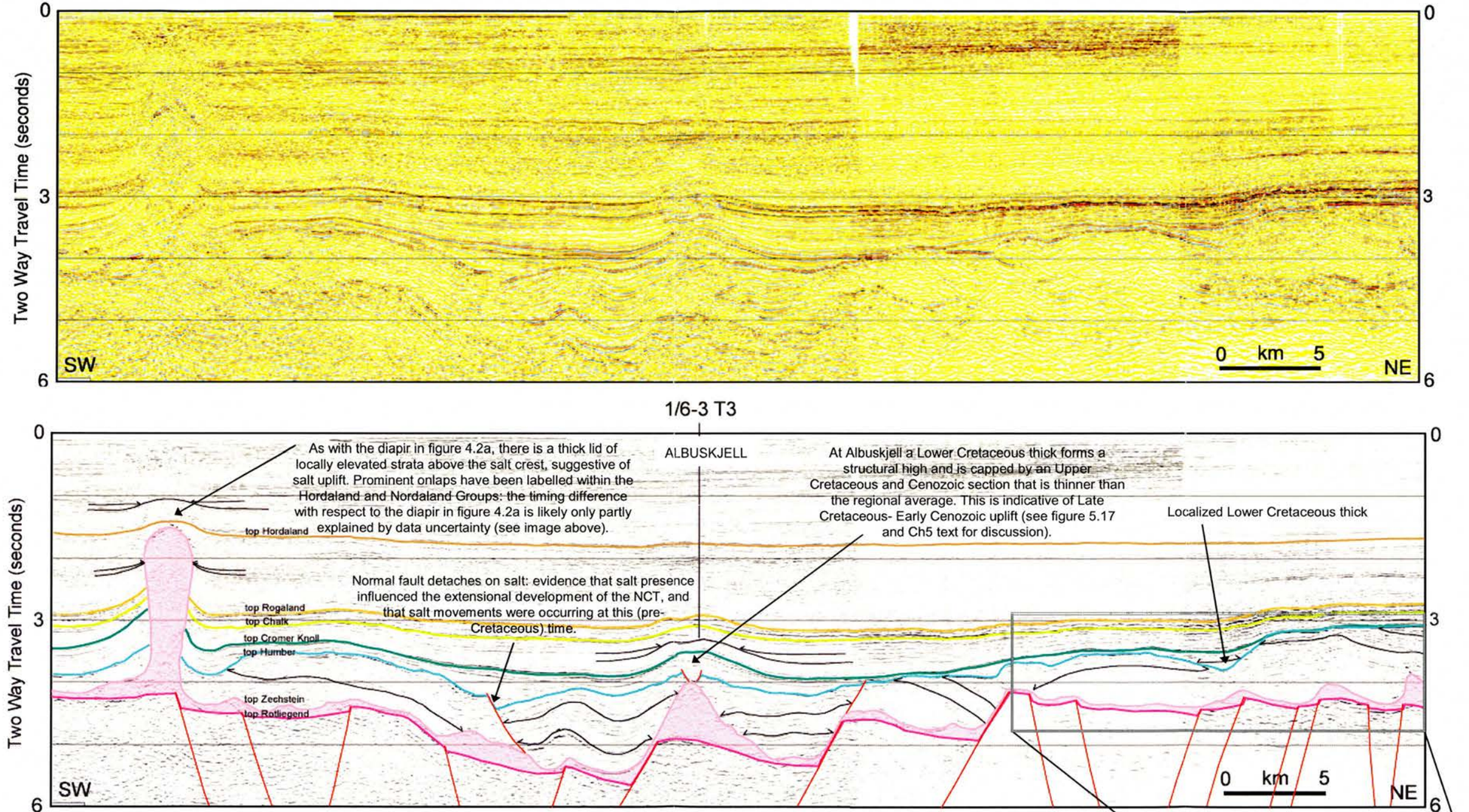

Figure 4.2b: Seismic cross section B-B'. The localized Lower Cretaceous thick on the NE part of the section (labelled) is attributed to the collapse of a salt wall dividing two Triassic minibasins, creating accommodation space at this time (see also figure 2.12).

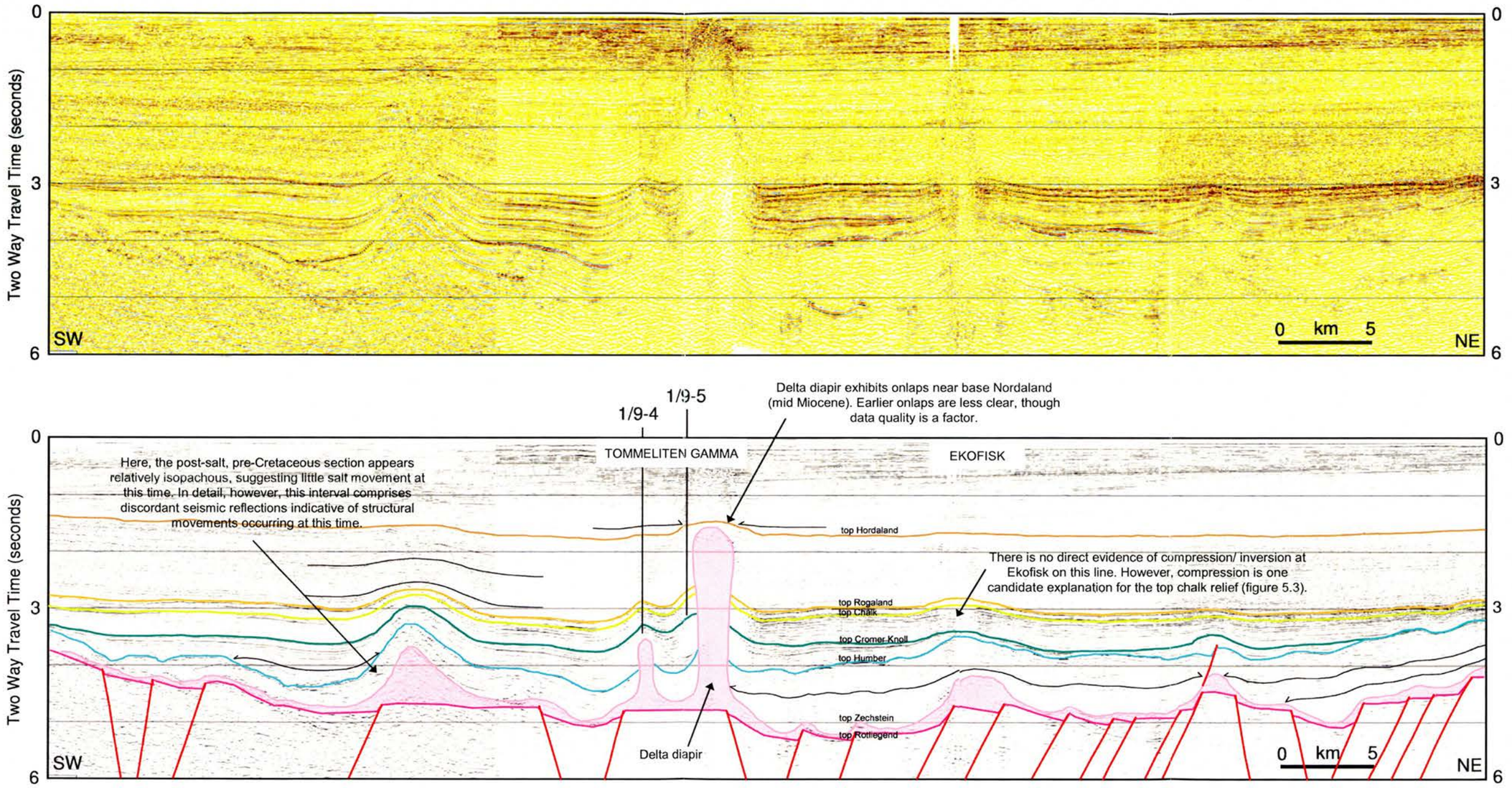

Figure 4.2c: Seismic cross section C-C'. Tommeliten Gamma and Ekofisk labels mark the locations of Chalk Group oil (and gas) fields.

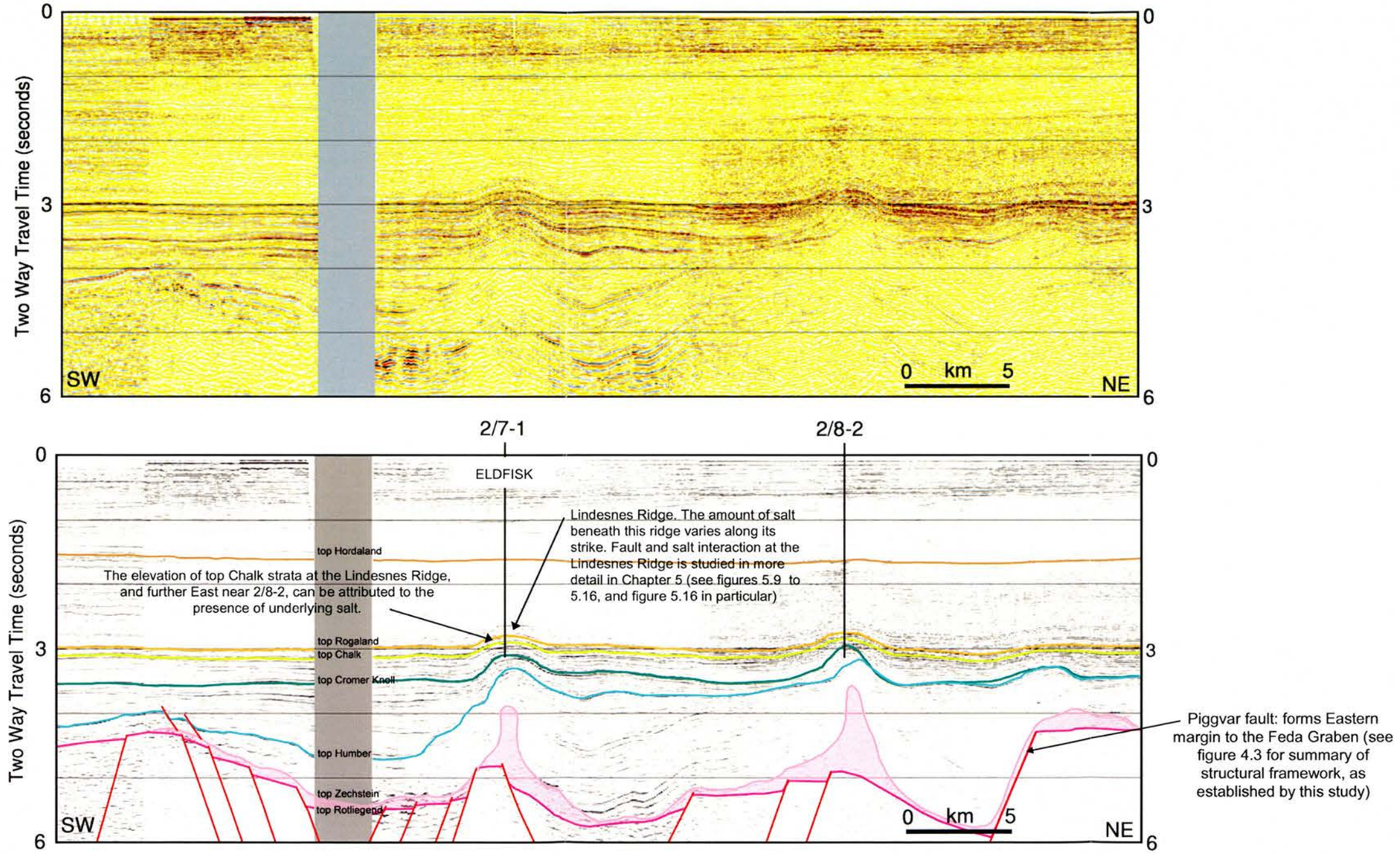

Figure 4.2d: Seismic cross section D-D'.

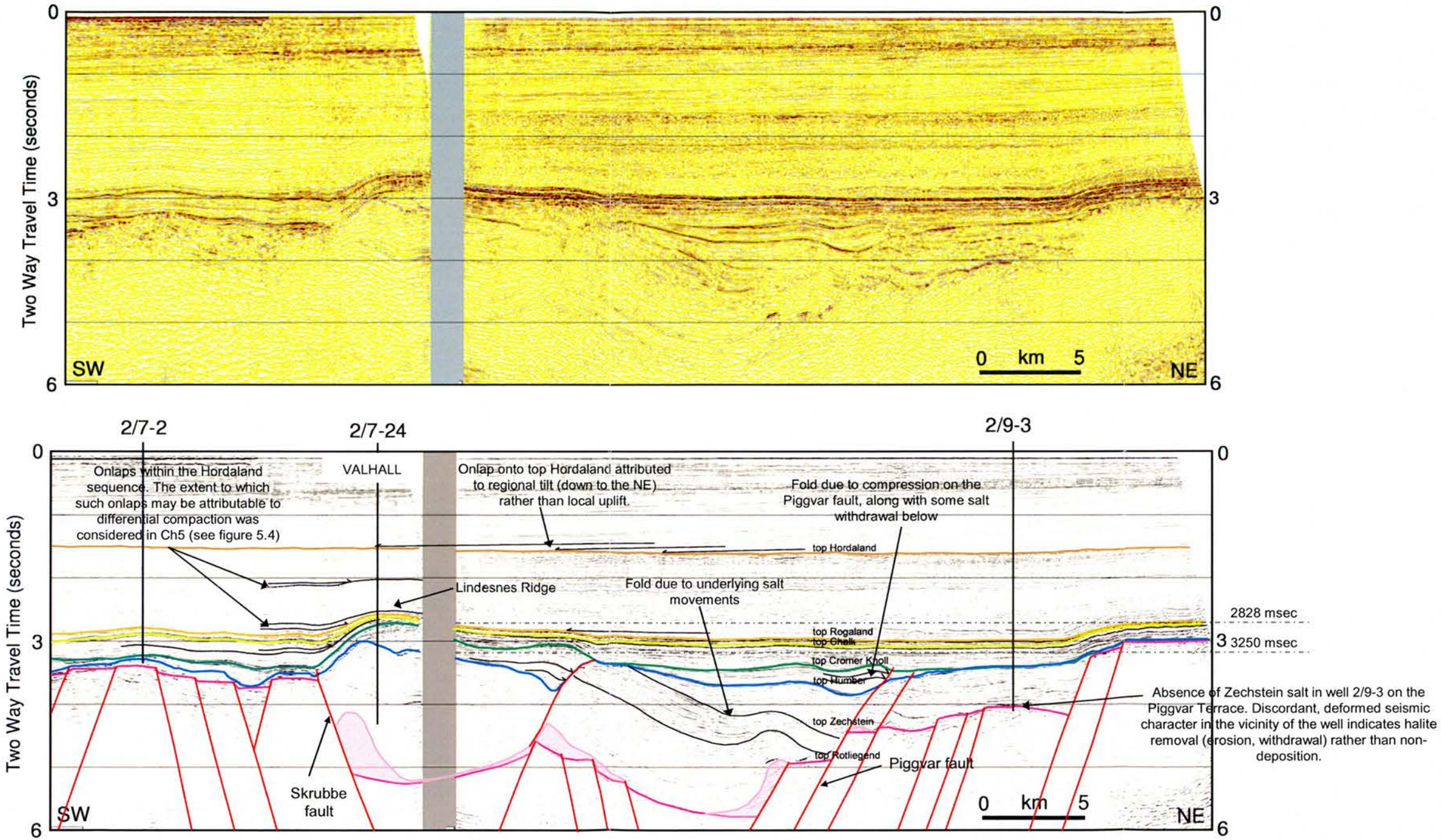

Figure 4.2e: Seismic cross section E-E'. Shows the location of two timeslices through the ga3d93 survey posted in figure 2.16

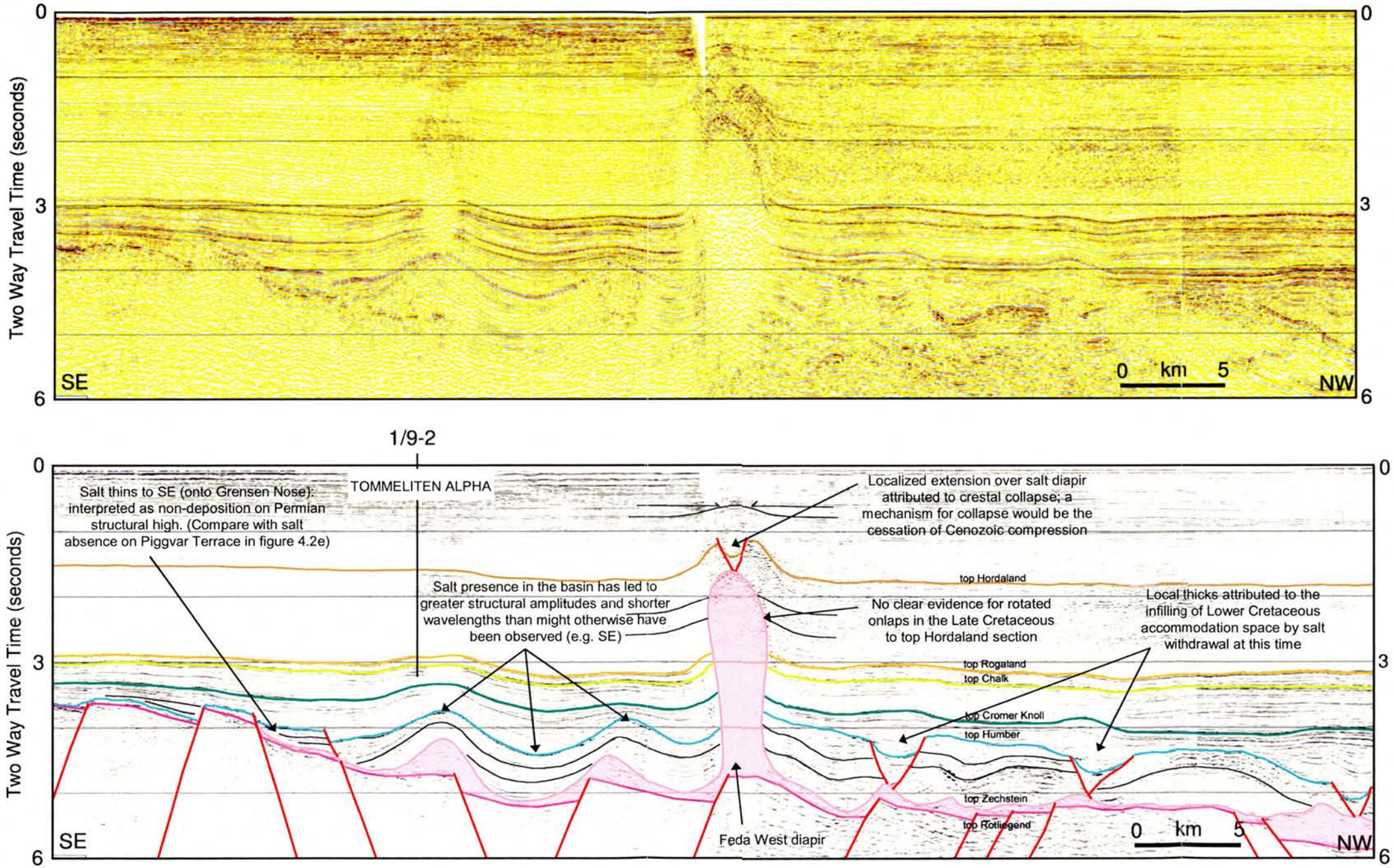

Figure 4.2f: Seismic cross section F-F'

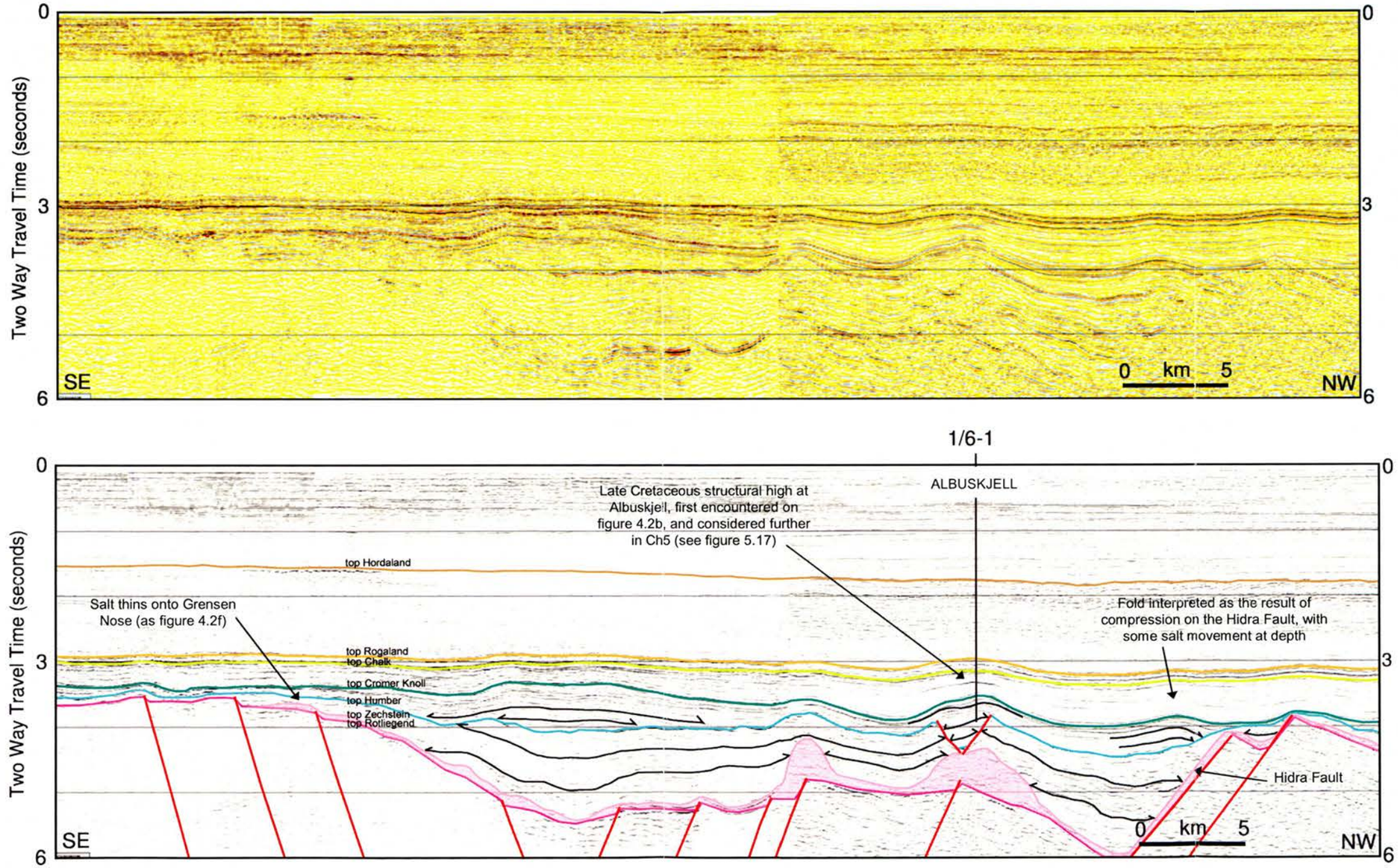

Figure 4.2g: Seismic cross section G-G'

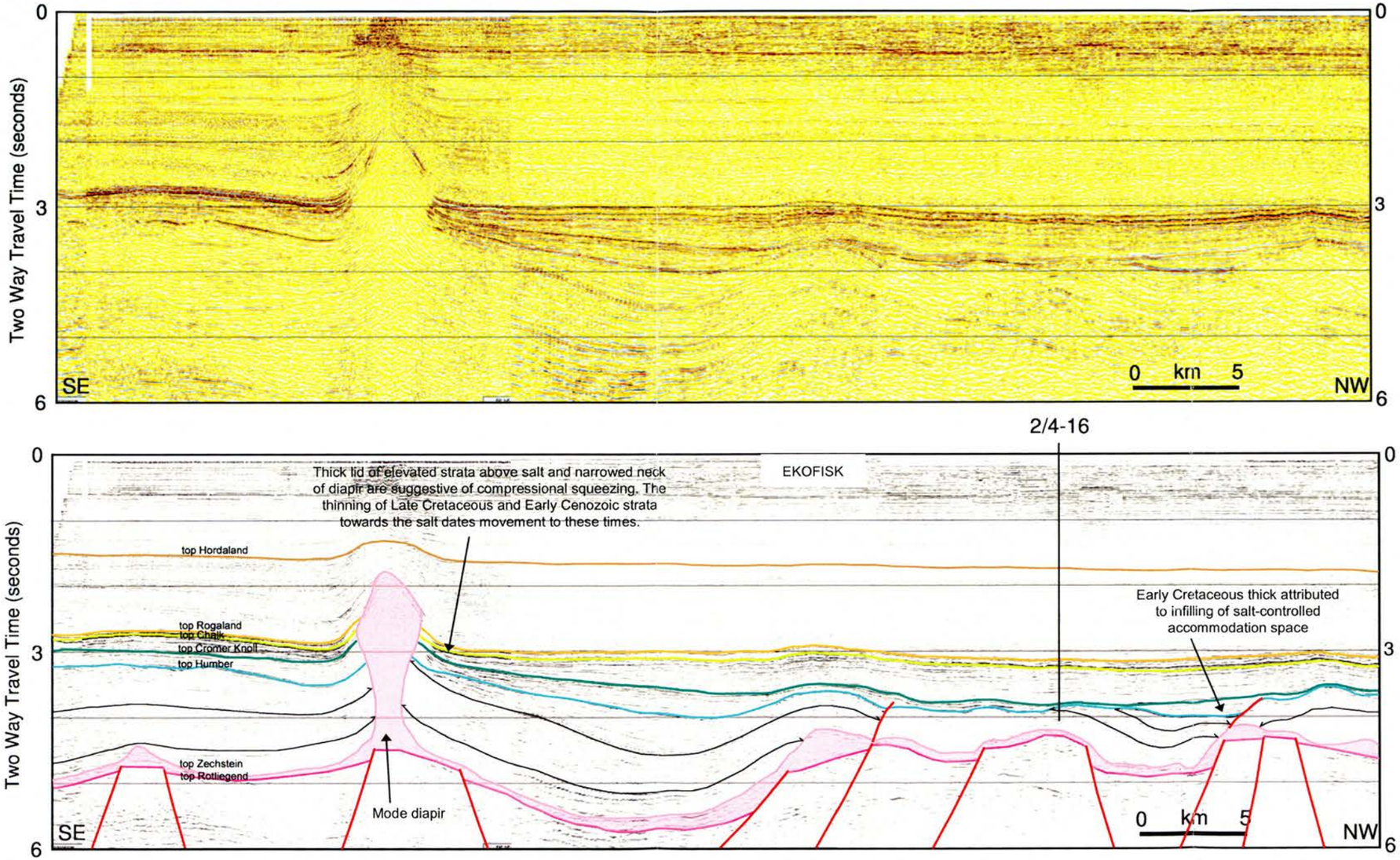

Figure 4.2h: Seismic cross section H-H'

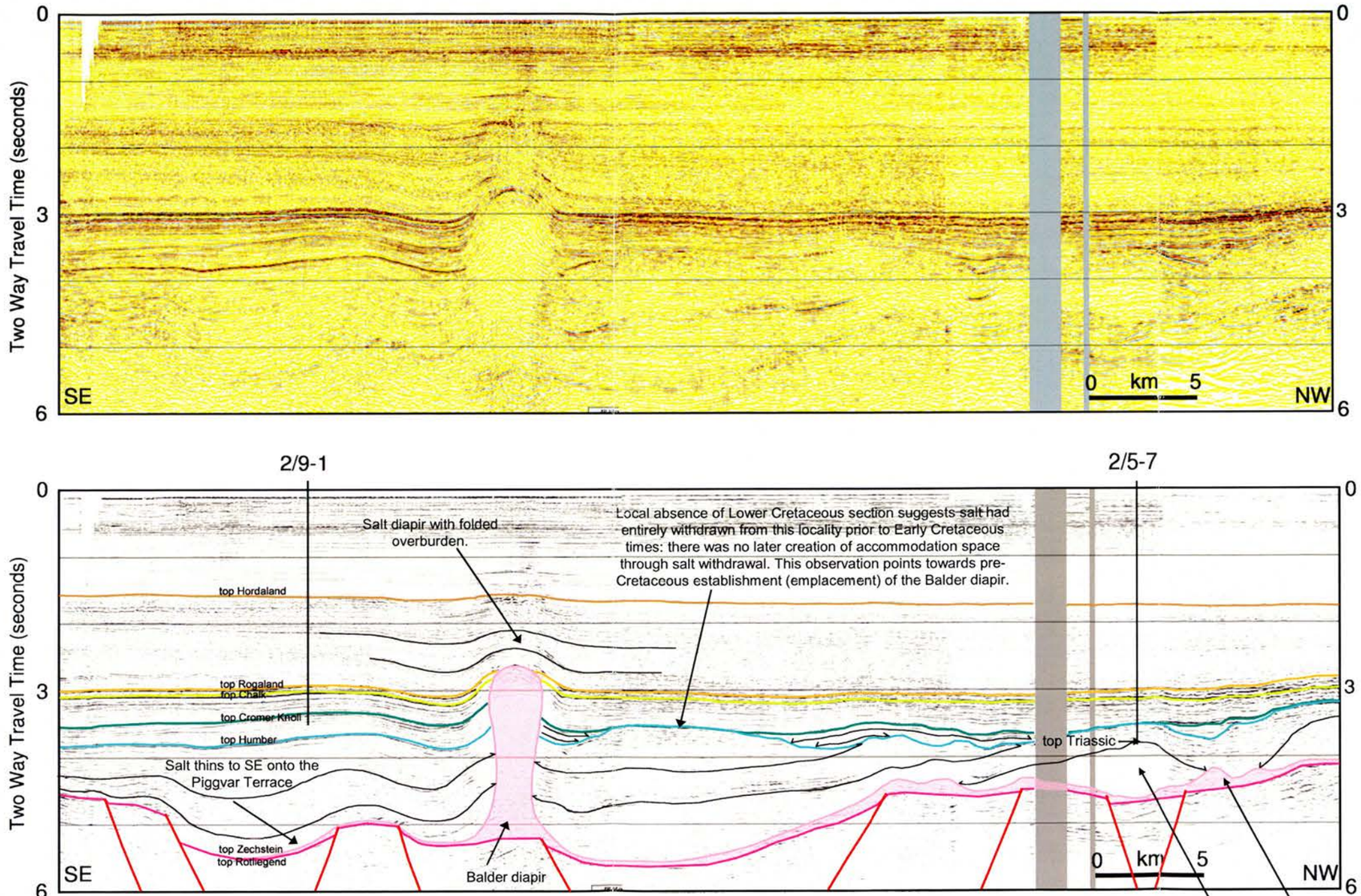

Figure 4.2i: Seismic cross section I-I'

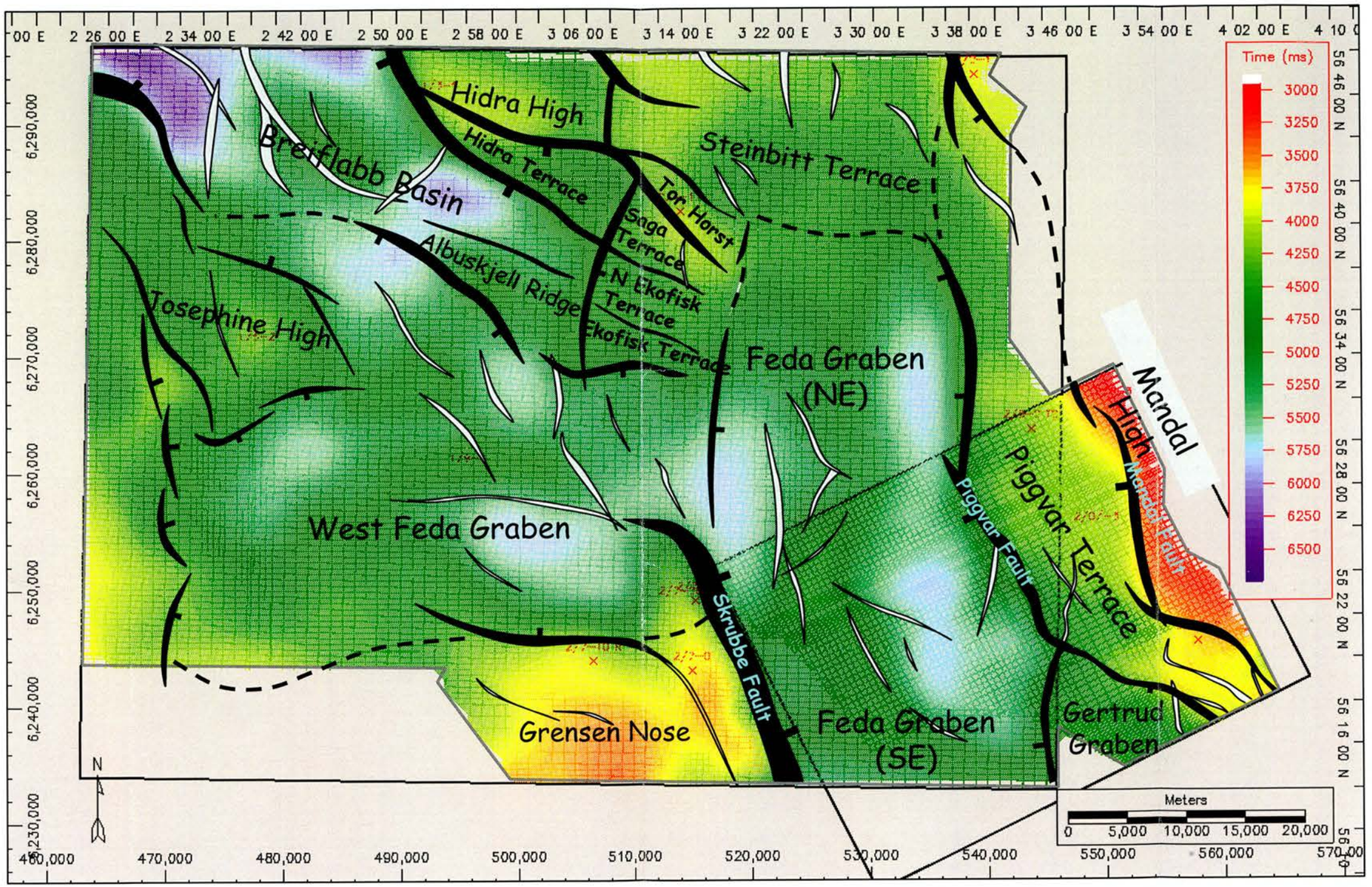

Figure 4.3: Top Rotliegend Group TWTT horizon map. The top Rotliegend surface is offset by faults, as shown. The basin depocentre is laterally restricted in the SE, where it is bounded by the large offset NNW-SSE trending Skrubbe, Piggvar and Mandal faults. Elsewhere in the Norwegian Central Trough fault throws are much less and fault orientations more variable.

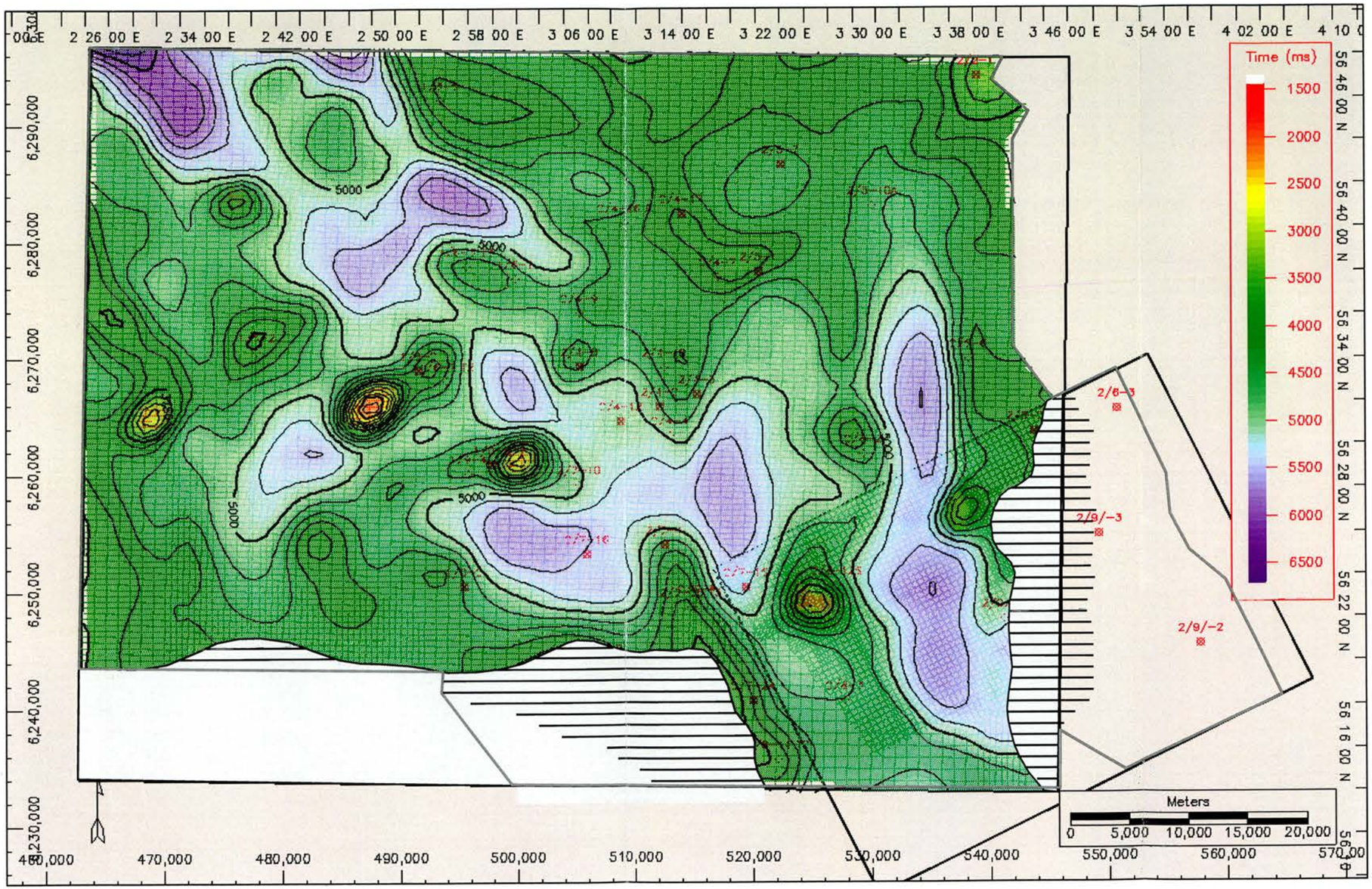

Figure 4.4: Top Zechstein Group TWTT horizon map (150ms contour interval). Line shading highlights areas of non-deposition and halite removal (erosion, dissolution).

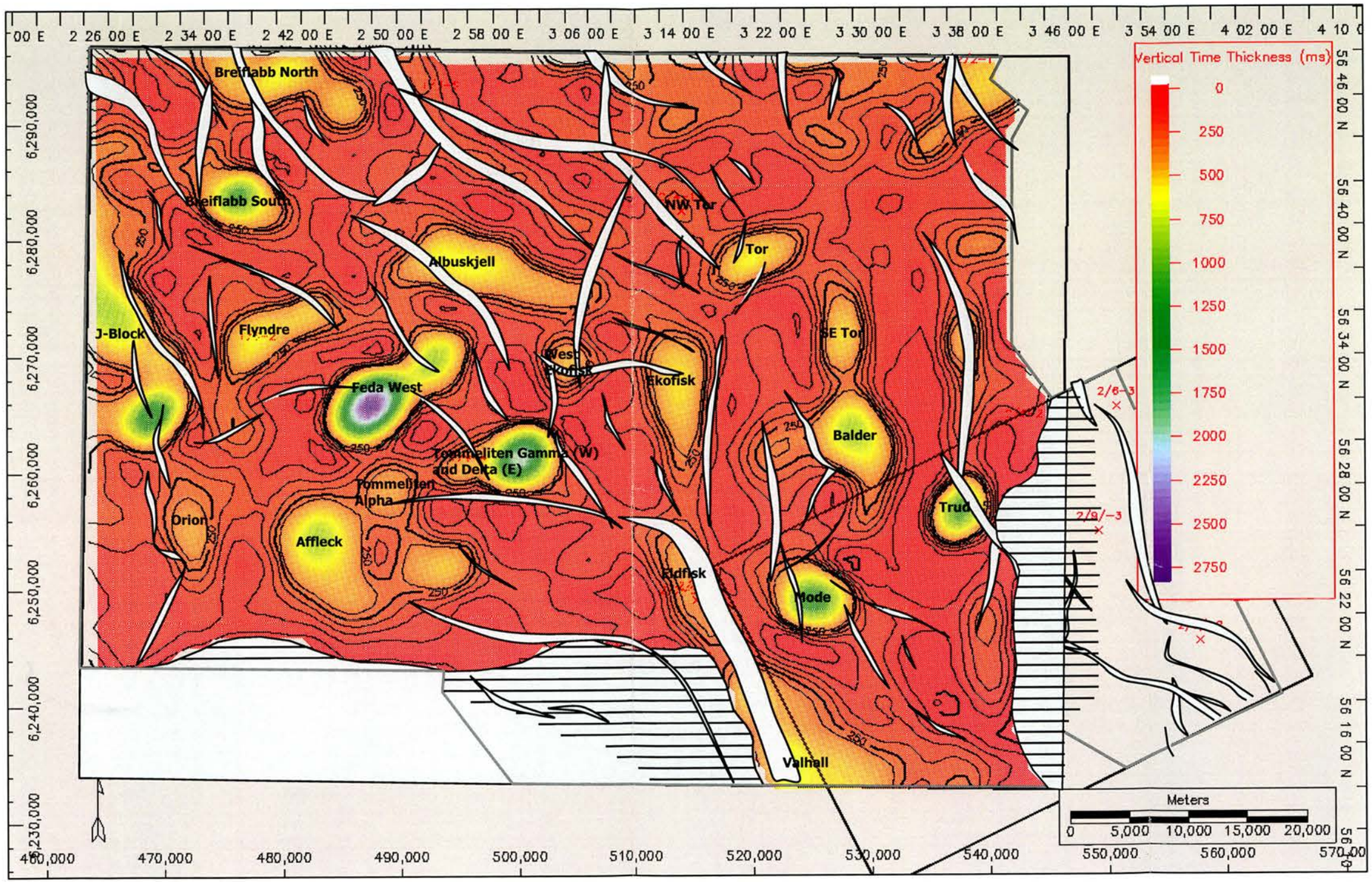

Figure 4.5: Top Rotliegend to Top Zechstein (Zechstein Group) isochron map (50ms contour interval, truncated at 300ms). The location of wells that penetrate Zechstein and/or Rotliegend is shown. This map illustrates the location of named Zechstein Group thicks (salt walls and salt diapirs) relative to structure at Top Rotliegend level. Line shading highlights areas of non-deposition and halite removal (erosion, dissolution).

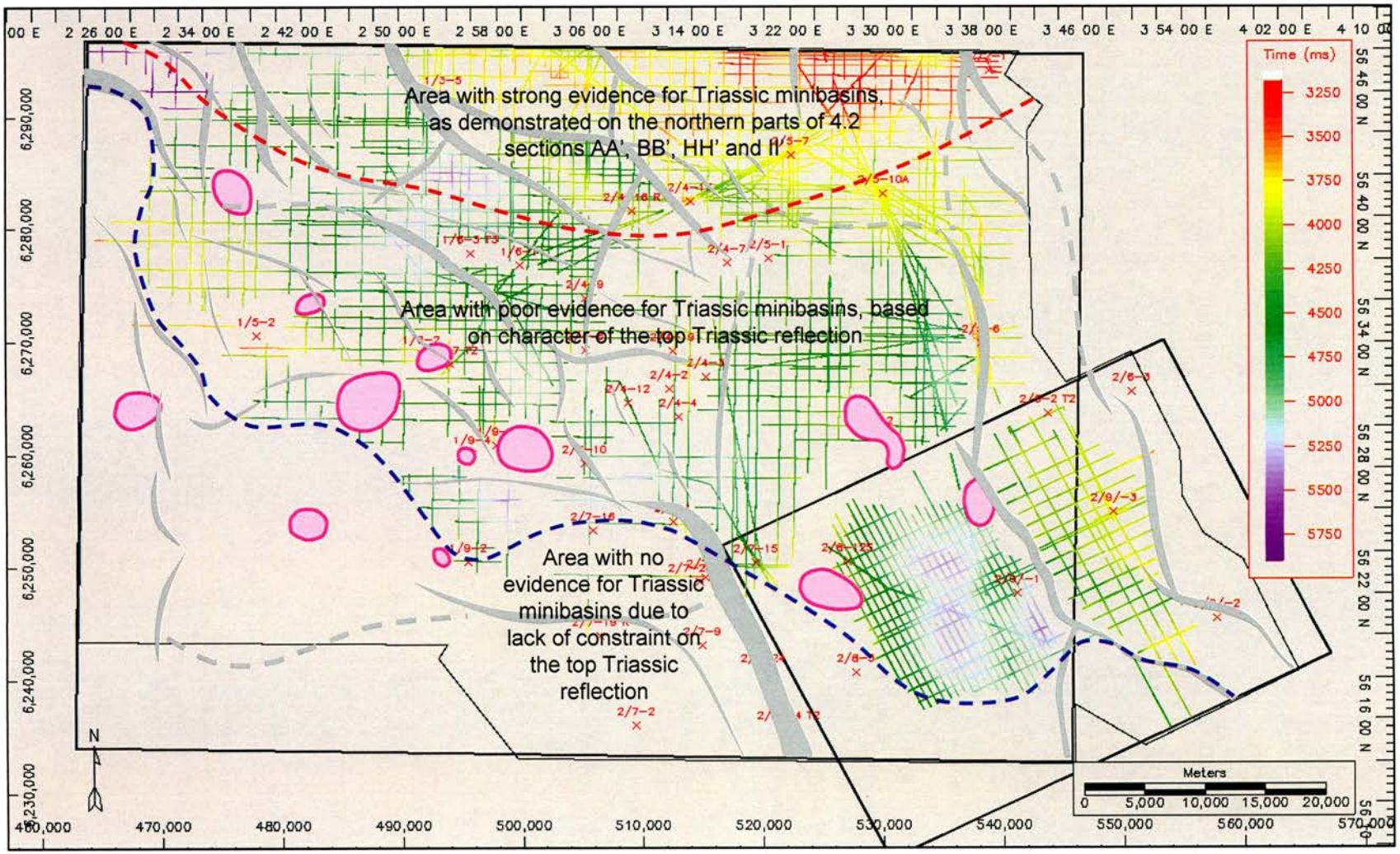

Figure 4.6: Top Triassic (Tr50) TWTT interpretations across the study area. More complete interpretation including surface contouring was not possible due to the difficulty of tracing this seismic reflection away from Tr50 well pick locations. Dashed red line divides northern area with strong evidence for Triassic salt movements from southern area, where this evidence is less clear. Pink blobs are salt structures that pierce the top Humber surface.

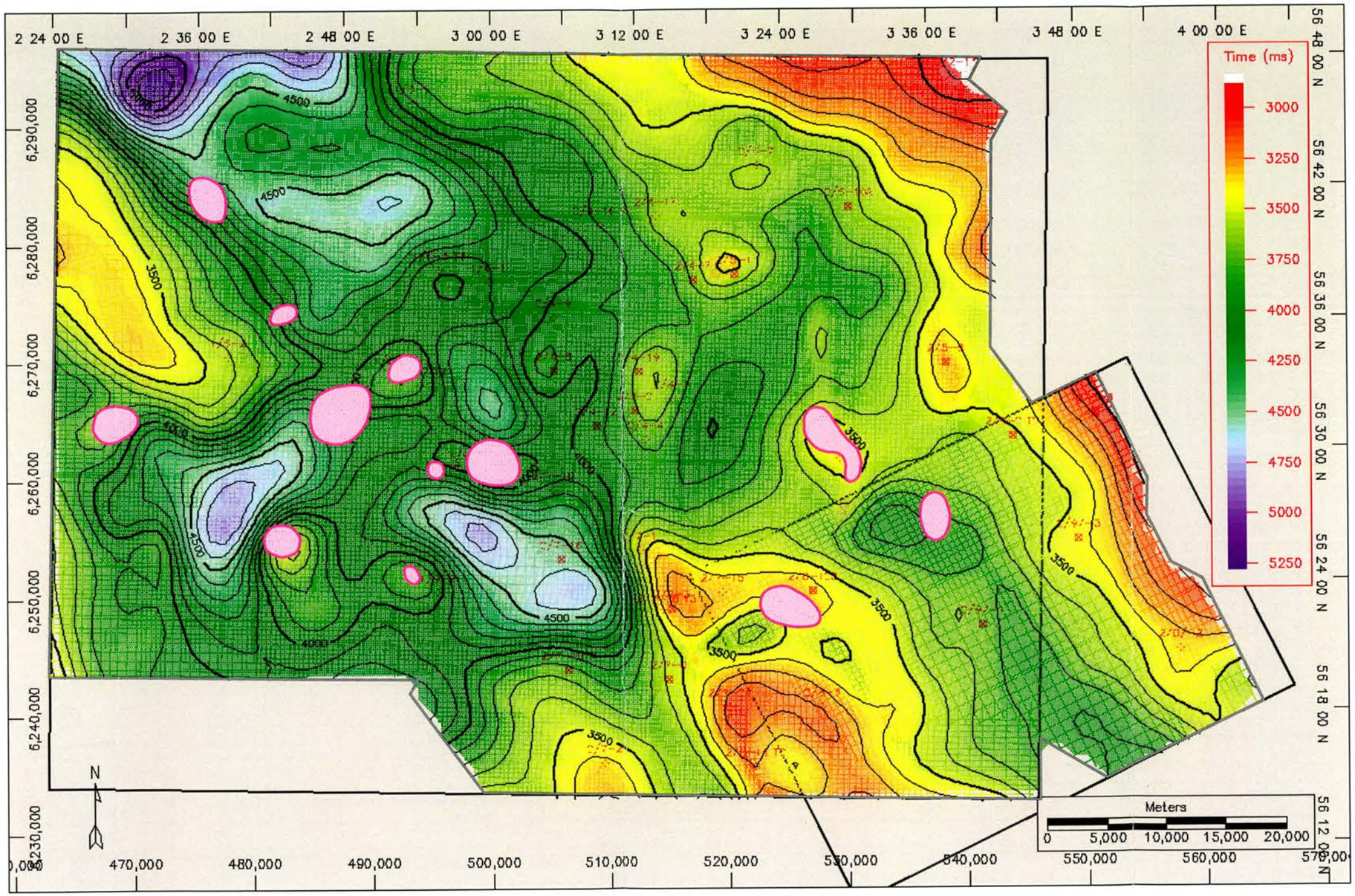

Figure 4.7: Top Humber Group TWTT horizon map (50ms contour interval). Pink blobs are salt structures that pierce the top Humber surface.

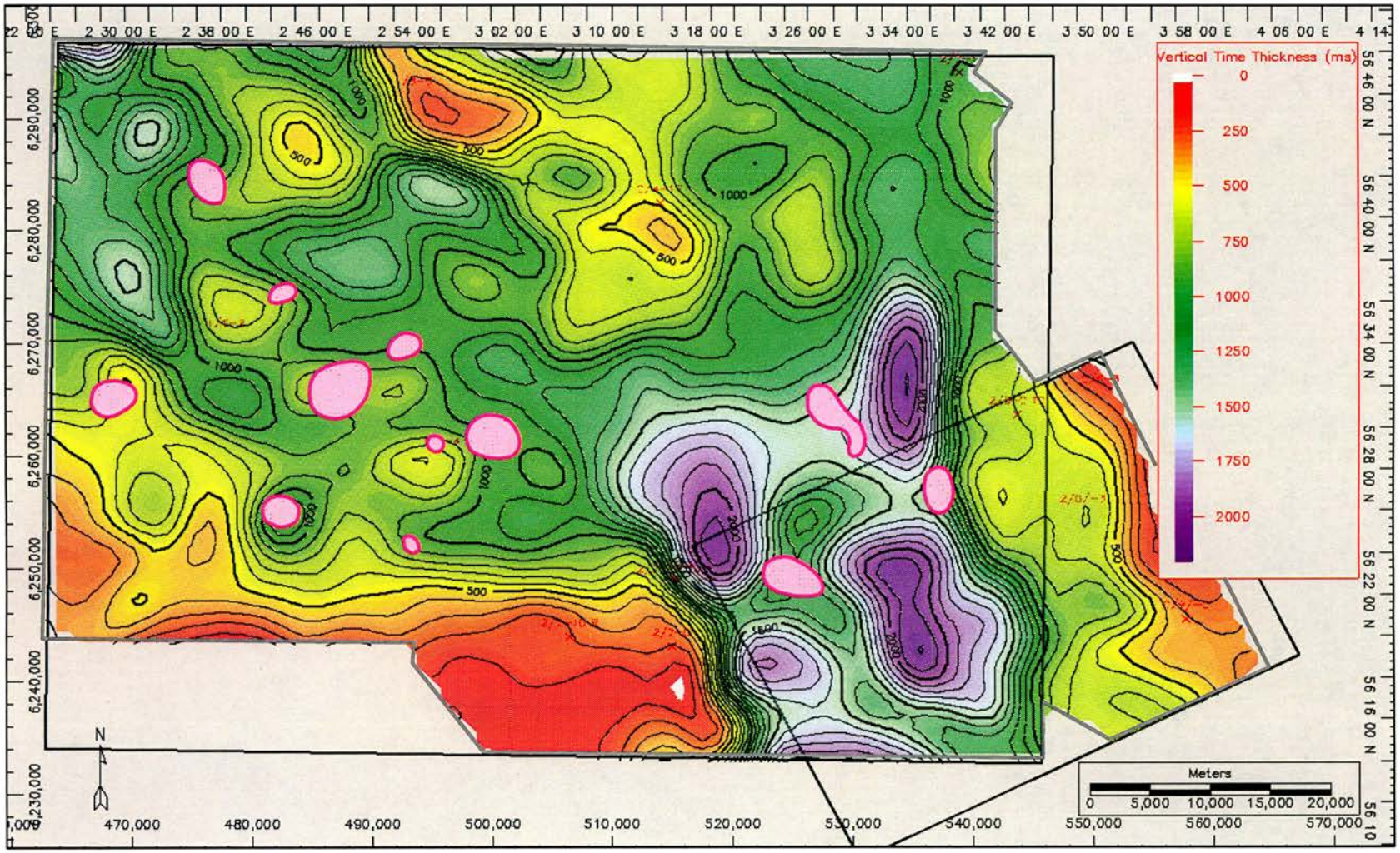

Figure 4.8: Top Zechstein to Top Humber (Hegre and Humber Groups) isochron map. Top Humber salt piercements (pink) are superimposed; the Triassic-Jurassic time thickness in these areas is zero.

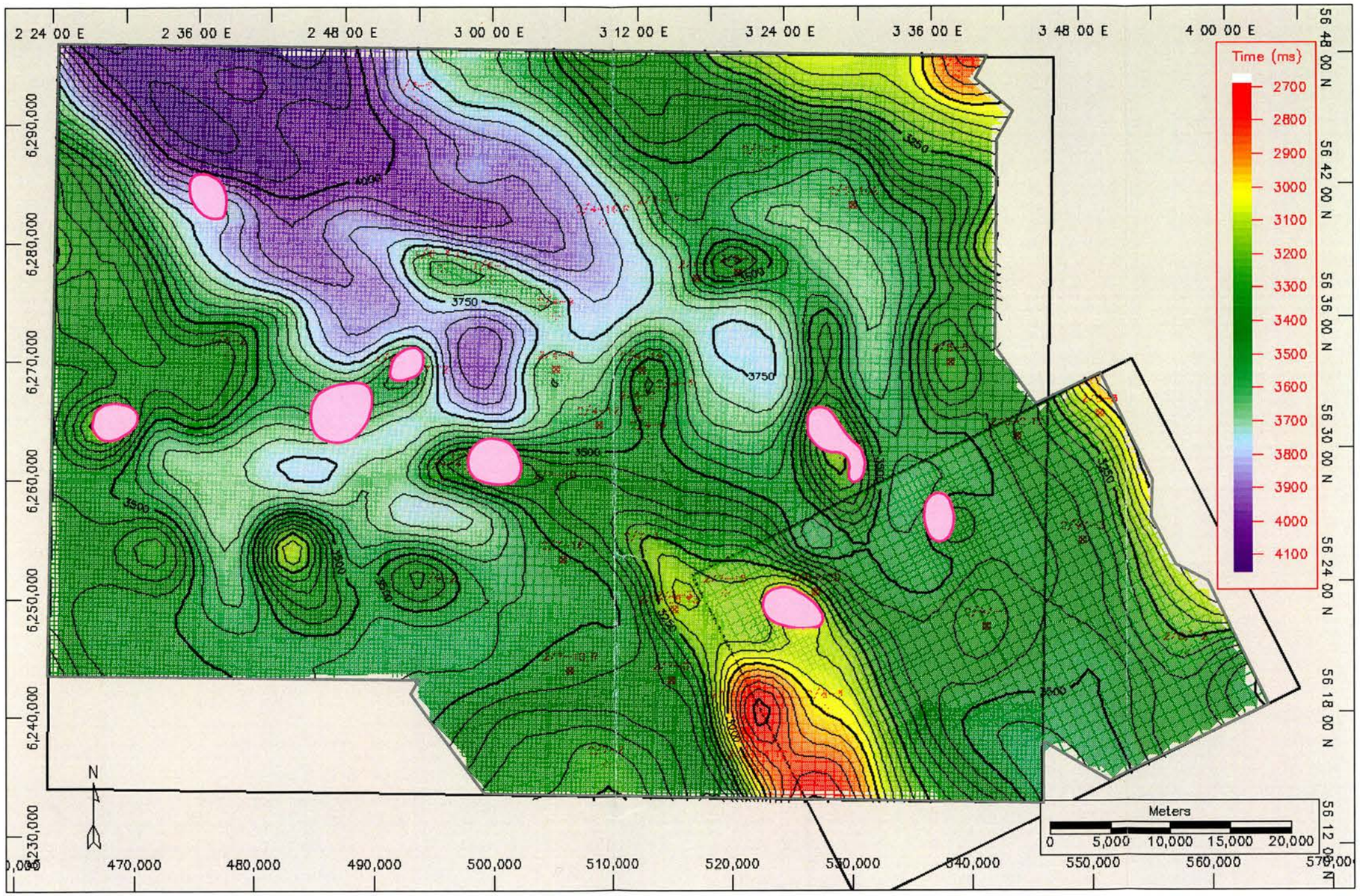

Figure 4.9: Top Cromer Knoll Group TWTT horizon map (50ms contour interval). Pink blobs are salt structures that pierce the top Cromer Knoll surface.

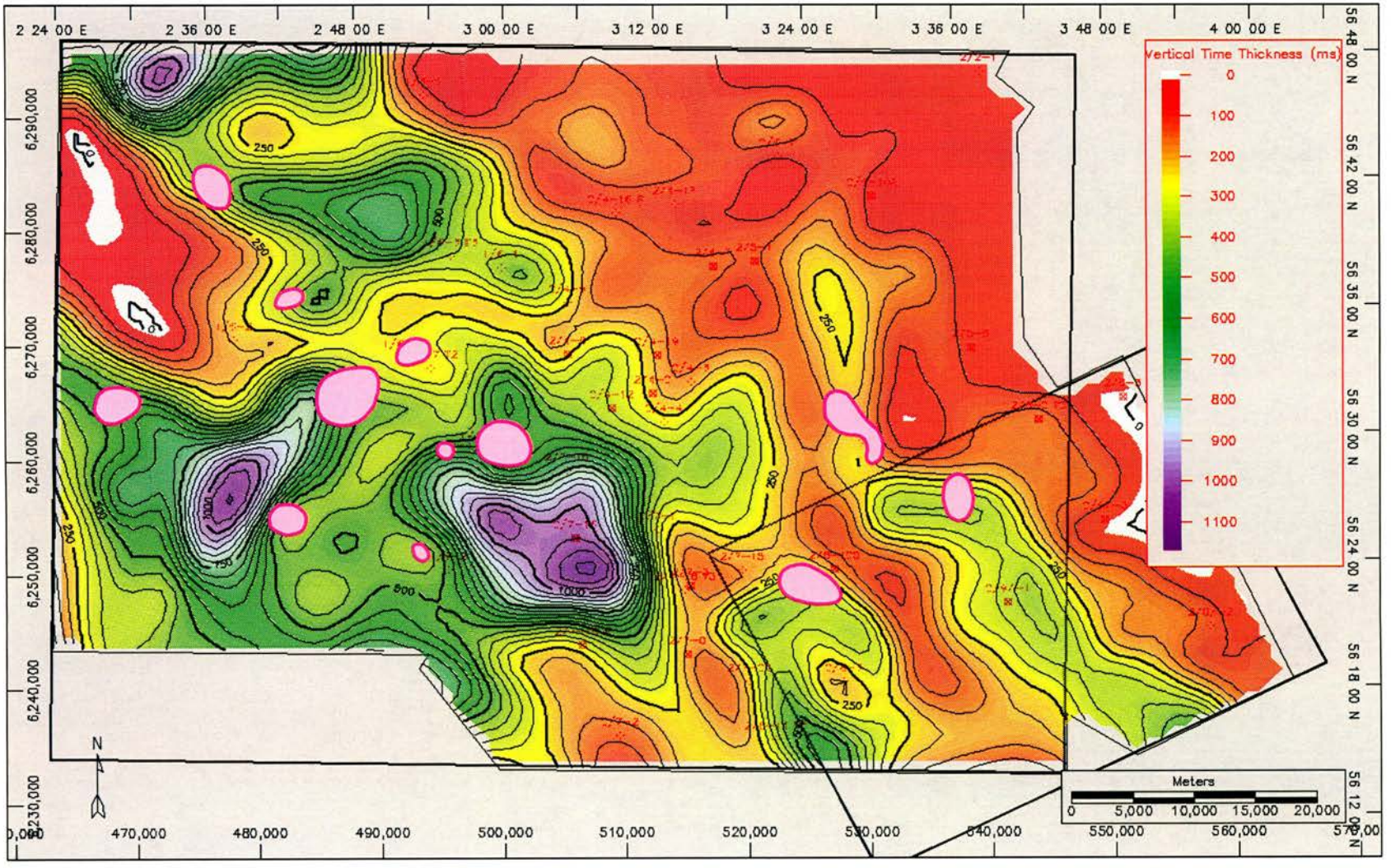

Figure 4.10: Top Humber to Top Cromer Knoll (Cromer Knoll Group) isochron map. Salt piercements are shaded pink.

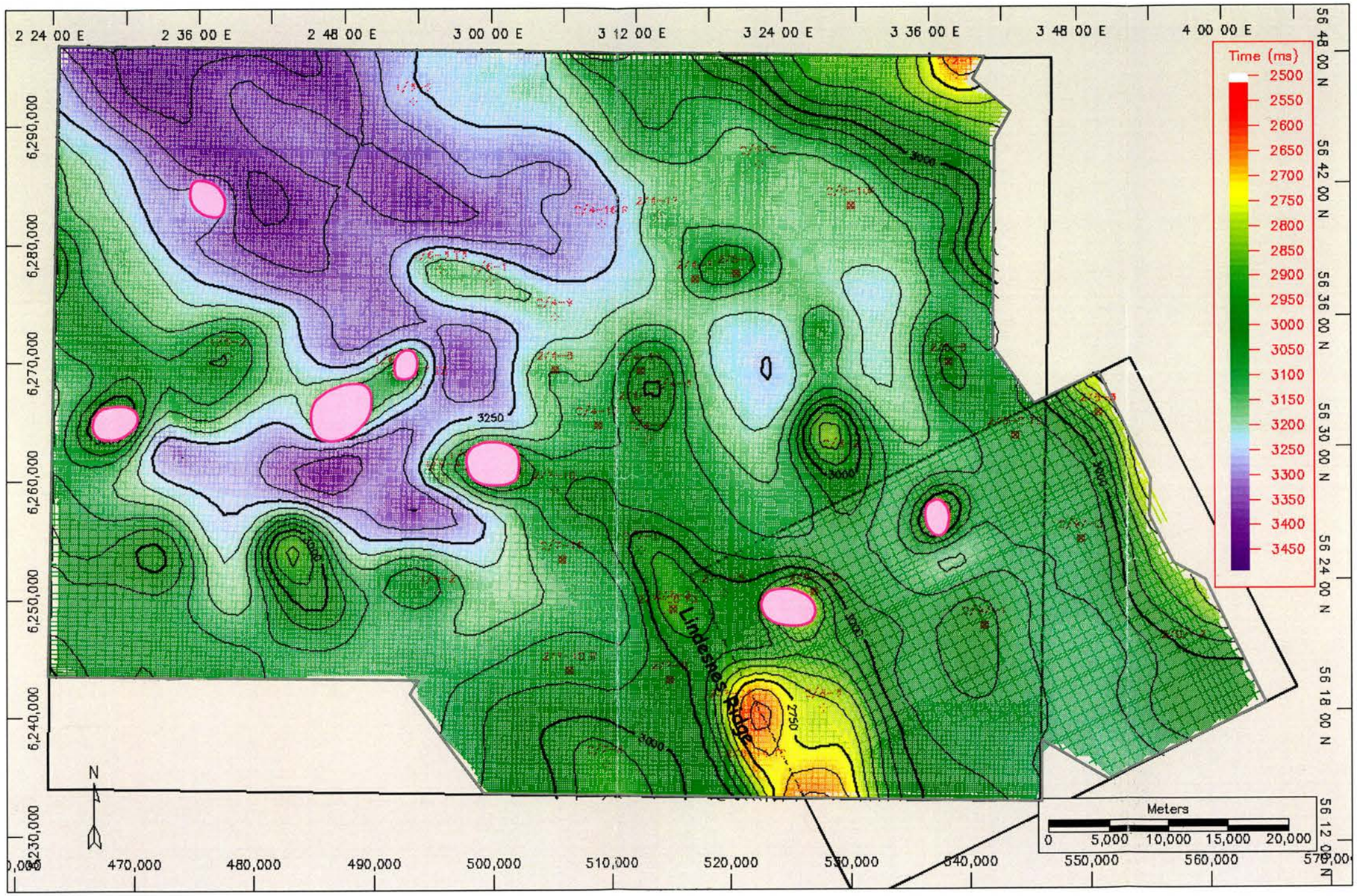

Figure 4.11: Top Chalk Group TWTT horizon map (50ms contour interval). Pink blobs are salt structures that pierce the top Chalk surface.

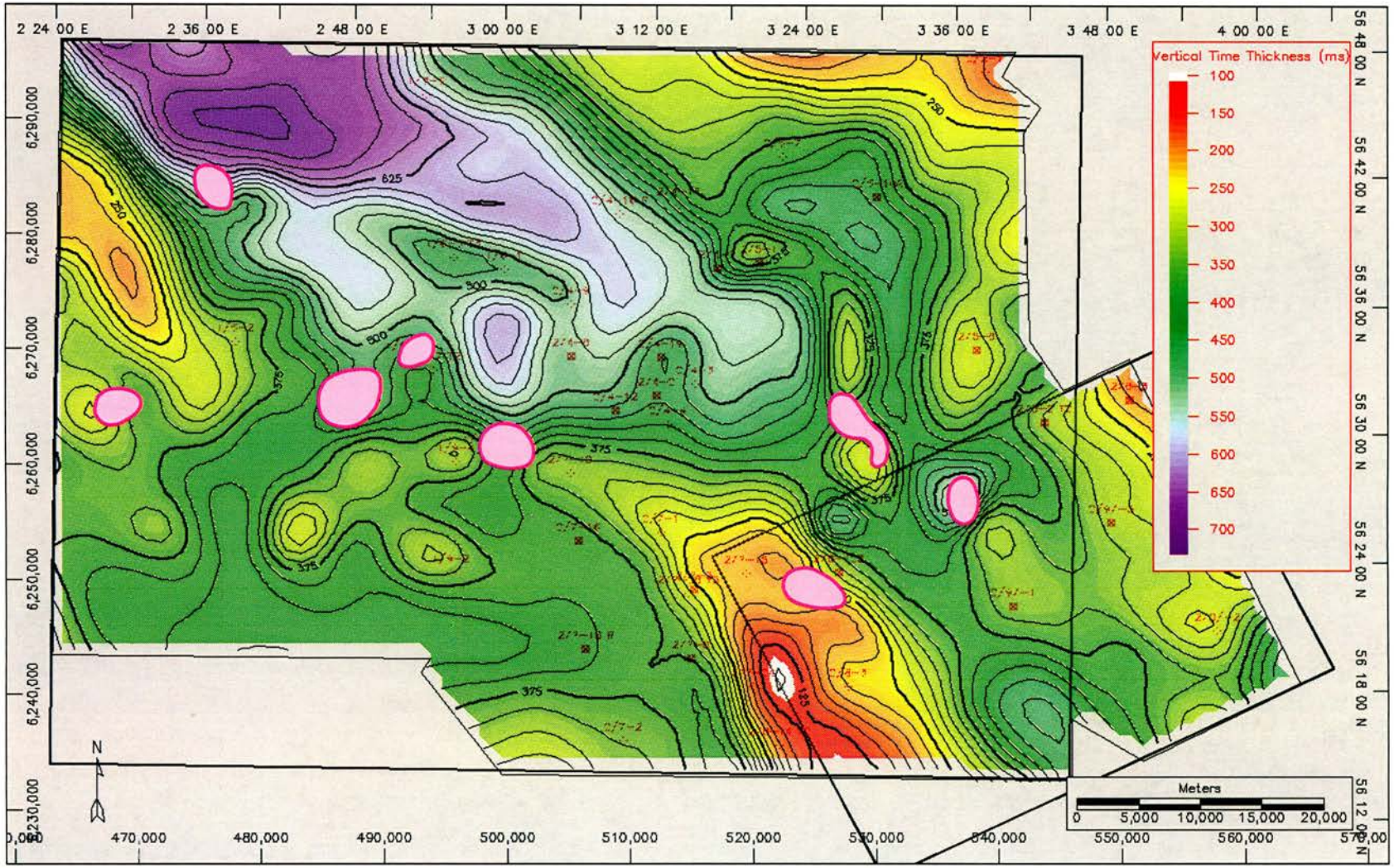

Figure 4.12: Top Cromer Knoll to Top Chalk (Chalk Group) isochron map. Salt piercements are shaded pink.

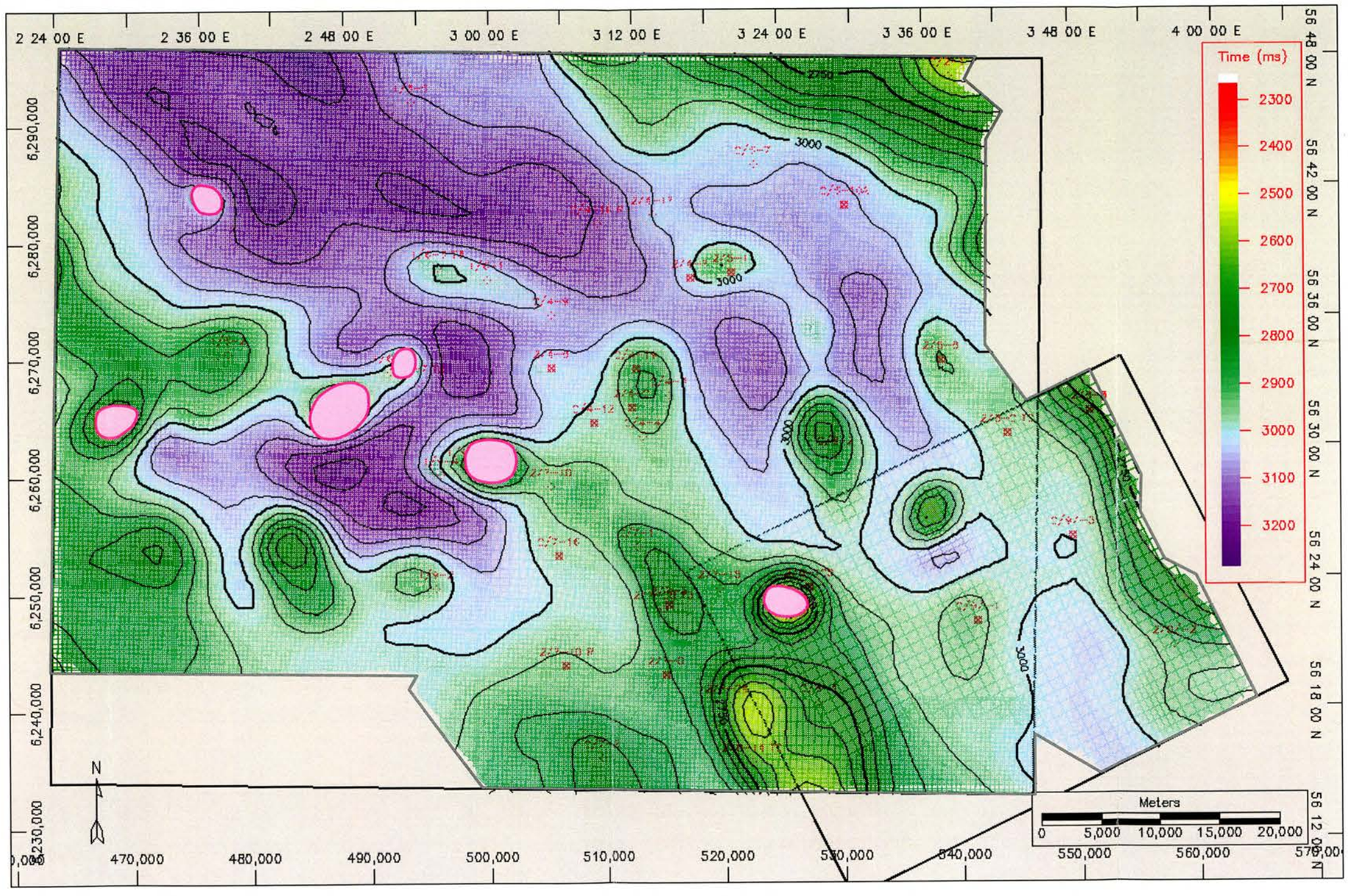

Figure 4.13: Top Rogaland Group TWTT horizon map (50ms contour interval). Pink blobs are salt structures that pierce the top Rogaland surface.

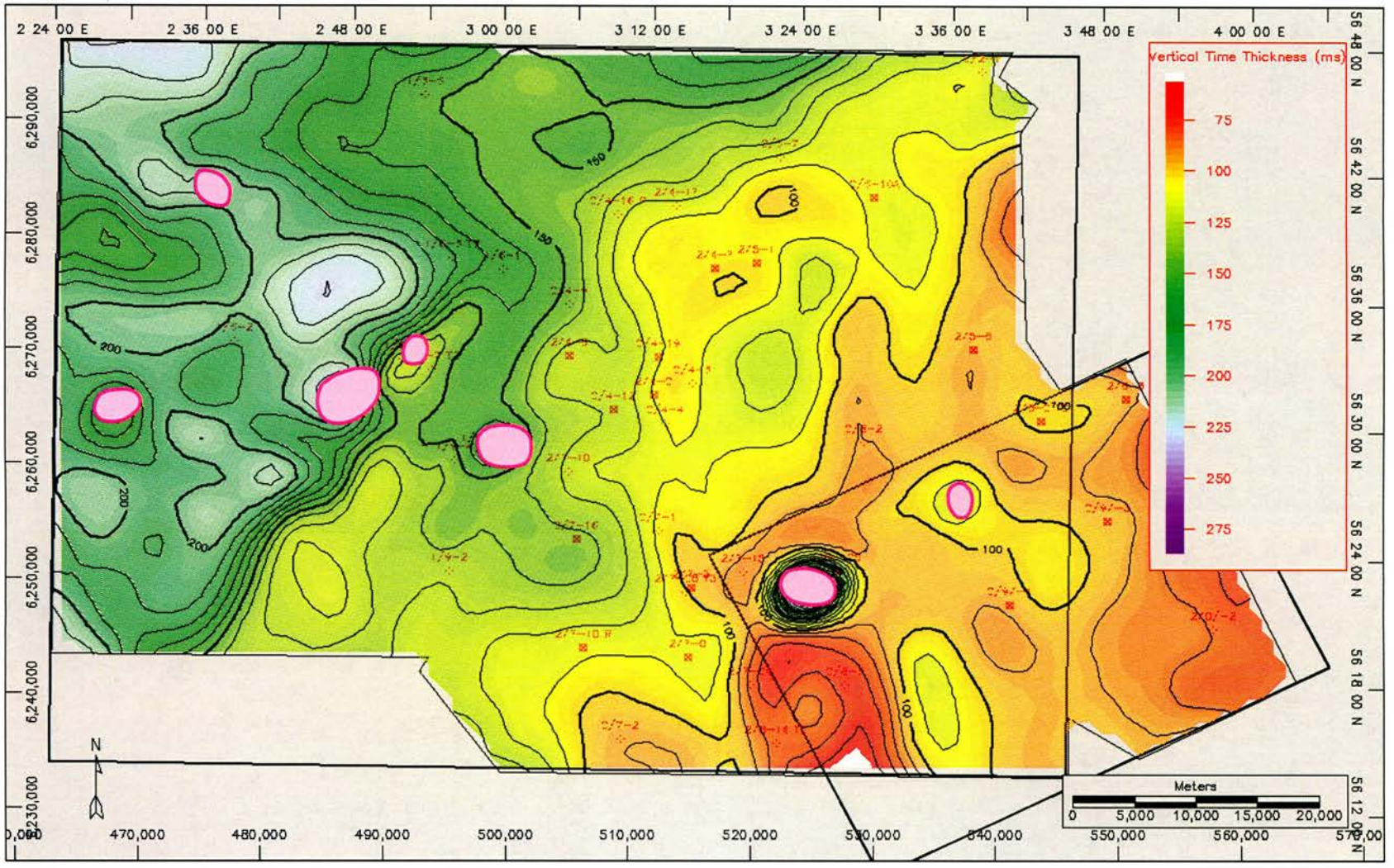

Figure 4.14: Top Chalk to Top Rogaland (Rogaland Group) isochron map. Salt piercements are shaded pink.

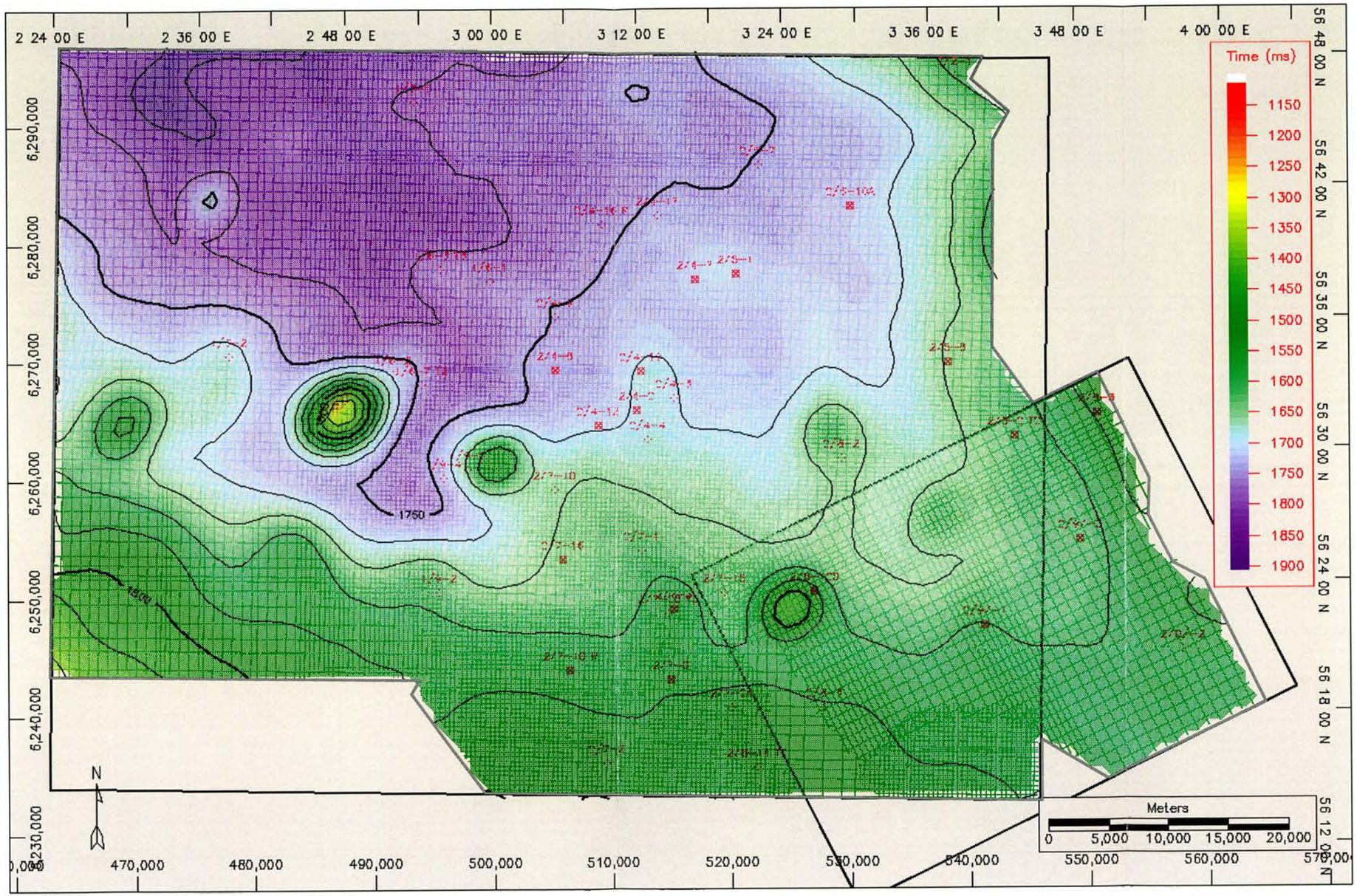

Figure 4.15: Top Hordaland Group TWTT horizon map (50ms contour interval)

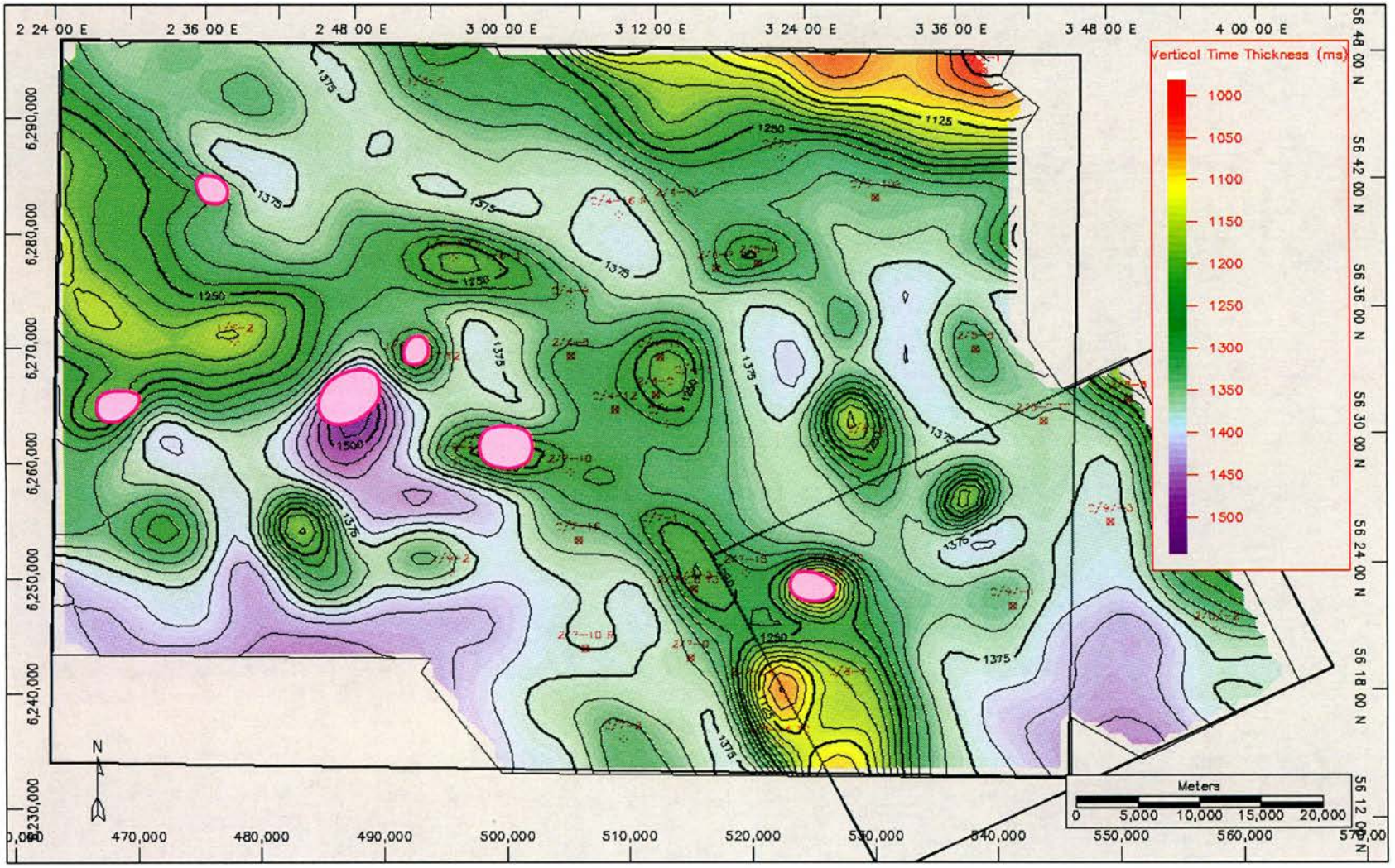

Figure 4.16: Top Rogaland to Top Hordaland (Hordaland Group) isochron map. Salt piercements are shaded pink.

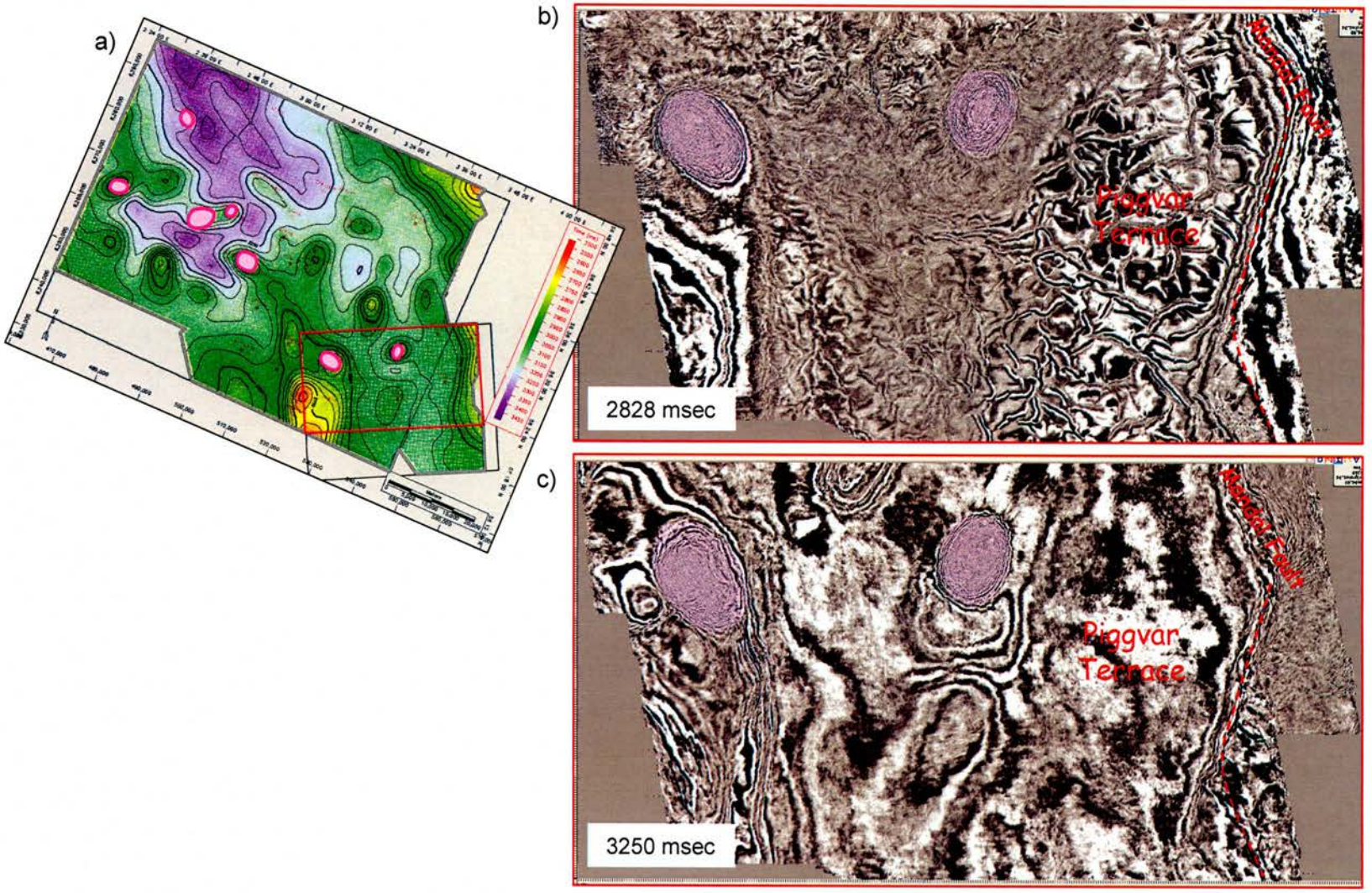

Figure 4.17: Timeslices through part of the ga3d93 survey. **a)** Location of the timeslice area relative to the Top Chalk Group TWTT map (figure 4.11). **b)** Timeslice at 2828msec (intersects mainly lower Hordaland reflections). **c)** Timeslice at 3250 msec (intersects mainly Chalk Group reflections). Salt piercements and the Mandal fault are visible on both slices. The shallower slice shows second order discontinuities not seen in the deeper slice: these features, seen most clearly over the Piggvar Terrace, are interpreted as polygonal faults and are attributed to the dewatering of shales associated with rapid deposition of the Hordaland section.

Compressional Style	Observations	Example
Faulting unrelated to salt mobility (Salt-absent inversion)	•Halite absent, or present but isopachous; no detachment effect on faults •Contractional offset on a fault that is in net extension at depth •Uplifted syn-rift sediment wedge •Monoclinal folding of overburden (post-rift)	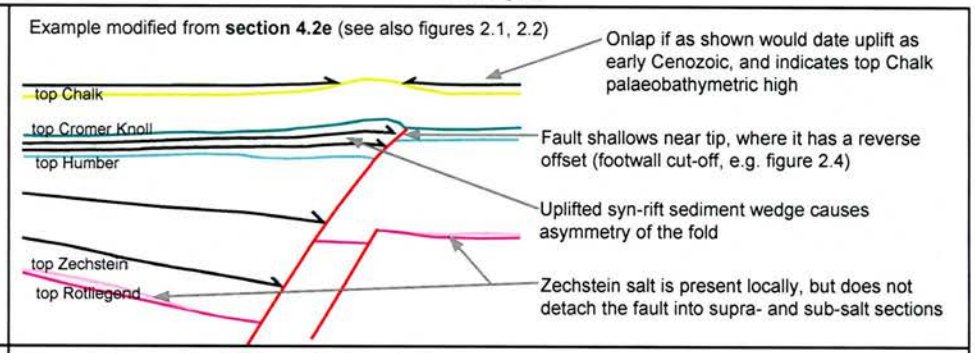
Salt movement unrelated to fault movement (Salt mobility in response to compression)	•Salt structures present, with rotated onlaps against the salt body. This is indicative of salt movement, but not necessarily compression •Thick lid of updomed strata over the salt body •Thinning in the neck of the salt body	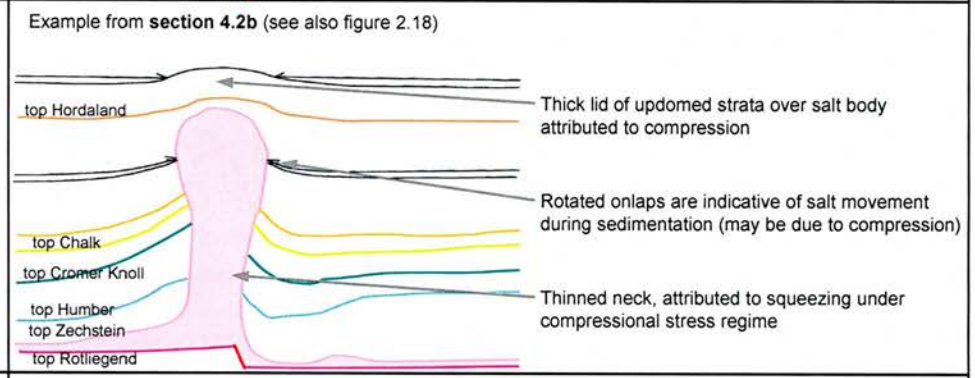
Fault and salt movement (Salt-influenced inversion)	•Salt structures present, with geometries often three-dimensionally complex (rather than simple diapirs or salt walls) •Uplifted syn-rift sediment wedge, spatially related to major sub-salt fault/s •Halite acting as fault detachment layer •Folding of overburden (post-rift)	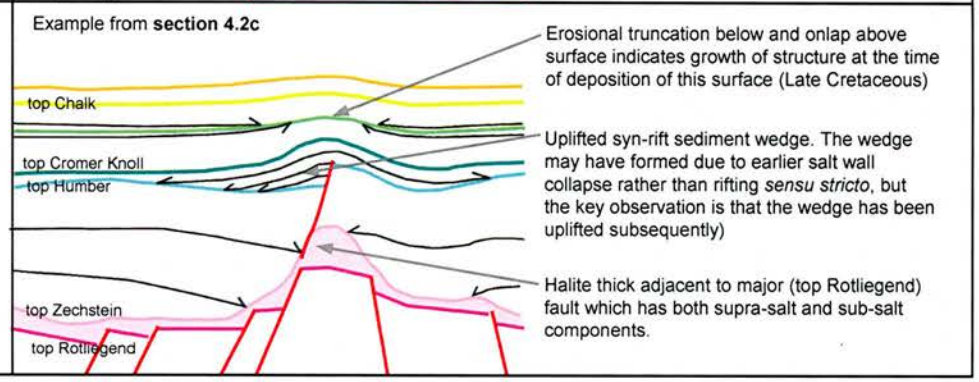

Figure 5.1: Seismic criteria for recognition of and discrimination between compressional structural styles in the salt-prone Norwegian Central Trough

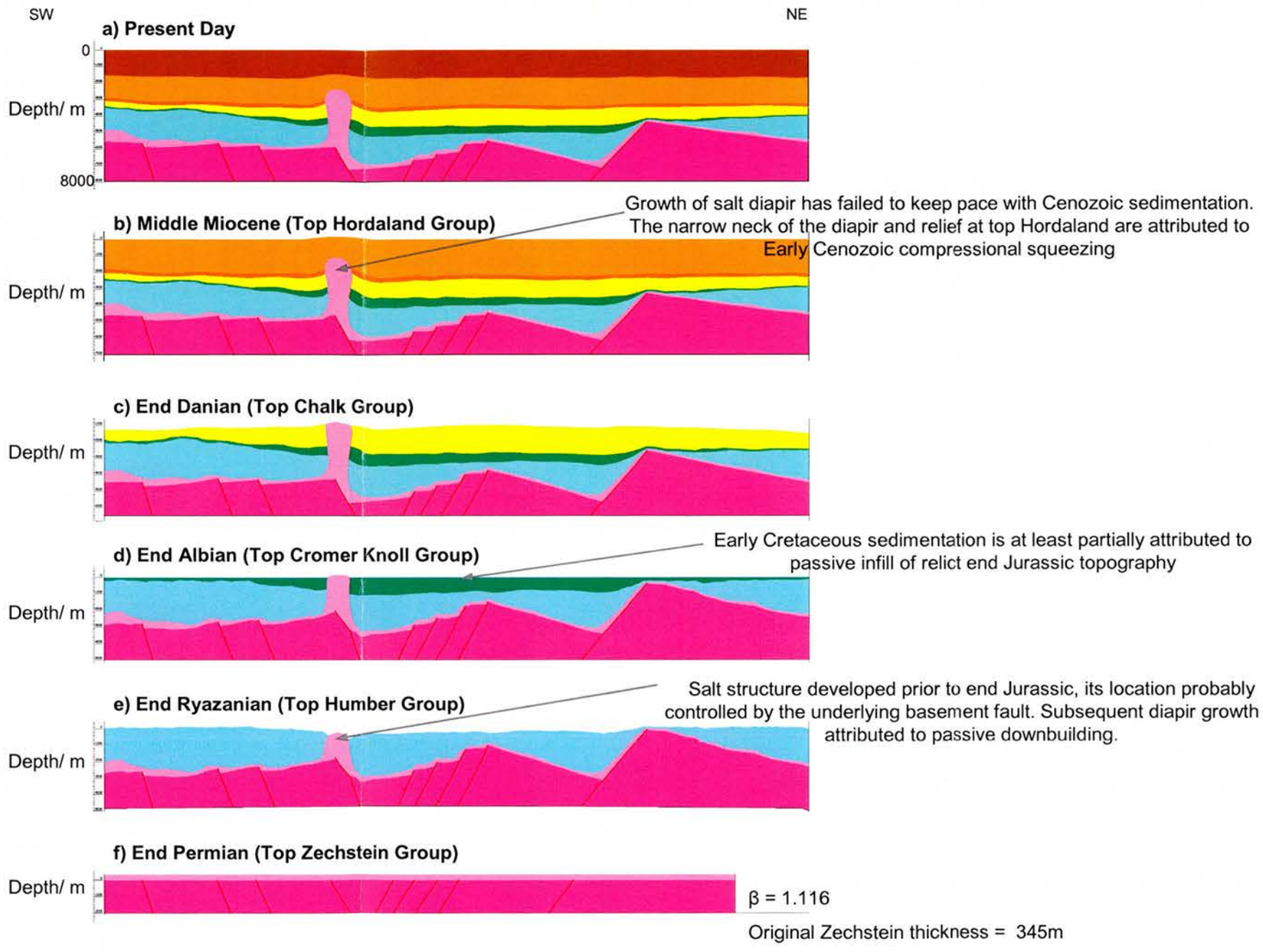

Legend

Horizon	Colour	Depth Coefficient	Porosity
Sea Bed		0.51	0.63
Top Hordaland		0.51	0.63
Top Rogaland		0.39	0.59
Top Chalk		0.71	0.7
Top Cromer Knoll		0.51	0.63
Top Humber		0.51	0.63
Top Zechstein		0.01	0.01
Top Rotliegend		0.27	0.49

Isostasy: None / Airy / Flex

Sub Marine / Sub Aerial

Load Dty.	2680
Mantle Dty.	3300
Elastic Th	5
Young's Modulus	7e+10

Figure 5.2: Structural restoration of seismic cross section A-A' (figure 4.2a) using 2dmove. Vertical and horizontal scales are equal.

The effects of compaction and isostasy, and faulting have been modelled for progressively older time steps. Parameters for decompaction and isostatic adjustment are recorded in the legend and justified in section 3.6. The same values were used for all shown restorations. Model layers are named and coloured according to their upper surface (a seismically mapped horizon). The β (stretching) factor records the amount of extension at top Rotliegend level since late Permian times. It is not possible to measure any shortening because the magnitude of that shortening is significantly less than the magnitude of extension, and may have been substantially accommodated by salt movement. 'Original' Zechstein thickness was calculated under the assumptions of constant area (no salt movement perpendicular to the plane of section) and uniform initial thickness.

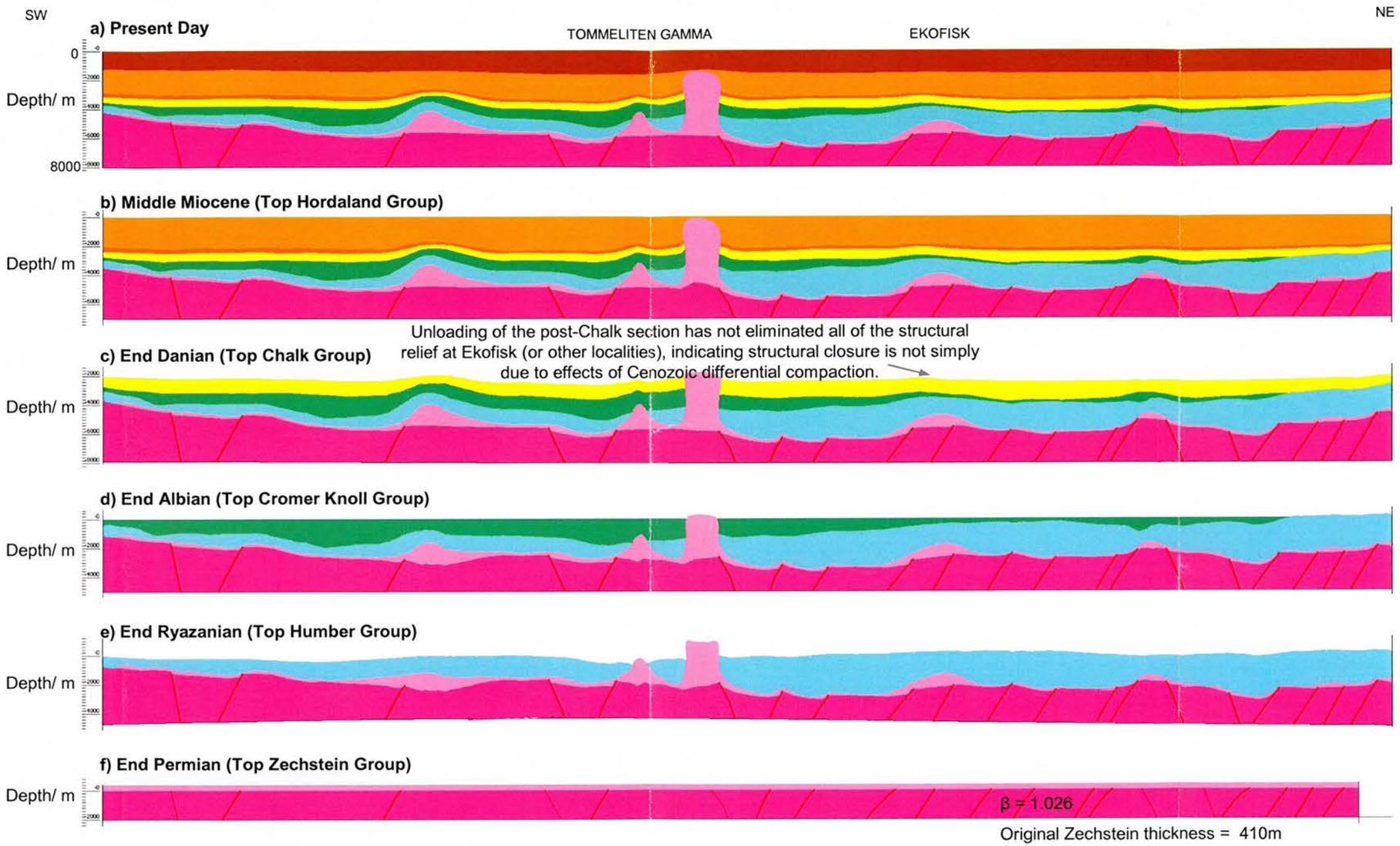

Legend

Horizon	Colour	Depth Coefficient	Porosity
Sea Bed		0.51	0.63
Top Hordaland		0.51	0.63
Top Rogaland		0.39	0.59
Top Chalk		0.71	0.7
Top Cromer Knoll		0.51	0.63
Top Humber		0.51	0.63
Top Zechstein		0.01	0.01
Top Rotliegend		0.27	0.49

Isostasy: None / Airy / Flex

Sub Marine / Sub Aerial

Load Dty.	2680
Mantle Dty.	3300
Elastic Th	5
Young's Modulus	7e+10

Figure 5.3: Structural restoration of seismic cross section C-C' (figure 4.2c) using 2dmove. Vertical and horizontal scales are equal.

The effects of compaction and isostasy, and faulting have been modelled for progressively older time steps. Legend records the parameters used for decompaction and isostatic adjustment. The β factor indicates 2.6% net extension since end Permian, and an original Zechstein thickness of 410m was calculated.

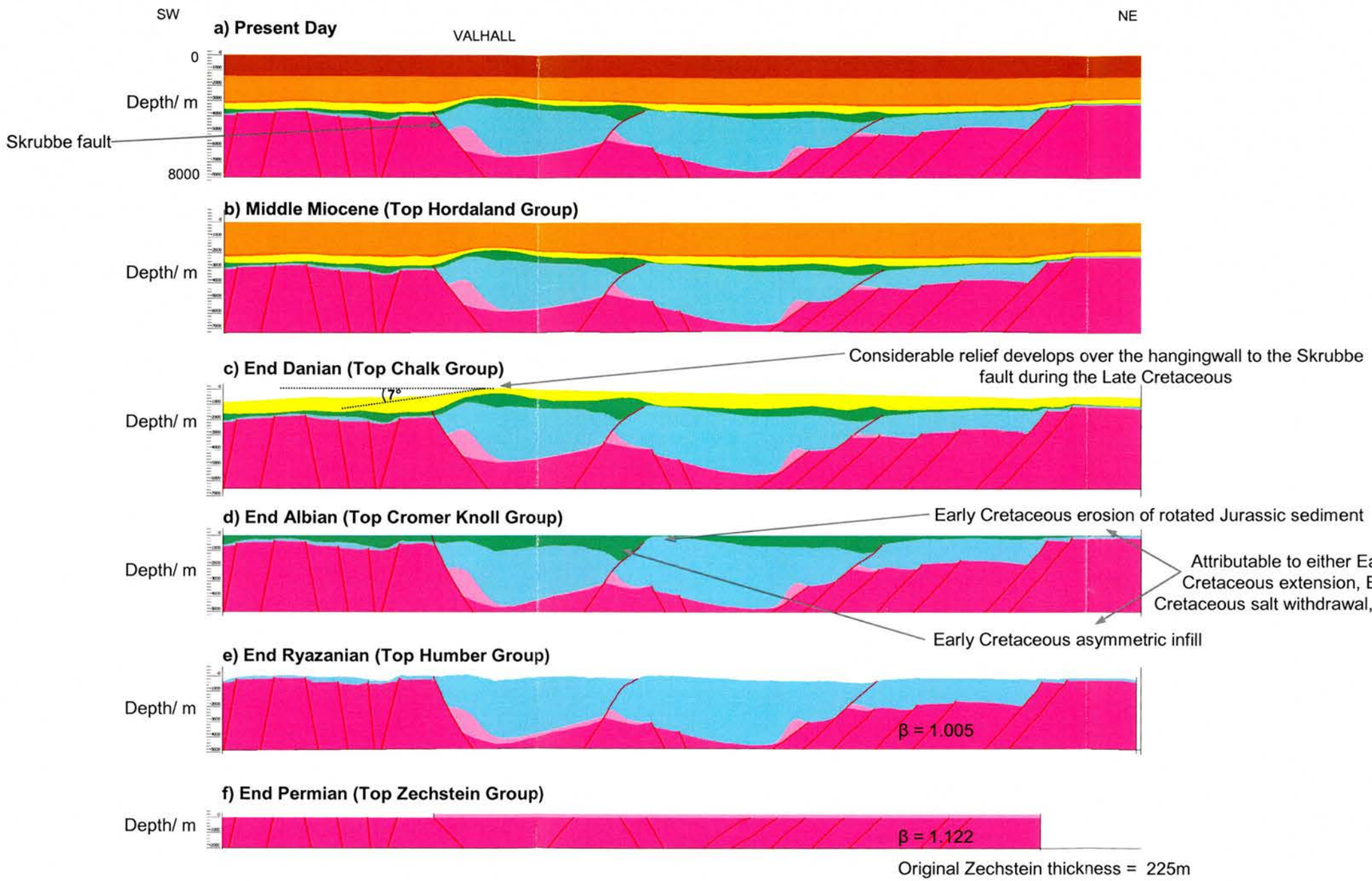

Legend

Horizon	Colour	Depth Coefficient	Porosity
Sea Bed		0.51	0.63
Top Hordaland		0.51	0.63
Top Rogaland		0.39	0.59
Top Chalk		0.71	0.7
Top Cromer Knoll		0.51	0.63
Top Humber		0.51	0.63
Top Zechstein		0.01	0.01
Top Rotliegend		0.27	0.49

Isostasy: None / Airy / Flex

Sub Marine / Sub Aerial

Load Dty.	2680
Mantle Dty.	3300
Elastic Th	5
Young's Modulus	7e+10

Figure 5.4: Structural restoration of seismic cross section E-E' (figure 4.2e) using 2dmove. Vertical and horizontal scales are equal.

The effects of compaction and isostasy, and faulting have been modelled for progressively older time steps. Legend records the parameters used for decompaction and isostatic adjustment. The β factor indicates 12.2% net extension since end Permian, including a small but measurable component attributed to the Early Cretaceous (assuming the Early Cretaceous asymmetric infill was due to extension rather than salt withdrawal). An original Zechstein thickness of 225m was calculated.

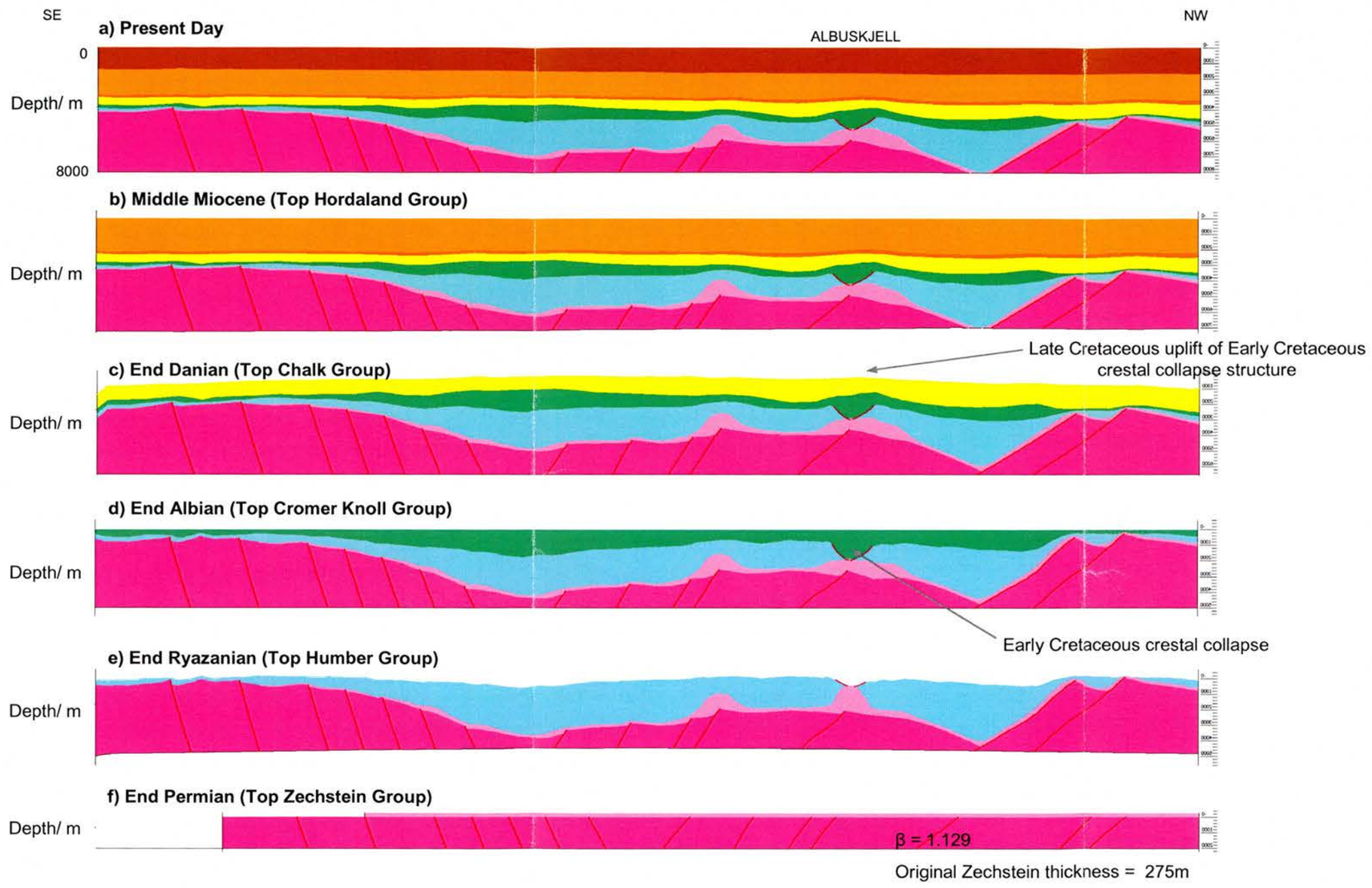

Legend

Horizon	Colour	Depth Coefficient	Porosity
Sea Bed		0.51	0.63
Top Hordaland		0.51	0.63
Top Rogaland		0.39	0.59
Top Chalk		0.71	0.7
Top Cromer Knoll		0.51	0.63
Top Humber		0.51	0.63
Top Zechstein		0.01	0.01
Top Rotliegend		0.27	0.49

Isostasy: None / Airy / Flex

Sub Marine / Sub Aerial

Load Dty.	2680
Mantle Dty.	3300
Elastic Th	5
Young's Modulus	7e+10

Figure 5.5: Structural restoration of seismic cross section G-G' (figure 4.2g) using 2dmove. Vertical and horizontal scales are equal.

The effects of compaction and isostasy, and faulting have been modelled for progressively older time steps. Legend records the parameters used for decompaction and isostatic adjustment. The β factor indicates 12.9% net extension since end Permian, and an original Zechstein thickness of 275m was calculated.

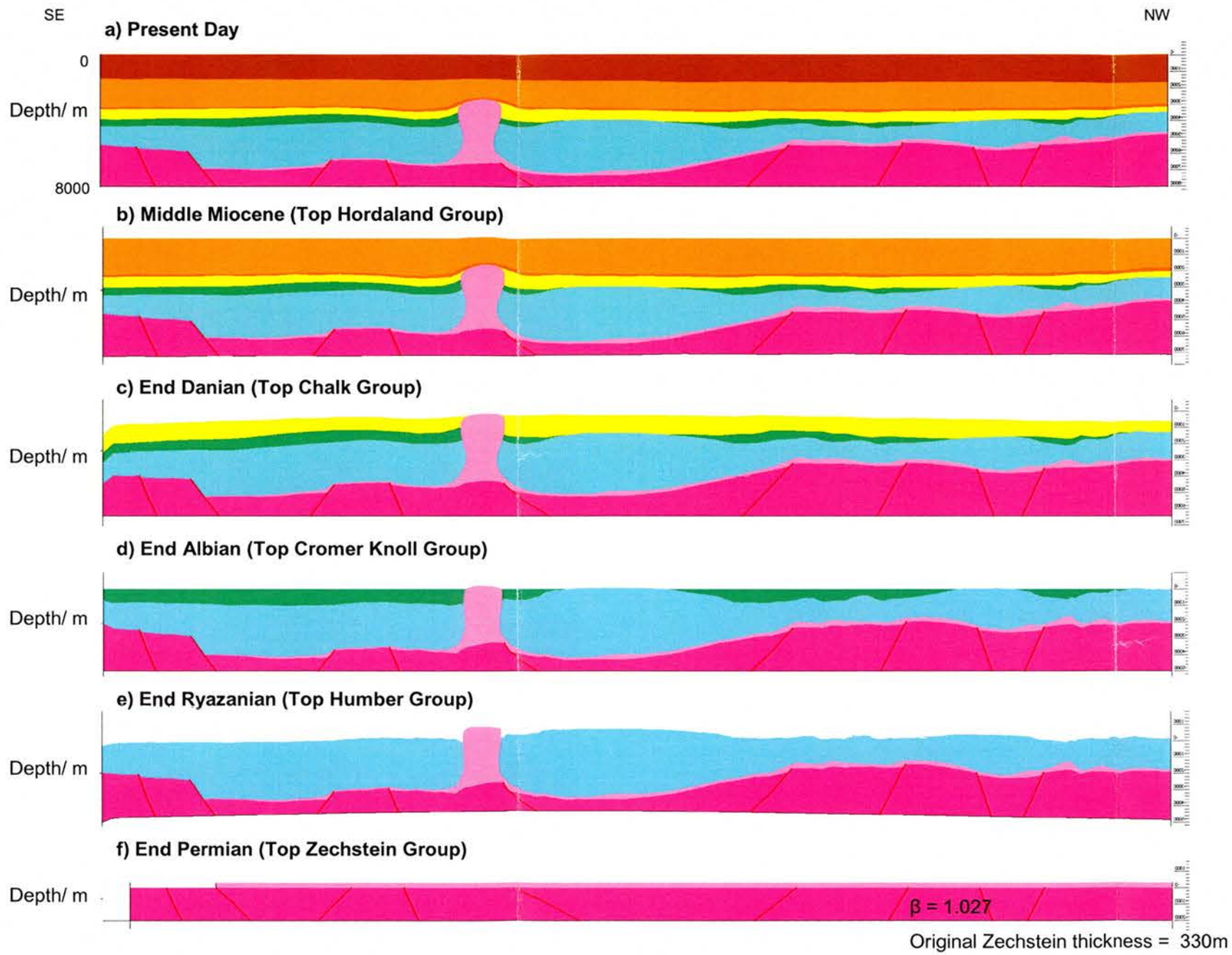

Legend

Horizon	Colour	Depth Coefficient	Porosity
Sea Bed		0.51	0.63
Top Hordaland		0.51	0.63
Top Rogaland		0.39	0.59
Top Chalk		0.71	0.7
Top Cromer Knoll		0.51	0.63
Top Humber		0.51	0.63
Top Zechstein		0.01	0.01
Top Rotliegend		0.27	0.49

Isostasy
- None
- Airy
- Flex

- Sub Marine
- Sub Aerial

Load Dty.	2680
Mantle Dty.	3300
Elastic Th	5
Young's Modulus	7e+10

Figure 5.6: Structural restoration of seismic cross section I-I' (figure 4.2i) using 2dmove. Vertical and horizontal scales are equal.

The effects of compaction and isostasy, and faulting have been modelled for progressively older time steps. Legend records the parameters used for decompaction and isostatic adjustment. The β factor indicates 2.7% net extension since end Permian, and an original Zechstein thickness of 330m was calculated.

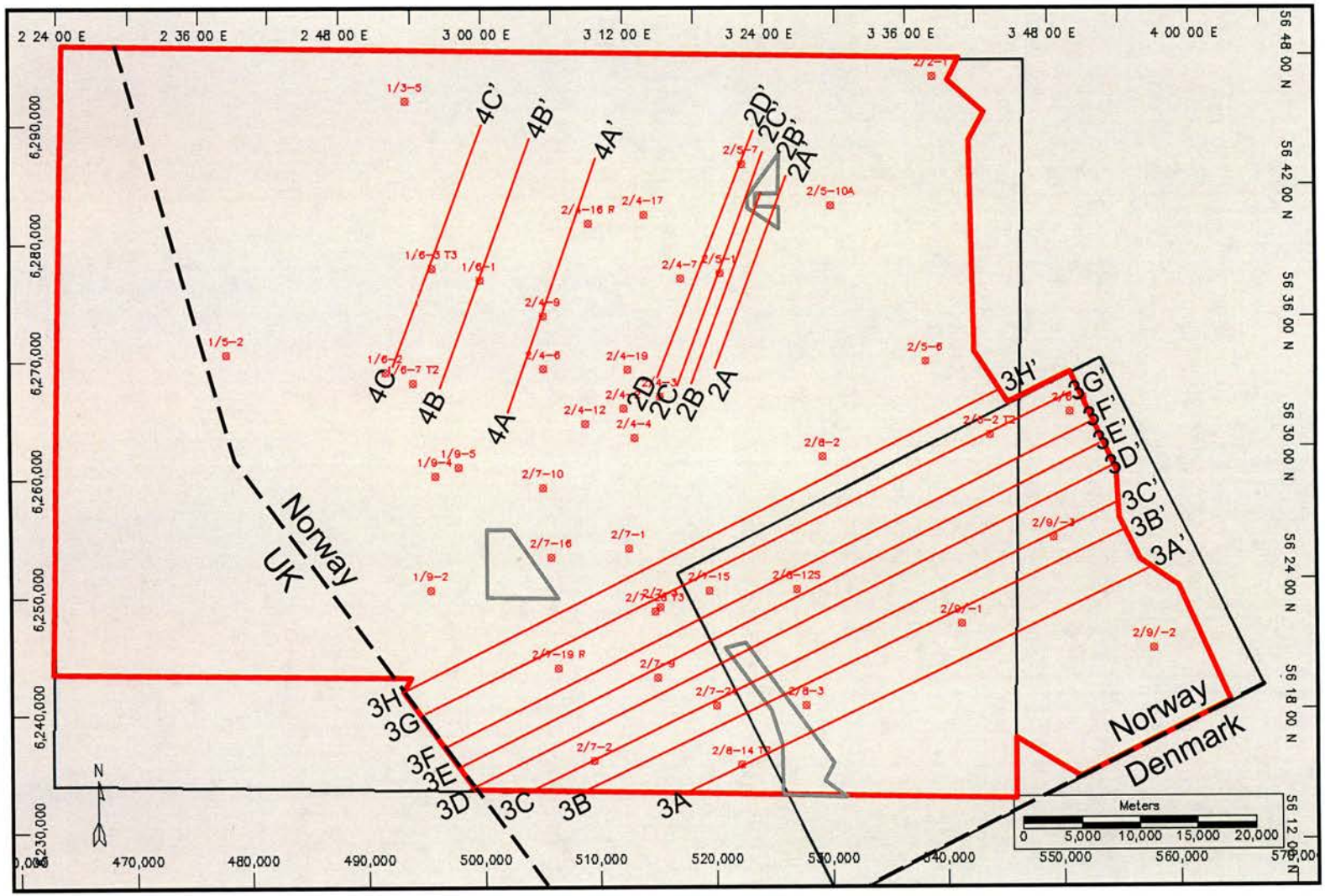

Figure 5.7: Key to sections discussed in chapter 5. Section 3C3C' is shown in chapter 4, as section EE'

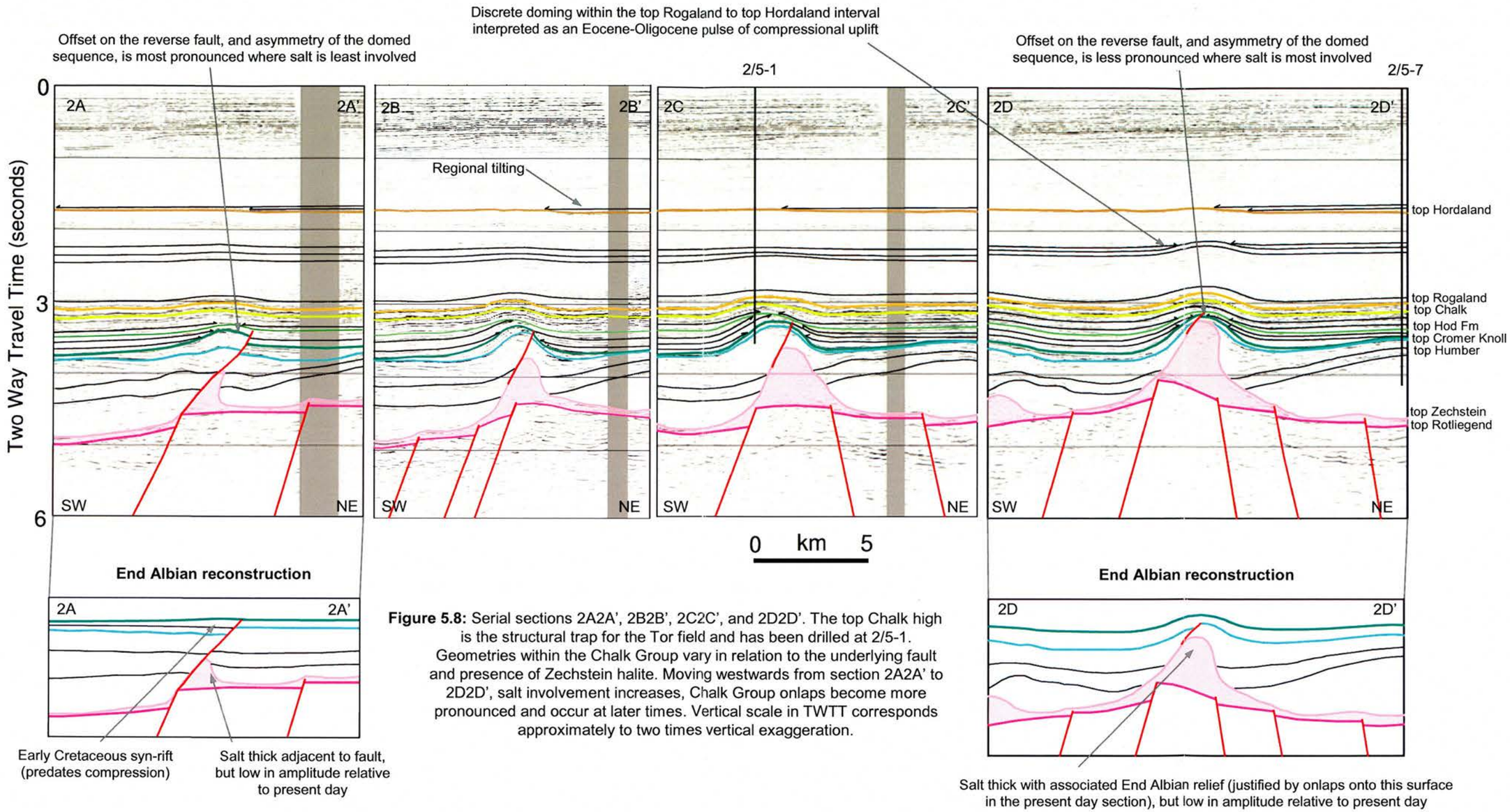

Figure 5.8: Serial sections 2A2A', 2B2B', 2C2C', and 2D2D'. The top Chalk high is the structural trap for the Tor field and has been drilled at 2/5-1. Geometries within the Chalk Group vary in relation to the underlying fault and presence of Zechstein halite. Moving westwards from section 2A2A' to 2D2D', salt involvement increases, Chalk Group onlaps become more pronounced and occur at later times. Vertical scale in TWTT corresponds approximately to two times vertical exaggeration.

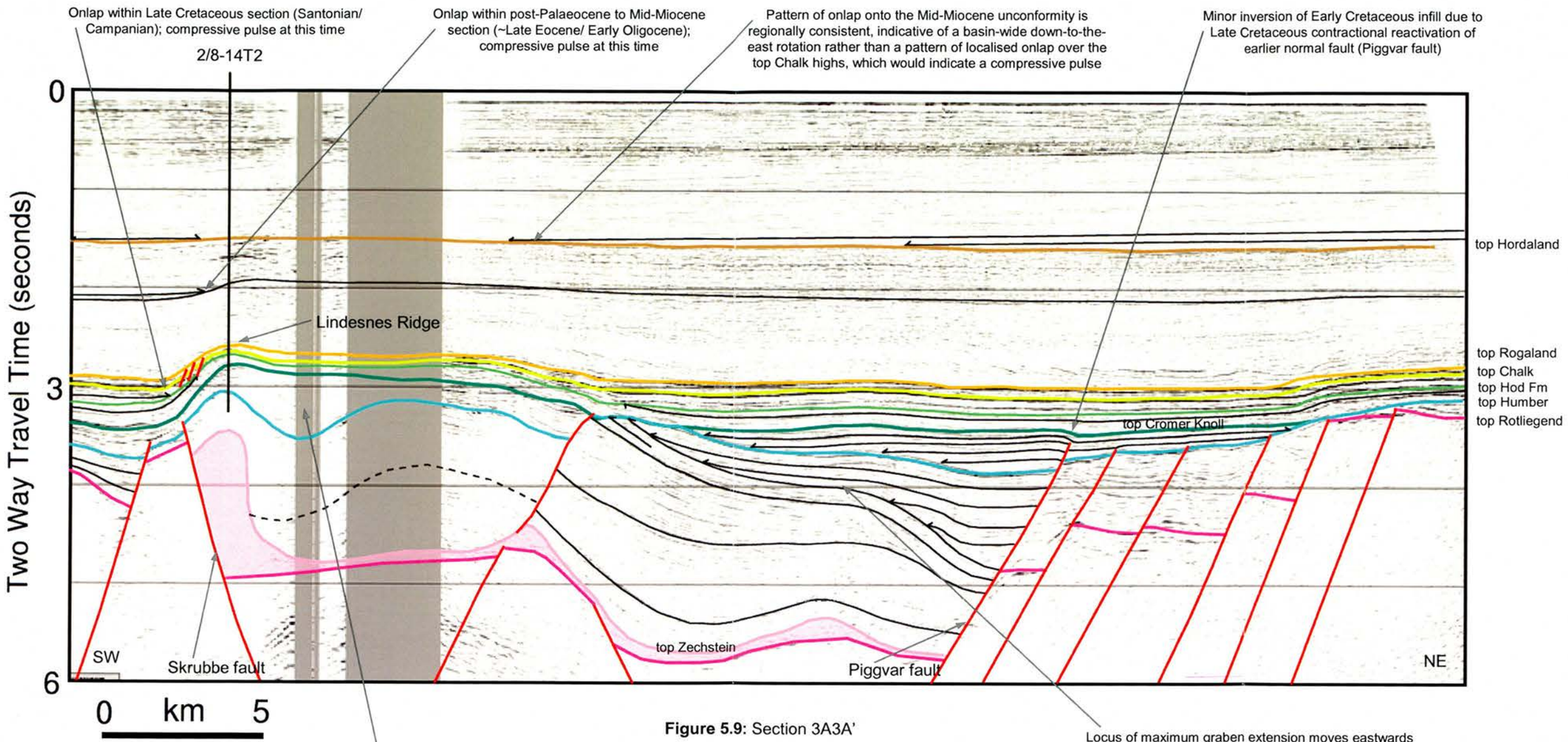

Figure 5.9: Section 3A3A'

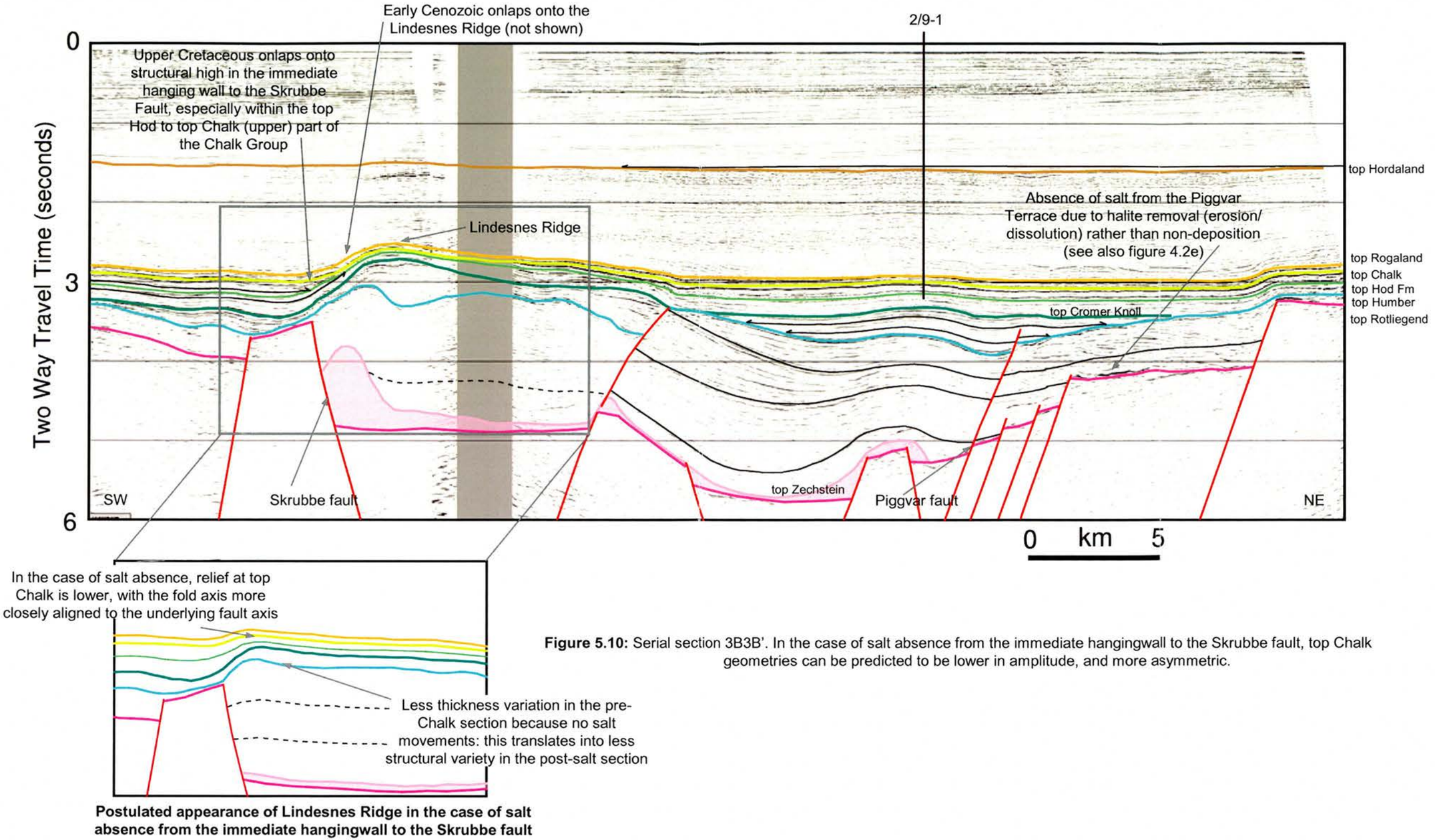

Figure 5.10: Serial section 3B3B'. In the case of salt absence from the immediate hangingwall to the Skrubbe fault, top Chalk geometries can be predicted to be lower in amplitude, and more asymmetric.

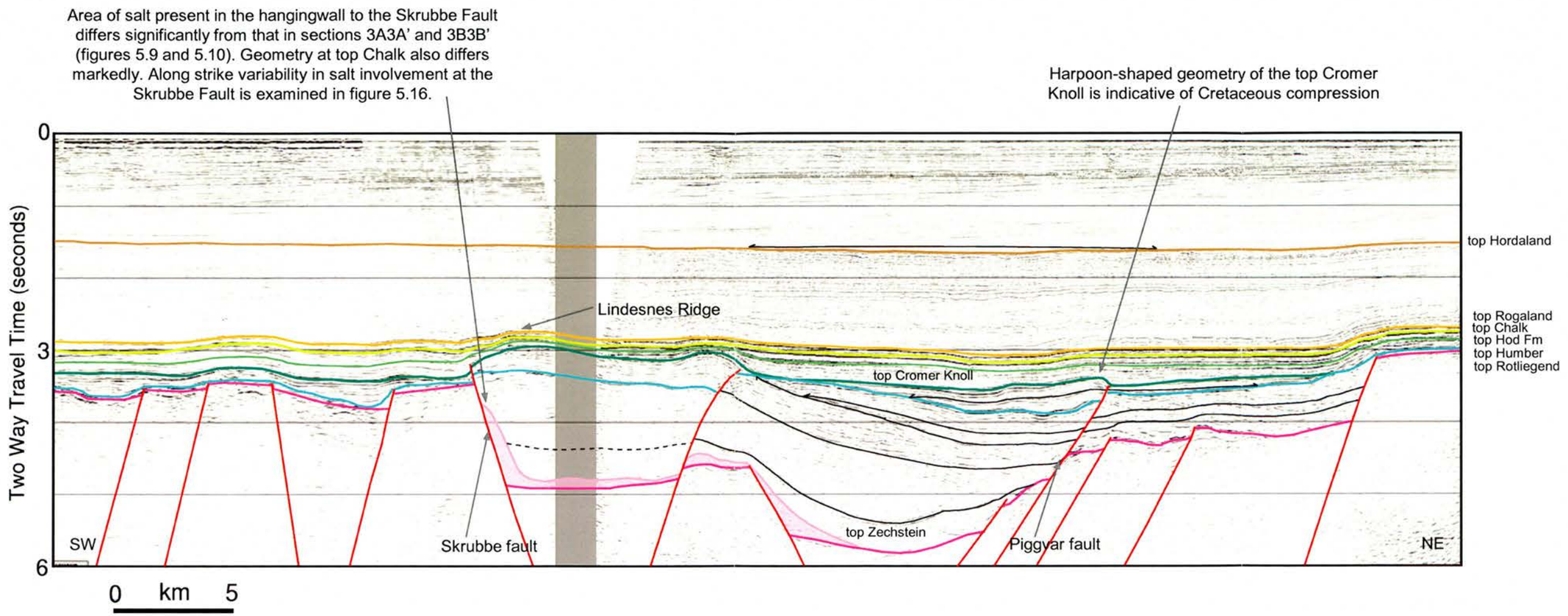

Figure 5.11: Serial section 3D3D'. Relative absence of salt against the Skrubbe fault coincides with low top Chalk relief on the Lindesnes Ridge

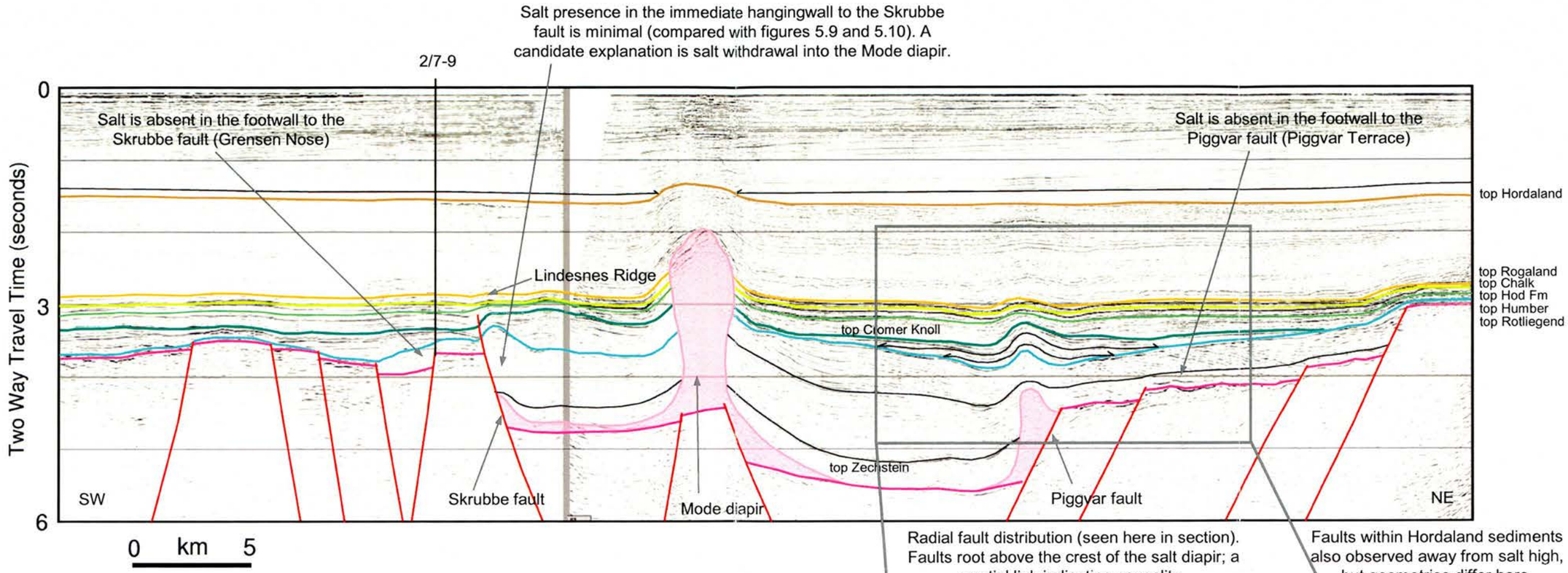

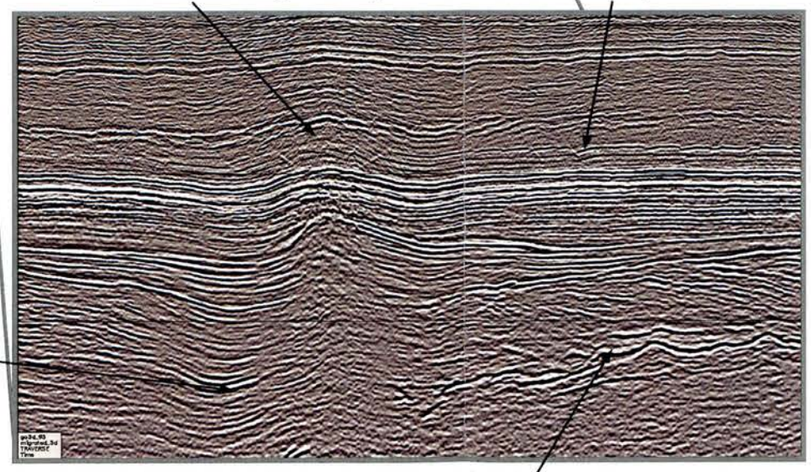

Figure 5.12: Serial section 3E3E'. Caption illustrates pattern of faulting in lowermost Rogaland sediments over crest of salt structure.

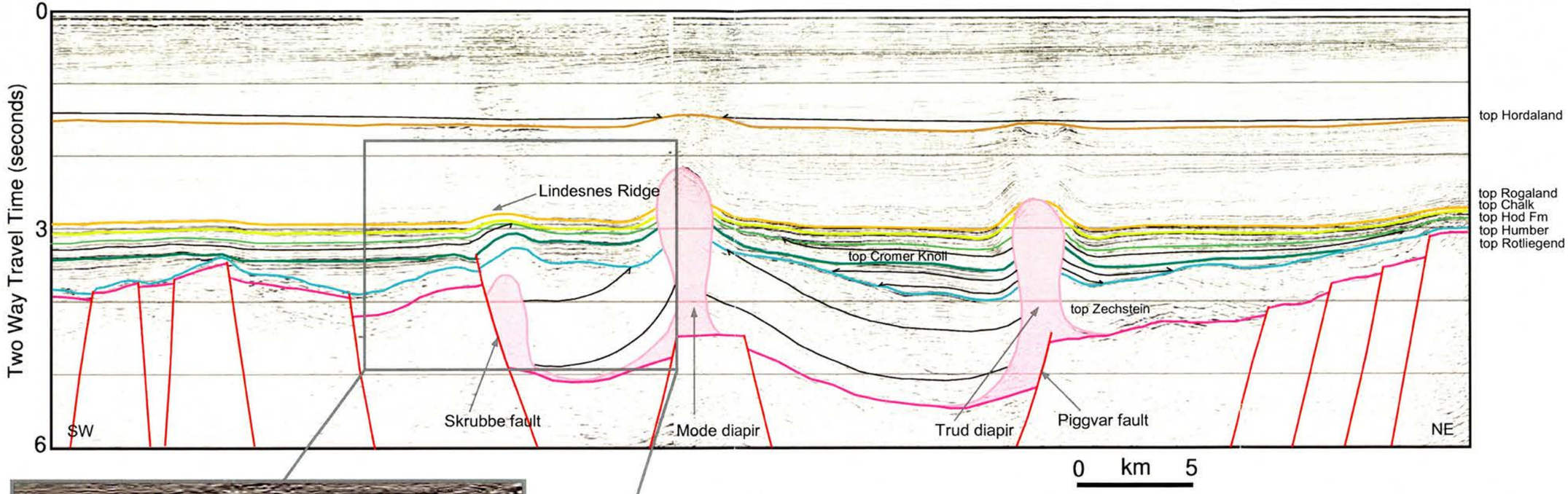

Post-Zechstein, pre-Cretaceous sediments rotated by Triassic-Jurassic salt movements

Figure 5.13: Serial section 3F3F'. Caption illustrates quality of cnsmerge seismic data on which interpretation of salt-fault interaction beneath the Lindesnes Ridge is based.

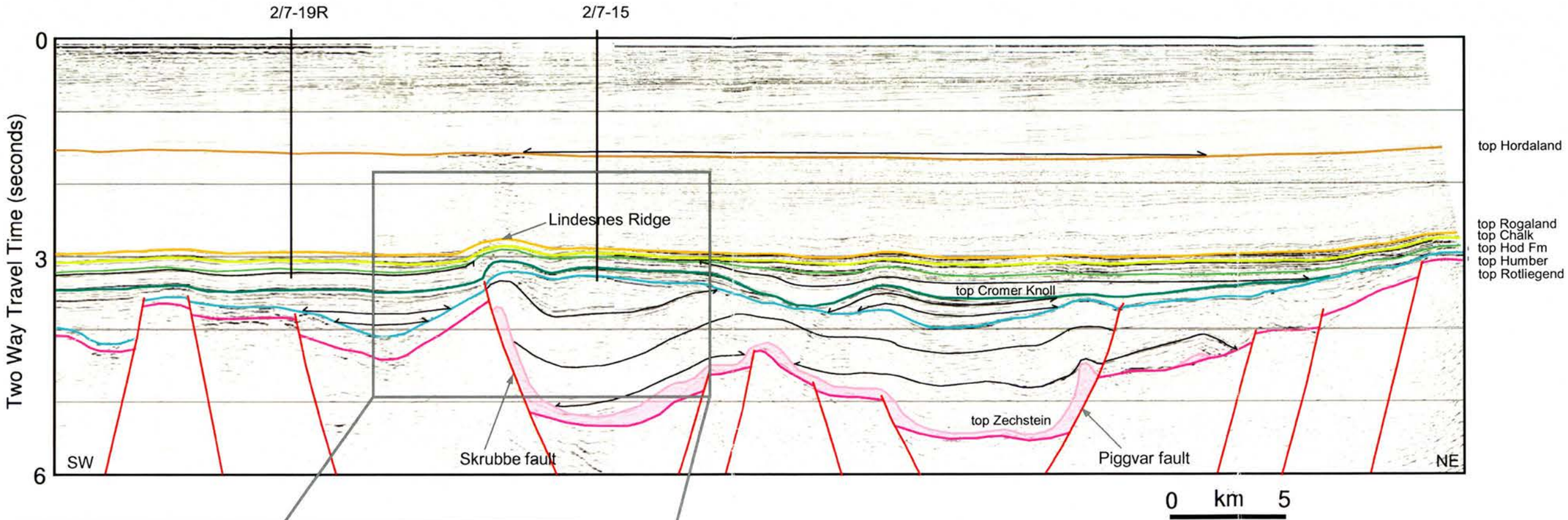

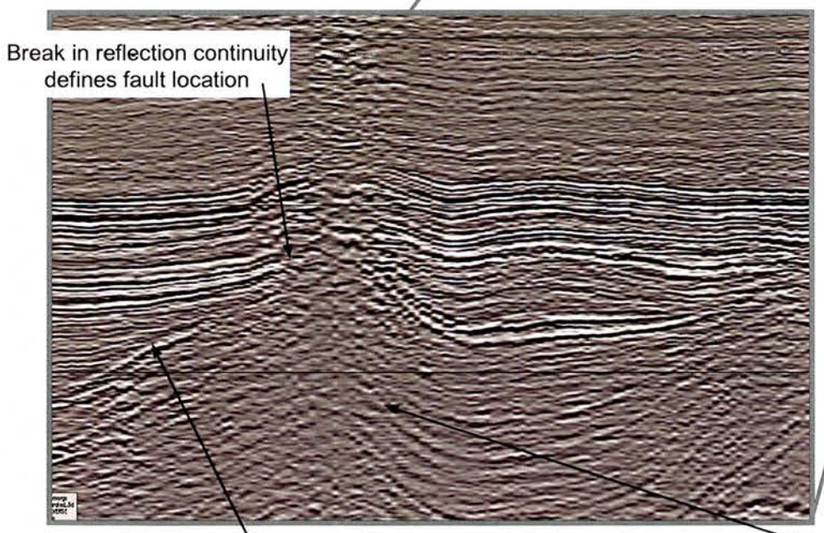

Figure 5.14: Serial section 3G3G'. Caption illustrates quality of cnsmerge seismic data on which interpretation of salt-fault interaction beneath the Lindesnes Ridge is based.

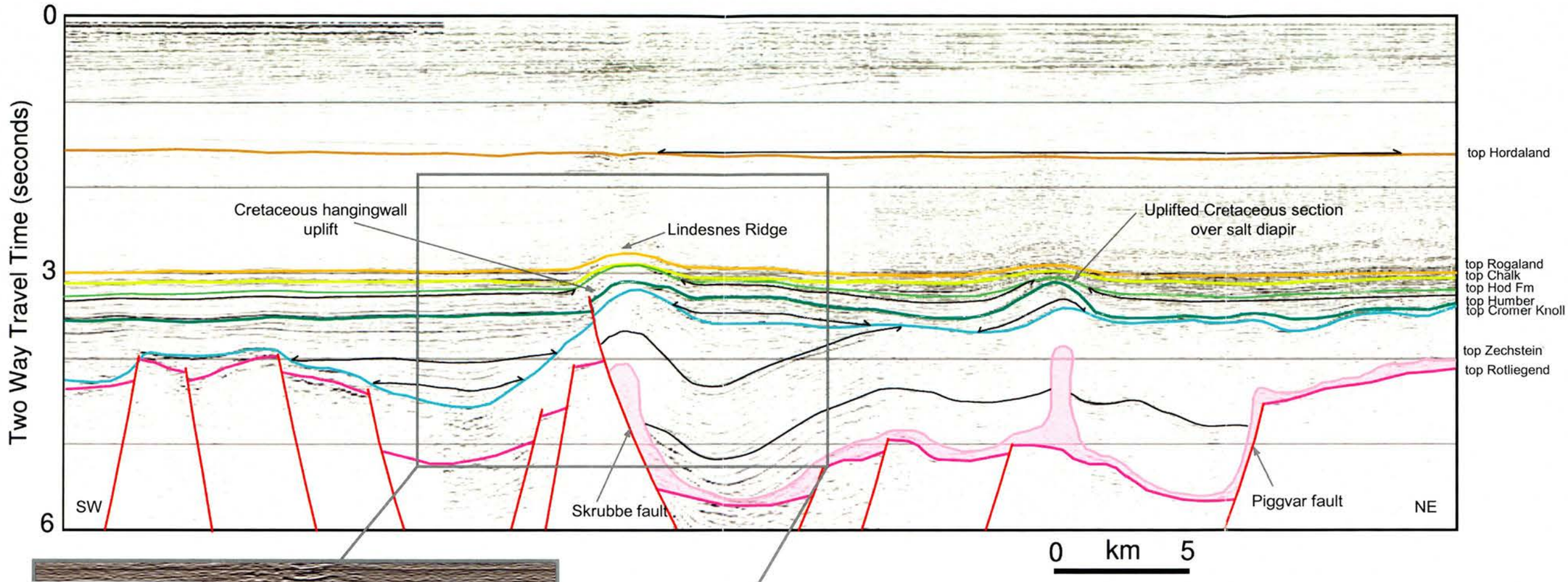

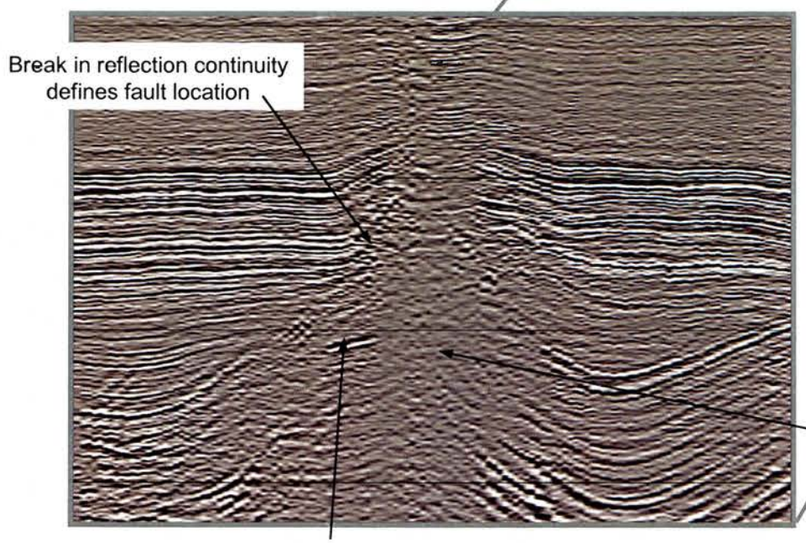

Seismic transparency due to salt presence in hangingwall to Skrubbe fault. The fault position has been interpreted from detailed 3D mapping. (While there is positional uncertainty on any given section, this uncertainty reduces significantly when individual interpretations are iteratively adjusted.)

Figure 5.15: Serial section 3H3H'. Caption illustrates quality of cnsmerge seismic data on which interpretation of salt-fault interaction beneath the Lindesnes Ridge is based.

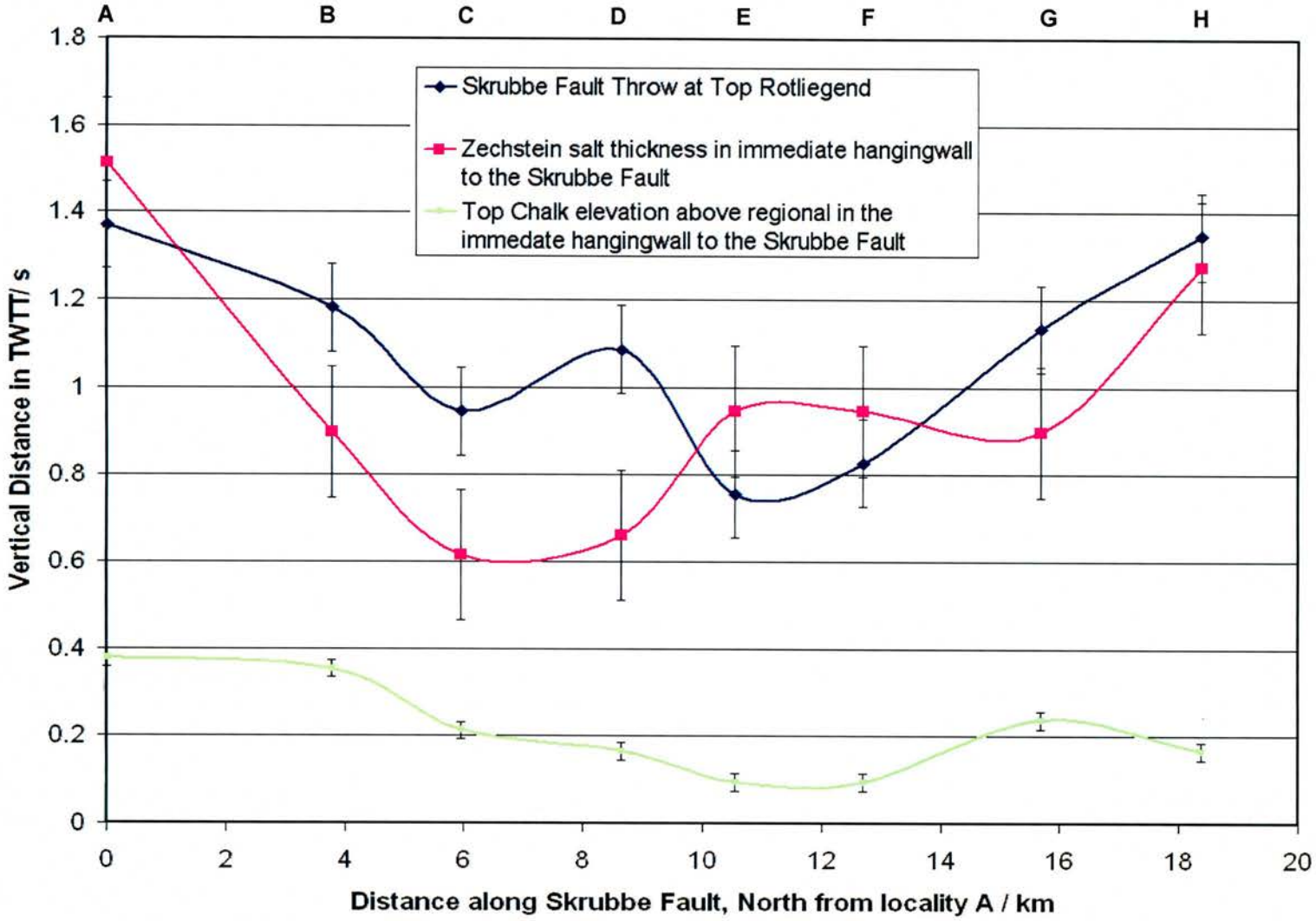

Figure 5.16: Along-strike variability in fault displacement (blue) and salt-involvement (pink) at the Skrubbe fault (Lindesnes Ridge) and how these parameters influence top Chalk Group relief (green). Along-strike variations in salt presence affect structural geometries and fault displacement-length profiles. See text for discussion.

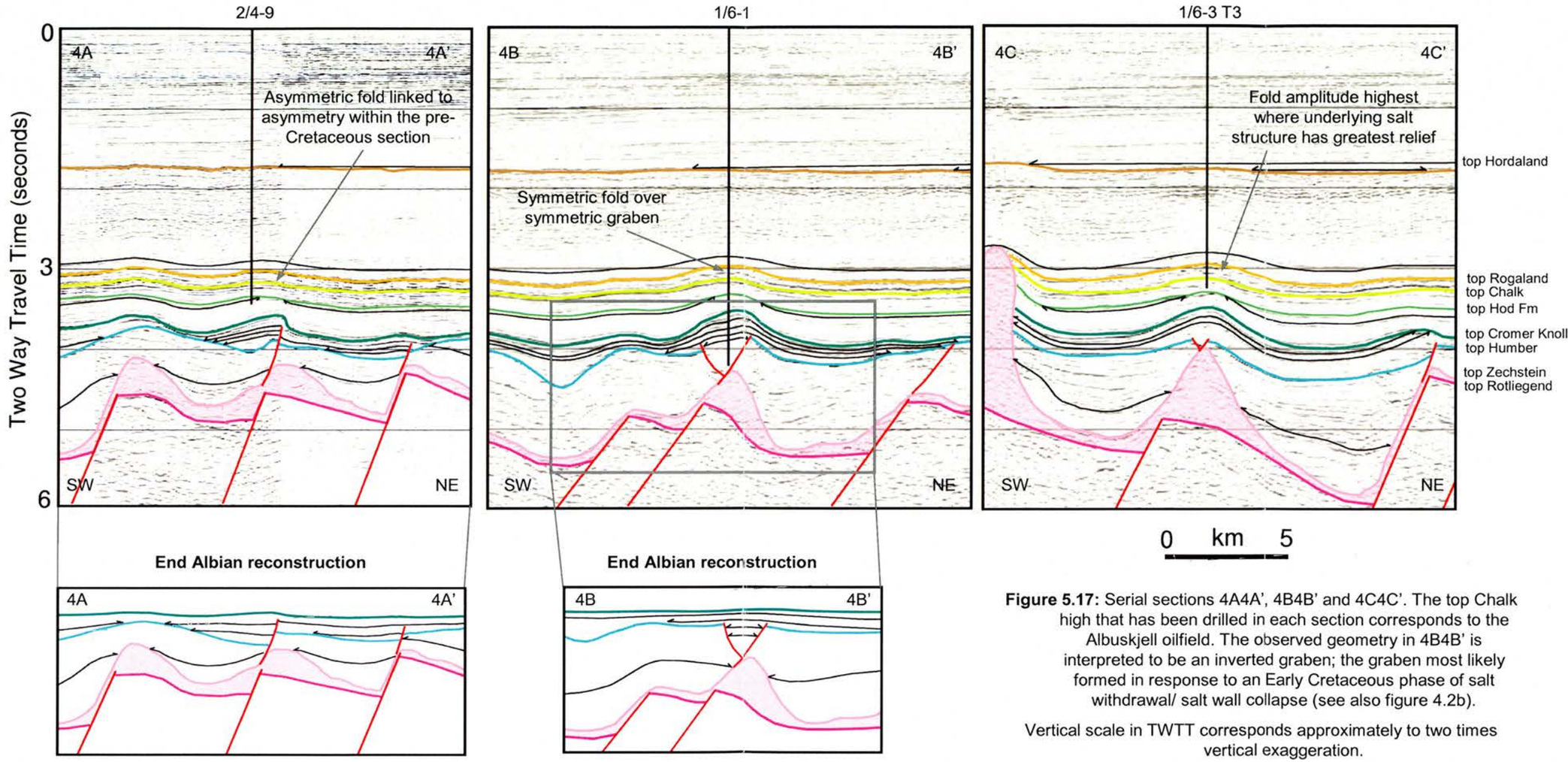

Figure 5.17: Serial sections 4A4A', 4B4B' and 4C4C'. The top Chalk high that has been drilled in each section corresponds to the Albuskjell oilfield. The observed geometry in 4B4B' is interpreted to be an inverted graben; the graben most likely formed in response to an Early Cretaceous phase of salt withdrawal/ salt wall collapse (see also figure 4.2b).

Vertical scale in TWTT corresponds approximately to two times vertical exaggeration.

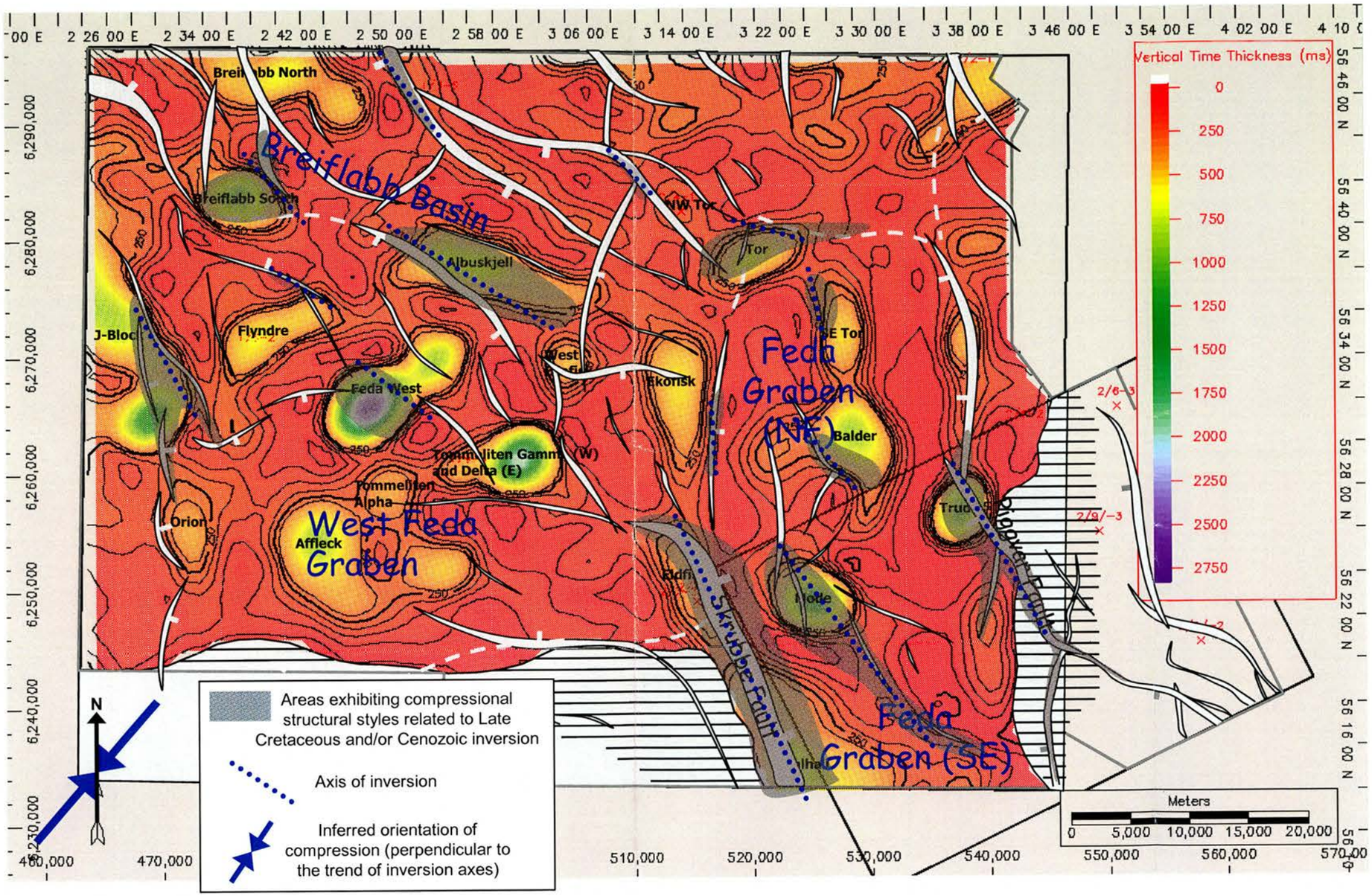

Figure 5.18: Summary map shows locations where structural inversion has been identified in the Norwegian Central Trough. The areas exhibiting compression are superimposed onto the Zechstein isochron (as figure 4.5) and the top Rotliegend fault interpretation (figure 4.3).

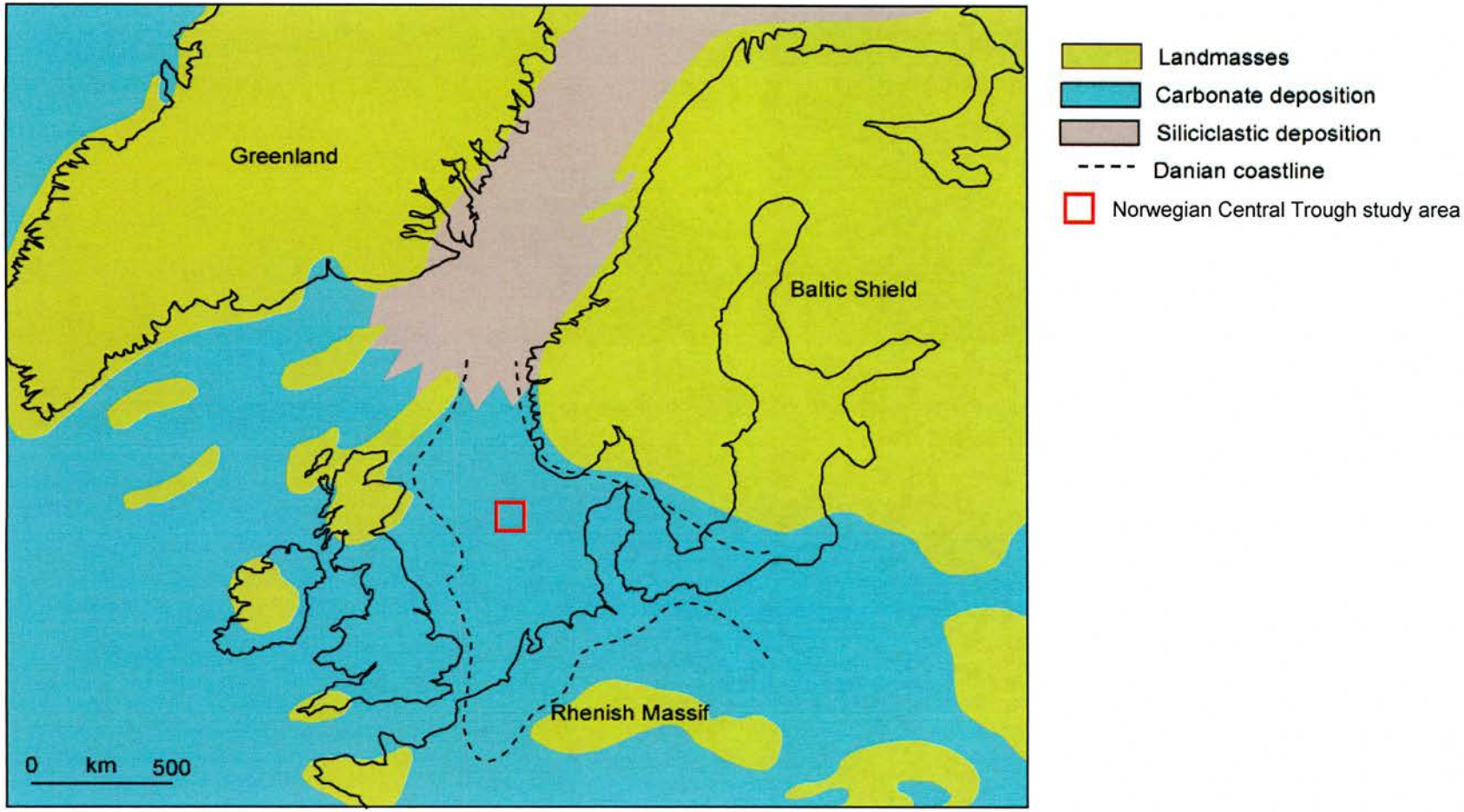

Figure 6.1: Illustration of Chalk Group deposition in NW Europe. Eustatic sea level rise and associated marine transgression severely restricted clastic input to the North Sea area, giving rise to a thick sequence of mostly pelagic marine deposits. Chalk thicknesses were as much as 2 km in the basin interior. *(After Surlyk et al 2003)*

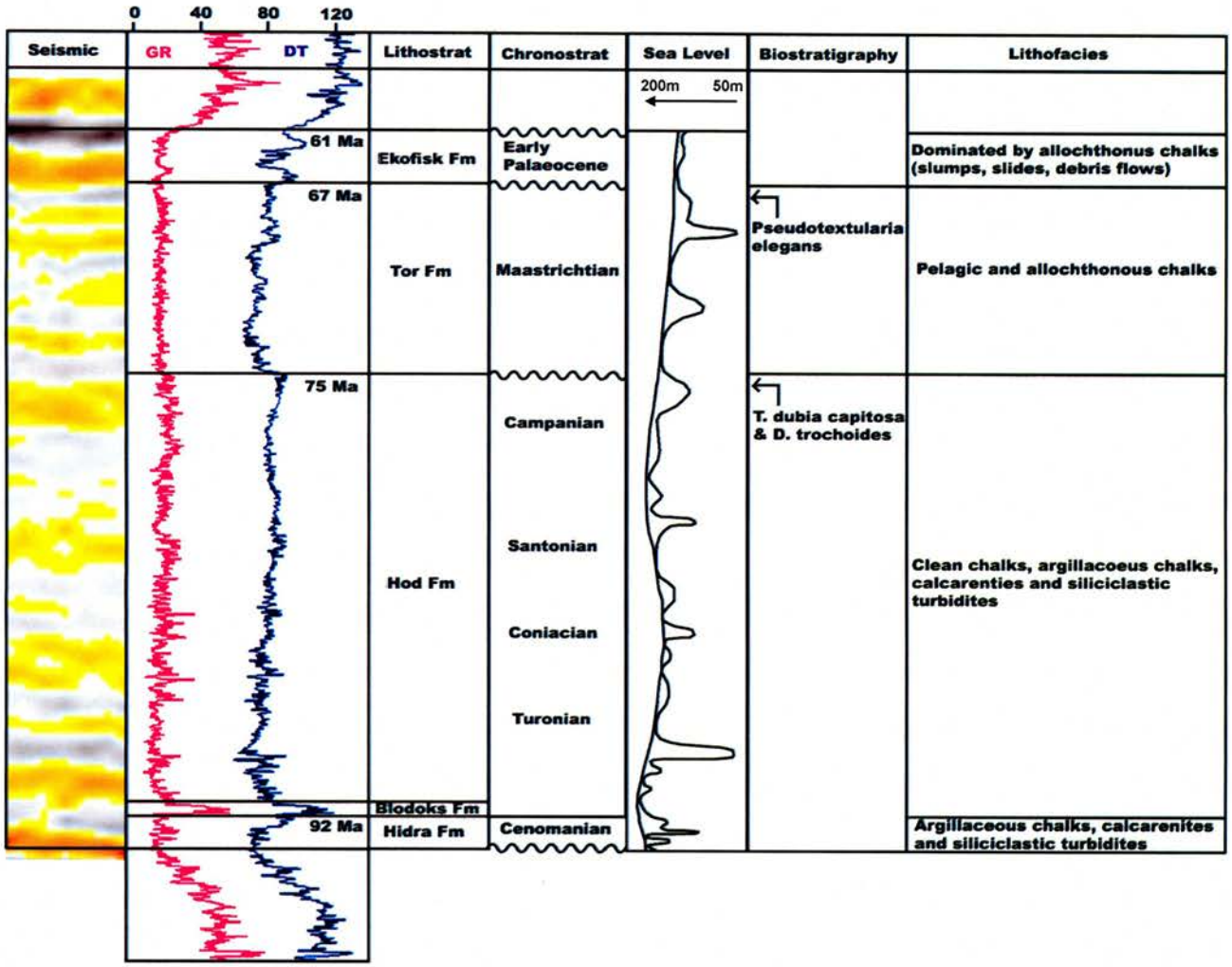

Figure 6.2: Detailed stratigraphic column for the Chalk Group. Seismic reflection data (red is positive amplitude, black negative), gamma ray (GR) and sonic (DT) log signatures are from well 2/7-15. The scale for the GR is API units, and the scale for the DT is microseconds/ft. Lower GR values are indicative of lower shale content. Lower DT values (higher interval velocities) are indicative of lower porosities, but can be strongly influenced by other factors such as fluid pressure and fracturing *(Rider , 2000)*. The eustatic sea level curves are based on *Haq et al., 1988* and biostratigraphic constraints are those defined by *Bramwell et al., 1999*.

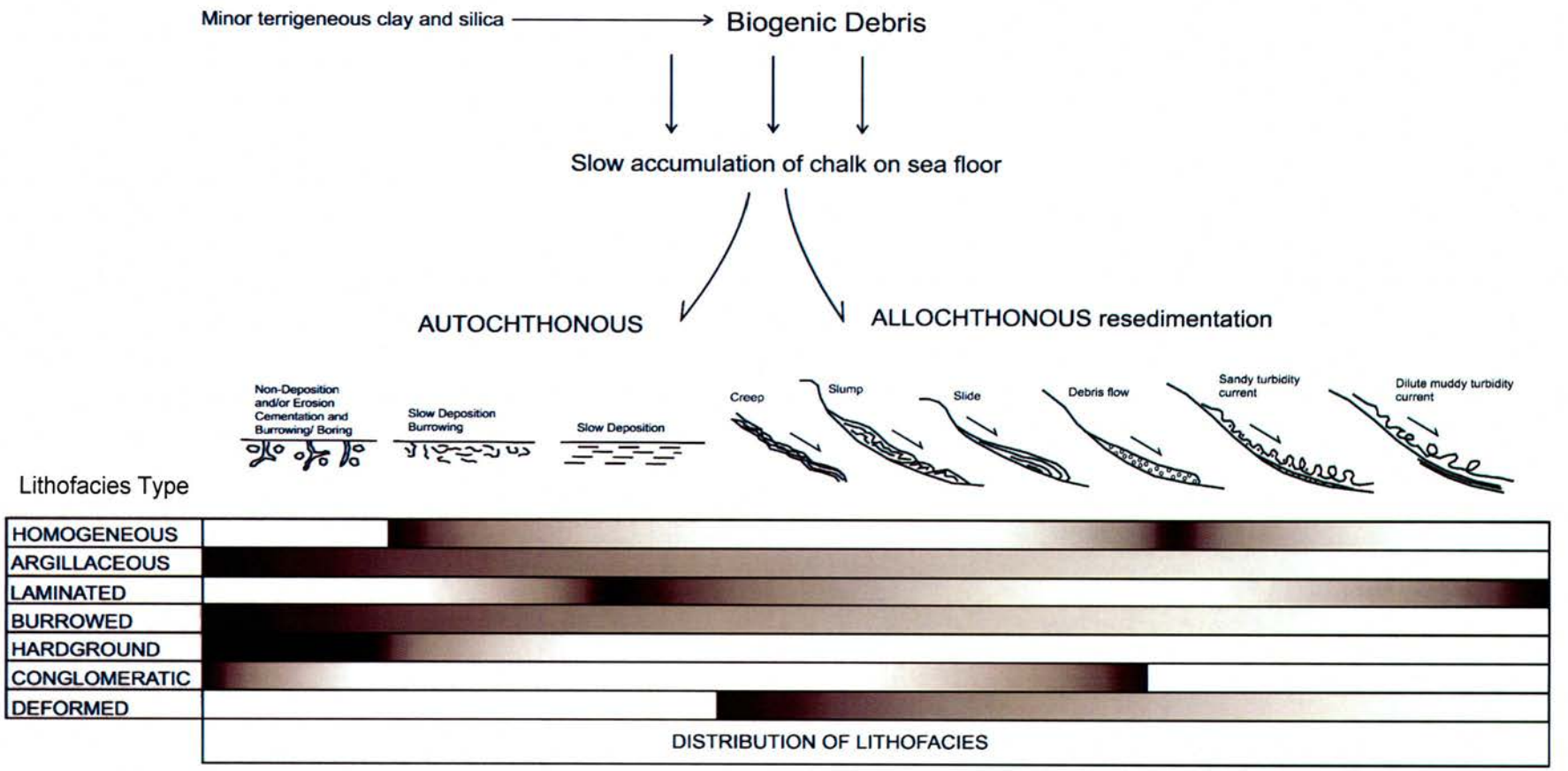

Figure 6.3: Summary illustration of the relationship between Chalk Group lithofacies and depositional environment. Greyscale shading highlights the environments associated with a particular lithofacies type; darker shades indicate a stronger association. *(After Surlyk, 1979; Bramwell et al., 1999)*

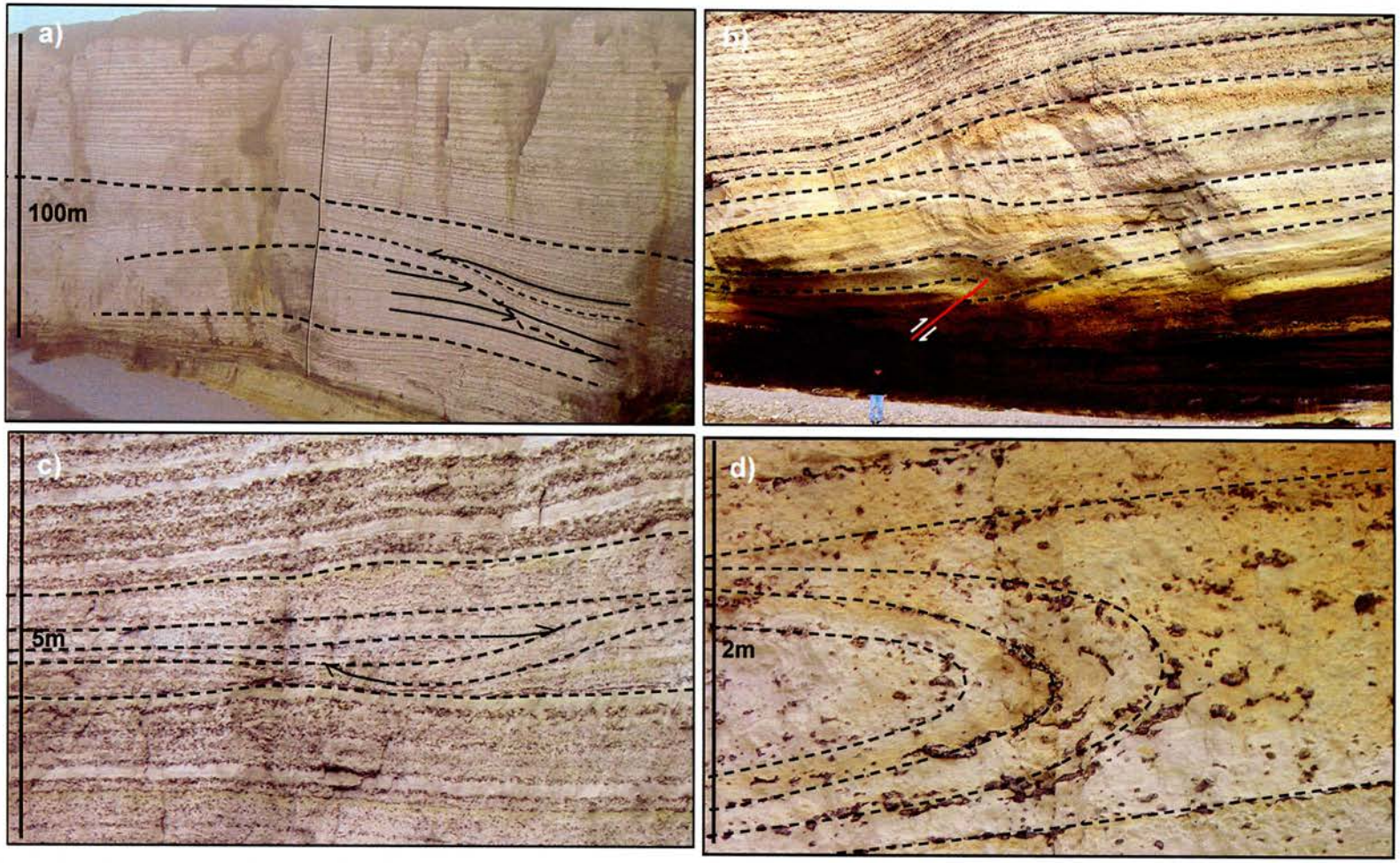

Figure 6.4: Sedimentary structures within the Chalk Group, as photographed at Etretat, Normandy. **a)** Chalk 'mounds' and erosive channel features. **b)** Reverse fault in lithified chalk, with associated soft-sediment reworking in the overlying strata. **c)** Soft-sediment deformation within a horizontally bedded sequence. **d)** Slump fold within an apparently horizontally bedded sequence.

a)

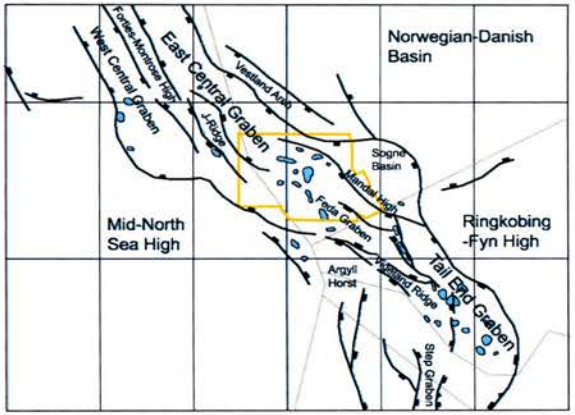

b)

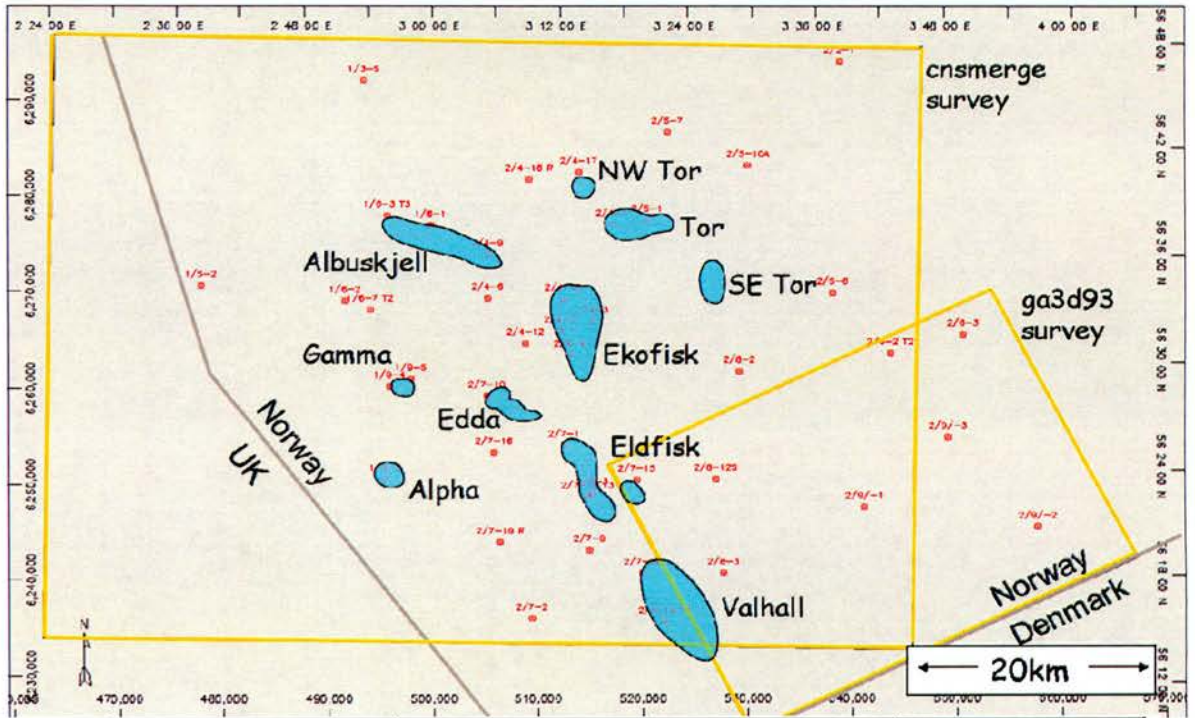

c)

Field name	Eldfisk	Ekofisk	Tor	Albuskjell
Year of Discovery	1970	1969	1970 by 2/5-1X	1972
Year of first Production	1979	1971	1978	1979
Producing Until	Present	Present	Present	1998
Original Recoverable Reserves (Oil in mscm, Gas in bscm)	124.7 Oil, 50.6 Gas	524.1 Oil, 184.9 Gas	26.7 Oil, 11.6 Gas	7.4 Oil, 15.5 Gas
Cumulative Production (Oil in mscm, Gas in bscm)	77.1 Oil, 35 Gas	345.8 Oil, 126.2 Gas	22.7 Oil, 0.9 Gas	7.4 Oil, 15.5 Gas
Producing Formations	Ekofisk, Tor, Hod (minor)	Ekofisk, Tor	Ekofisk (minor), Tor	No data
Total Number of Production Wells Drilled	dozens	dozens	21	<10

Figure 6.5: Introduction to the Norwegian Central Trough Chalk Group oilfields. **a)** Location of Chalk Group oilfields in the Central North Sea. **b)** Chalk fields of the Norwegian Central Trough. **c)** Production data from Chalk fields referred to in this study *(Data from the Norwegian Petroleum Directorate, 2007)*

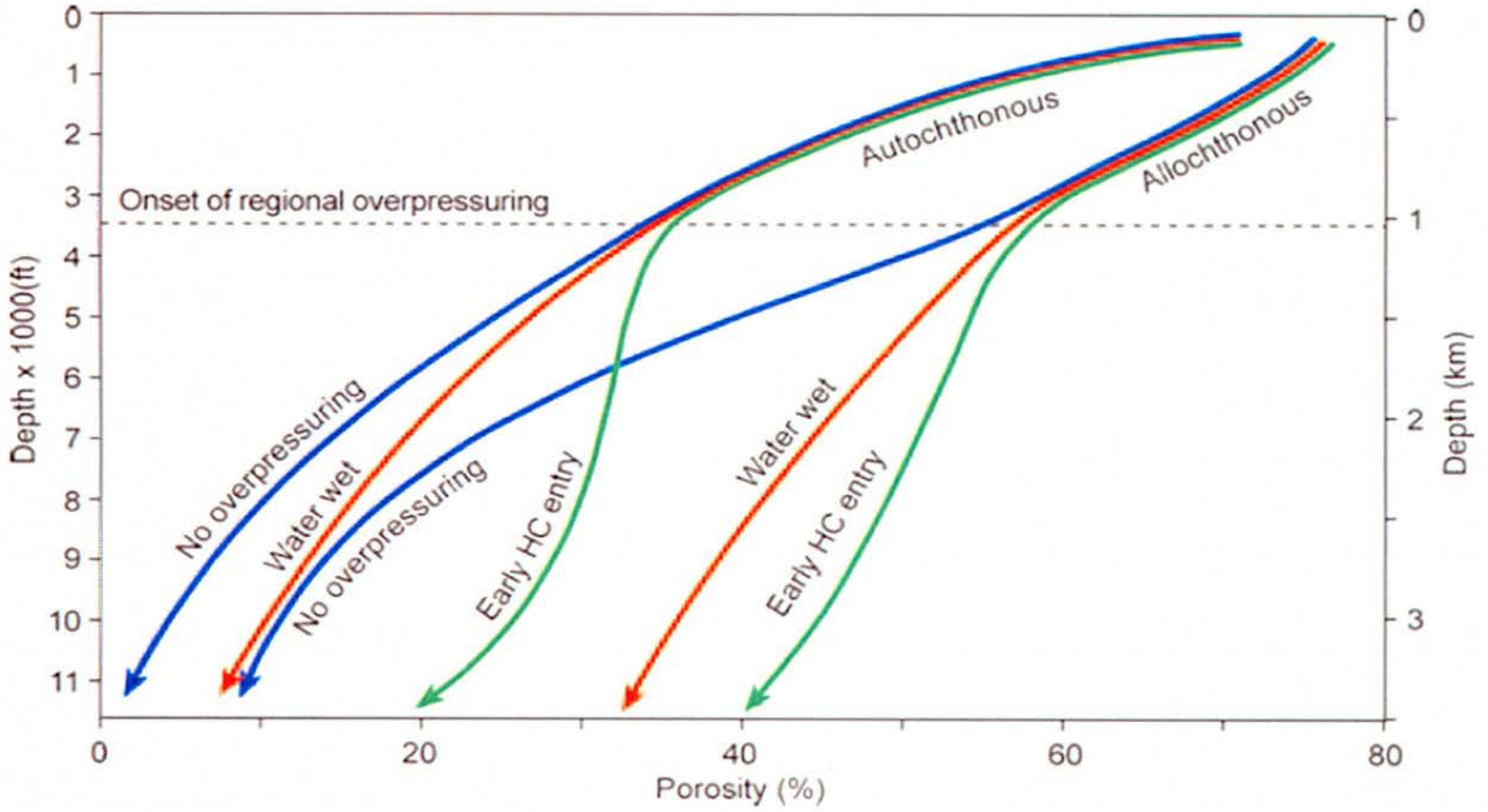

Figure 6.6: Schematic diagram summarising factors that affect porosity preservation during chalk burial. Porosity differences attributed to the primary sedimentology tend to be preserved or even accentuated during the burial process. *(From Megson and Hardman, 2001;* based on the original figure by *Brasher and Vagle, 1996)*

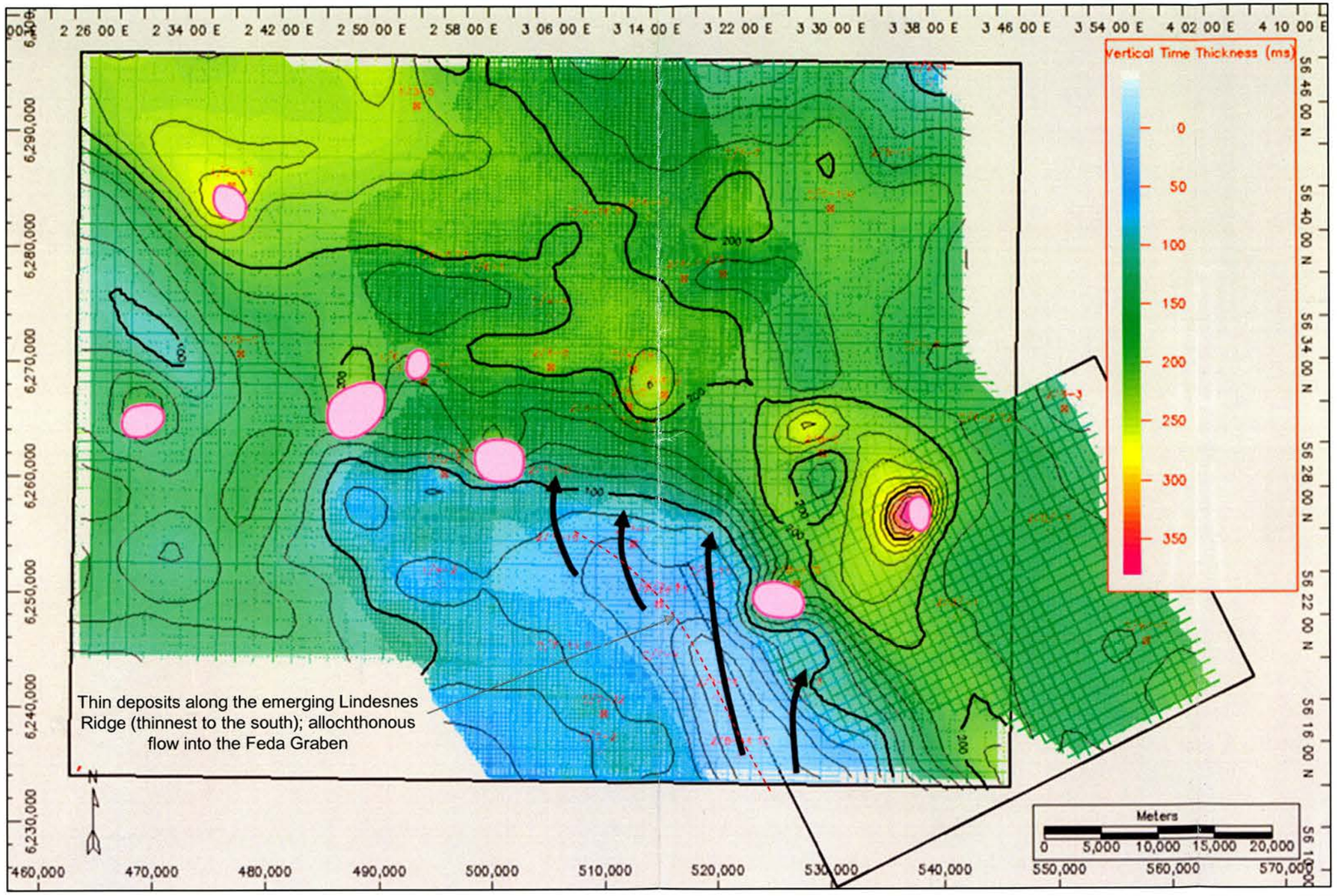

Figure 6.7: Time thickness map for the Maastrichtian to Early Palaeocene section of the Chalk Group (Tor and Ekofisk Formations), annotated to show allochthonous chalk movements off the uplifting Lindesnes Ridge and into the NE Feda Graben. Top Chalk salt piercements (pink) are superimposed on to the figure. There are thick Tor and Ekofisk sequences immediately adjacent to some of the diapirs (e.g. Trud) and these thicks are indicative of salt movements (withdrawal and squeezing) synchronous with Tor and Ekofisk Formation deposition.

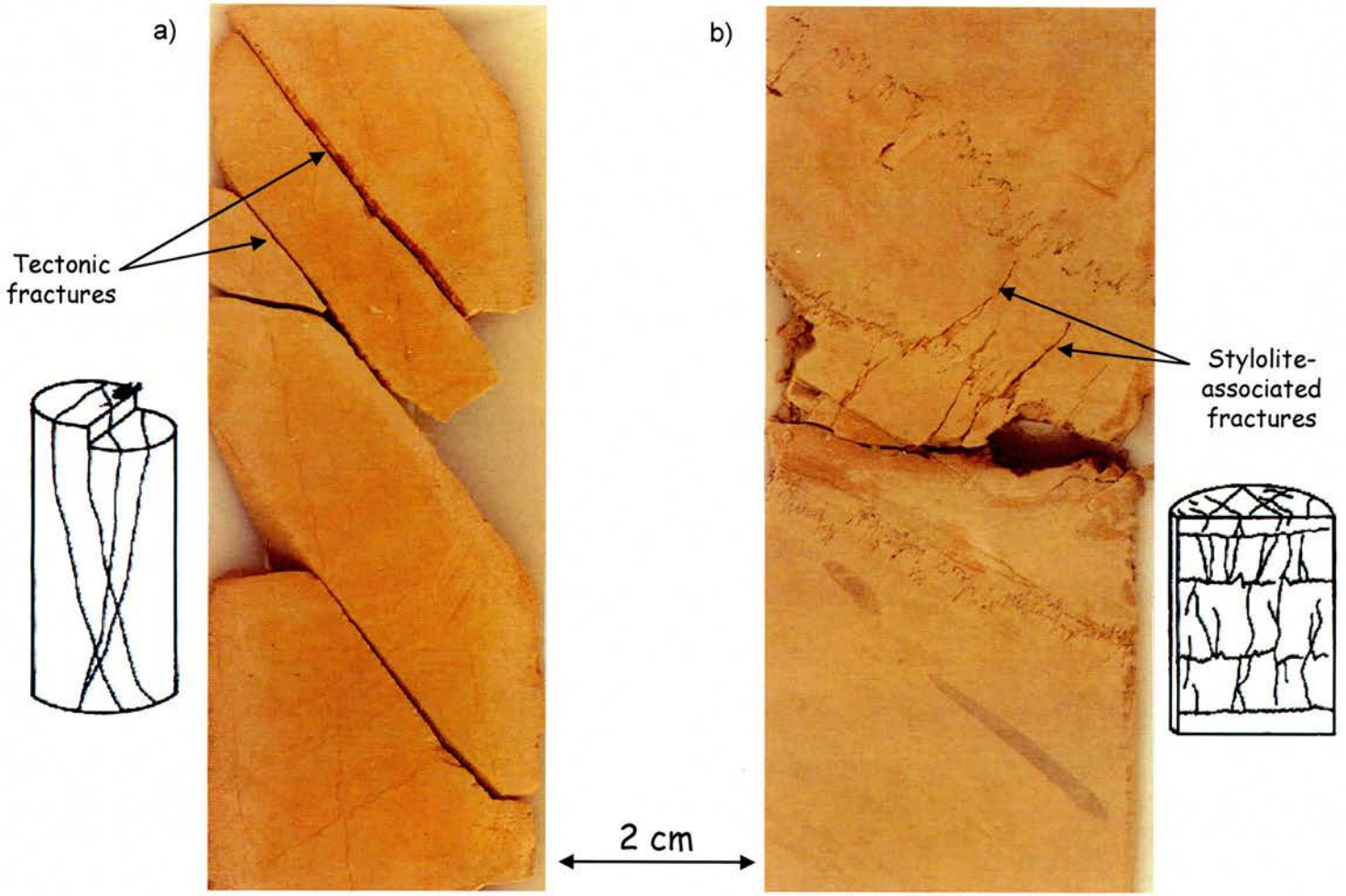

Figure 6.8: Types of fracture observed in Chalk core **a)** Tectonic fractures from Eldfisk field well 2/7-18A **b)** Stylolite- associated fractures from Eldfisk field well 2/7-13B *(Images courtesy of ConocoPhillips)*

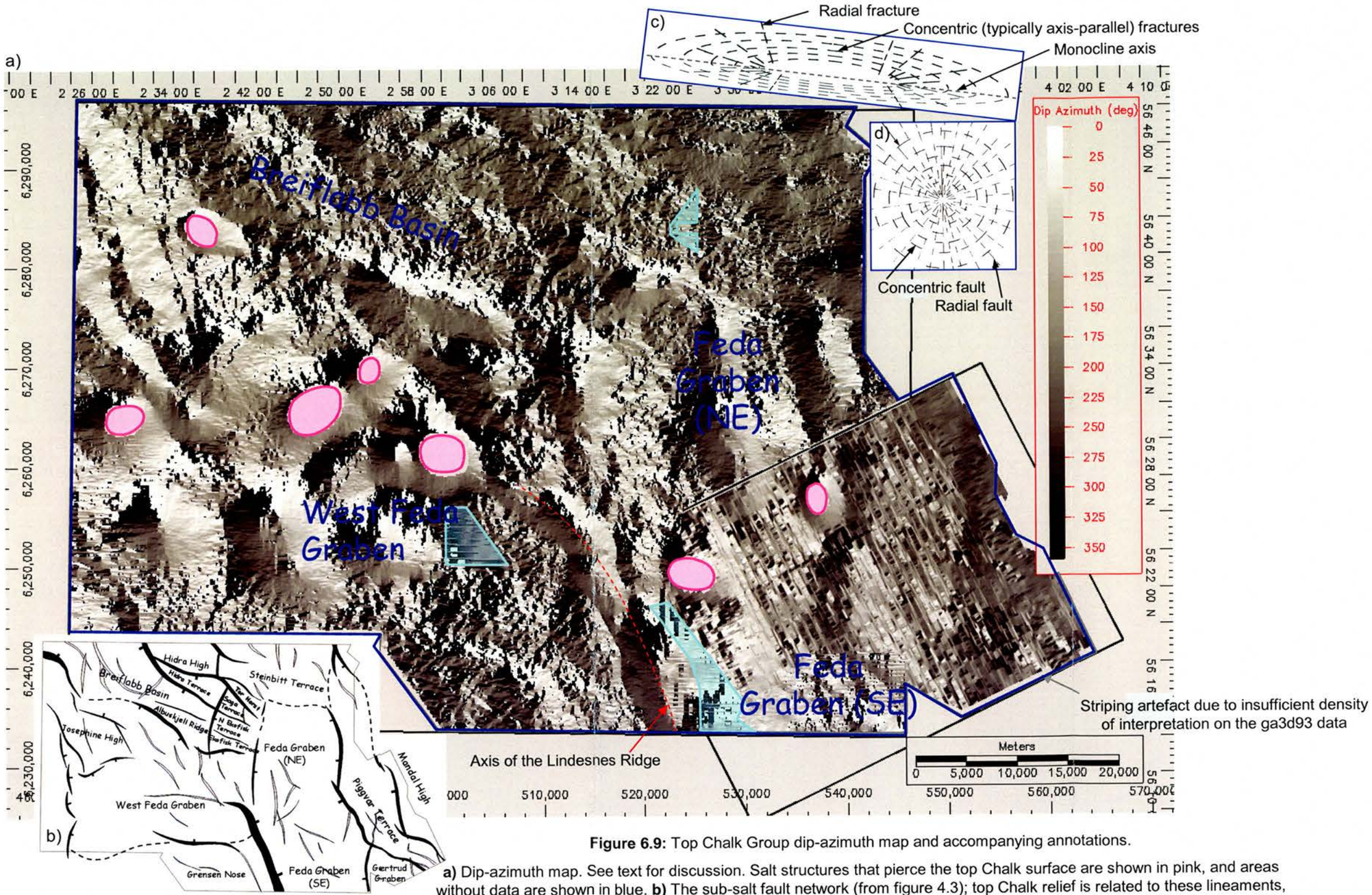

Figure 6.9: Top Chalk Group dip-azimuth map and accompanying annotations.

a) Dip-azimuth map. See text for discussion. Salt structures that pierce the top Chalk surface are shown in pink, and areas without data are shown in blue. **b)** The sub-salt fault network (from figure 4.3); top Chalk relief is related to these lineaments, but is also affected by the distribution of salt structures. **c)** Idealised pattern of radial and concentric tectonic fractures predicted for an inversion monocline (e.g. Breiflabb Basin localities) **d)** Pattern of radial and concentric tectonic fractures predicted for the crest of a salt diapir (e.g. West Feda Graben localities). Fracture patterns associated with the Lindesnes Ridge are most likely include combinations of types in c) and d)

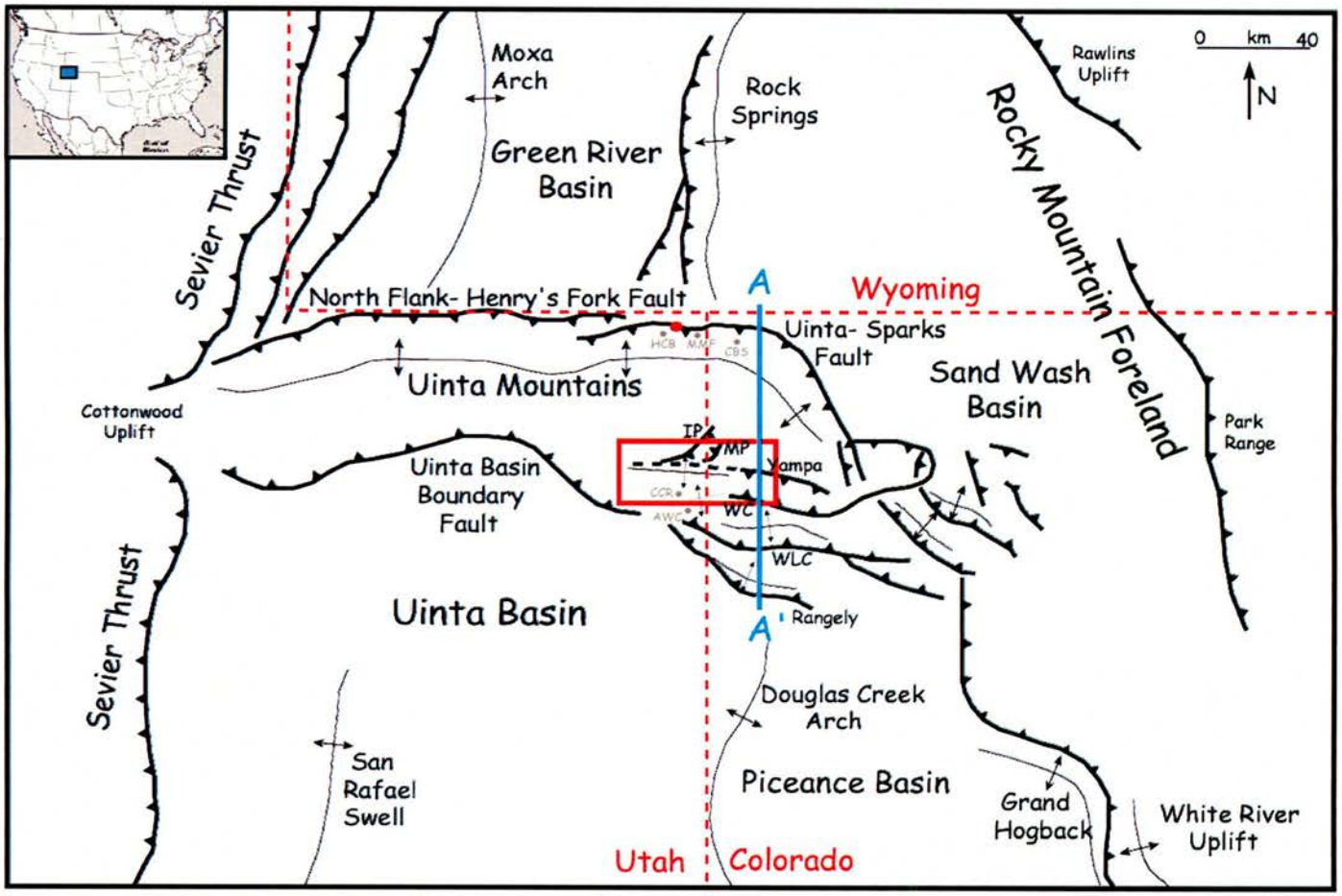

Figure 7.1: Location map of the Uinta Mountains, NE Utah/ NW Colorado *(Modified from Gregson and Chure, 2003)*. In addition to the major (named) tectonic lineaments there are numerous minor faults and associated monoclines, including; Island park (IP), Mitten Park (MP), Yampa, Wolf Creek (WC), Willow Creek (WLC) and Rangely. Borehole constraints have been derived from the Husky 7-3 Clay Basin well (HCB), the McMoran-Freeport 43-2A well (MMF), the Champlin 31-19 Bear Springs well (CBS), the ARCO Willow Creek #1 well (AWC) and the Celsius 1 Cliff Ridge well (CCR). Red dot shows location of figure 7.4 and red box shows location of the South flank study area, as illustrated in figure 7.5. Section A-A' is shown in figure 7.3.

System	Rock Unit	Thickness
Neogene	Alluvial-gravel deposits	Variable
Oligocene	Bishop Conglomerate	Variable
Eocene Palaeocene	Green River Fmn/ Uinta Fmn Duchesne River Fmn Wasatch Fmn	Variable up to 1,500m
Cretaceous	Mesaverde Group Mancos Shale Frontier Sst Mowry Shale Dakota Sst	
	Cedar Mountain Fmn	20m
Jurassic	Morrison Fmn	300m
	Stump/ Entrada/ Carmel Fmns	100m
	Glen Canyon Sst	200m
Triassic	Chinle Fmn	80m
	Moenkopi Fmn	200m
Permian	Park City Fmn	20m
Pennsylvanian	Weber Sst	300m
	Morgan Fmn	200m
	Round Valley Lst	100m
Mississippian	Doughnut Shale/ Humbug Fmn	80m
	Madison Lst	200m
Cambrian	Lodore Fmn	180m
Proterozoic	Uinta Mountain Group	>5,000m (base not exposed)

Figure 7.2: Simplified stratigraphic column for the Eastern Uinta Mountains. Cambrian to Jurassic stratigraphic thicknesses are appropriate for the area of the Southern flank shown in figure 7.5 and are based on field observations and data from *Hansen et al. (1983)* and *Gregson and Erslev (1997)*. Significant thicknesses of Cretaceous and younger deposits are exposed in the Uinta Basin to the south of the studied area *(e.g. Hefner and Barrow, 1992)*

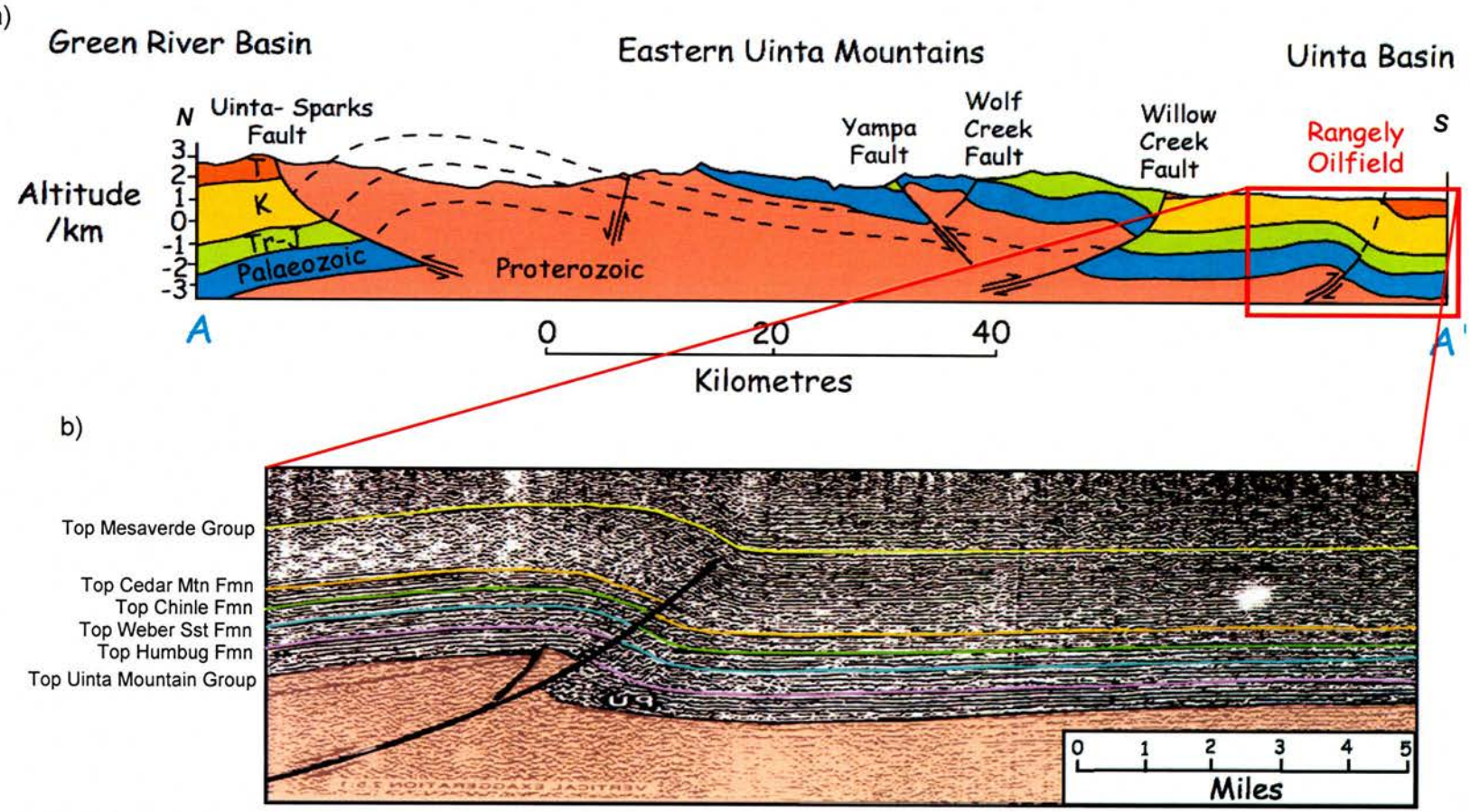

Figure 7.3: North-South cross section through the Eastern Uinta Mountains (longitude 108°52'30''). **a)** The Precambrian synrift was inverted during Late Cretaceous to Early Tertiary thick-skinned 'Laramide' compression. The large-scale geometry of the Southern flank is constrained by seismic data, such as that from the Rangely oilfield. *(After Hansen 1986)* **b)** Rangely: the largest oilfield in the Rocky Mountain region (cumulative oil production >1,000 MMBO). An inversion-induced structural trap, comprising a doubly-plunging, south-verging hanging wall anticline above a north-dipping thrust fault. Vertical exaggeration is 2.5. The North flank dips at ~4° and the South flank at up to 30°. *(After Stone 1989)*

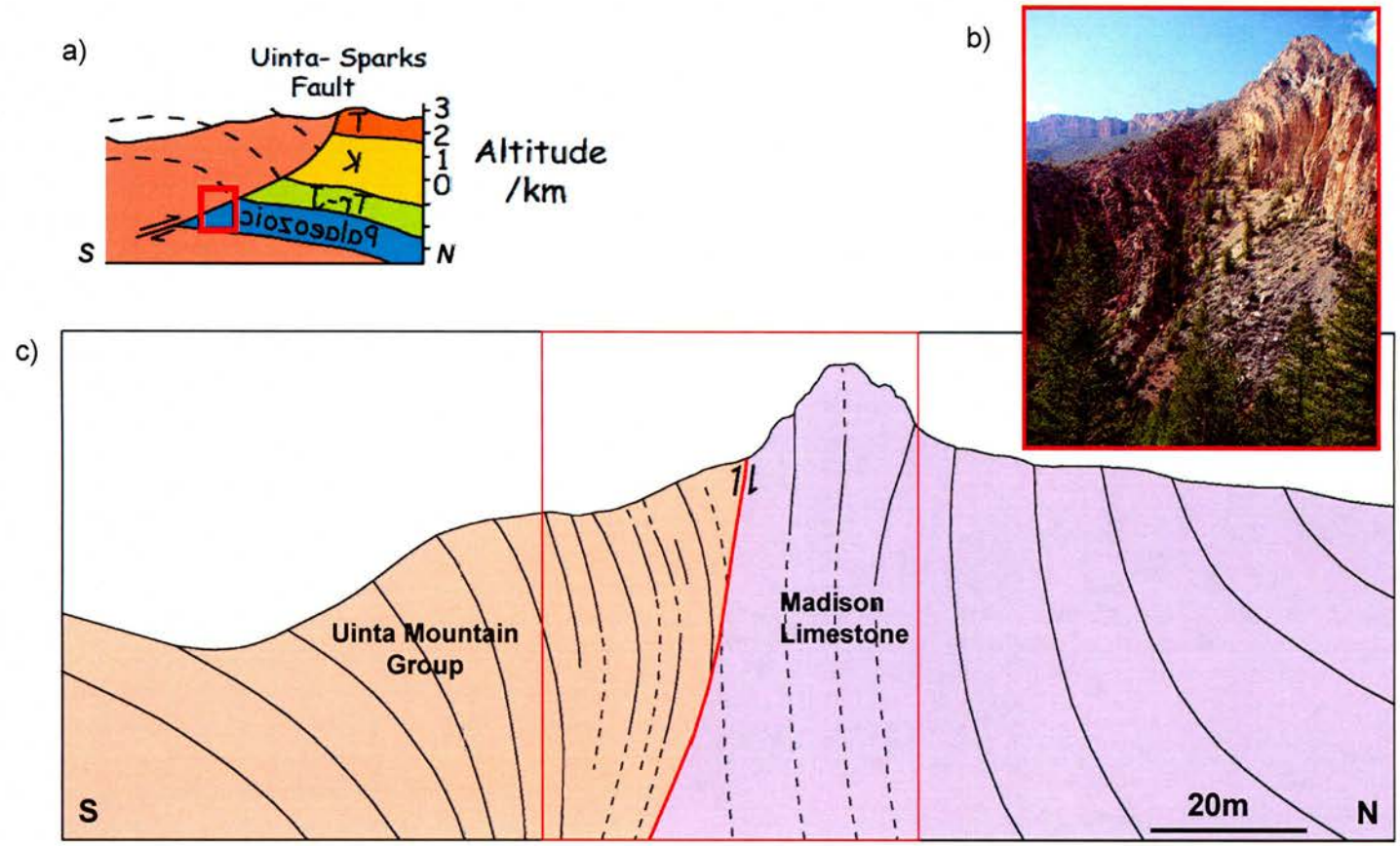

Figure 7.4: The Uinta Fault defines the northern margin of the Uinta Mountains uplift. It is visible in outcrop at Sheep Creek canyon (location shown in figure 7.1). Quartzites of the Precambrian Uinta Mountain Group are juxtaposed against limestone and cross-bedded sandstones of the Mississippian Madison Limestone Formation. **a)** Schematic illustration of the structural position. **b)** Photograph of the Uinta Fault viewed towards the WNW across Sheep Creek canyon. **c)** Field sketch clarifying the character of overturn in proximity to the Uinta fault. The area outside the photograph was not visible from a single vantage point due to obstruction by trees at the base of the canyon

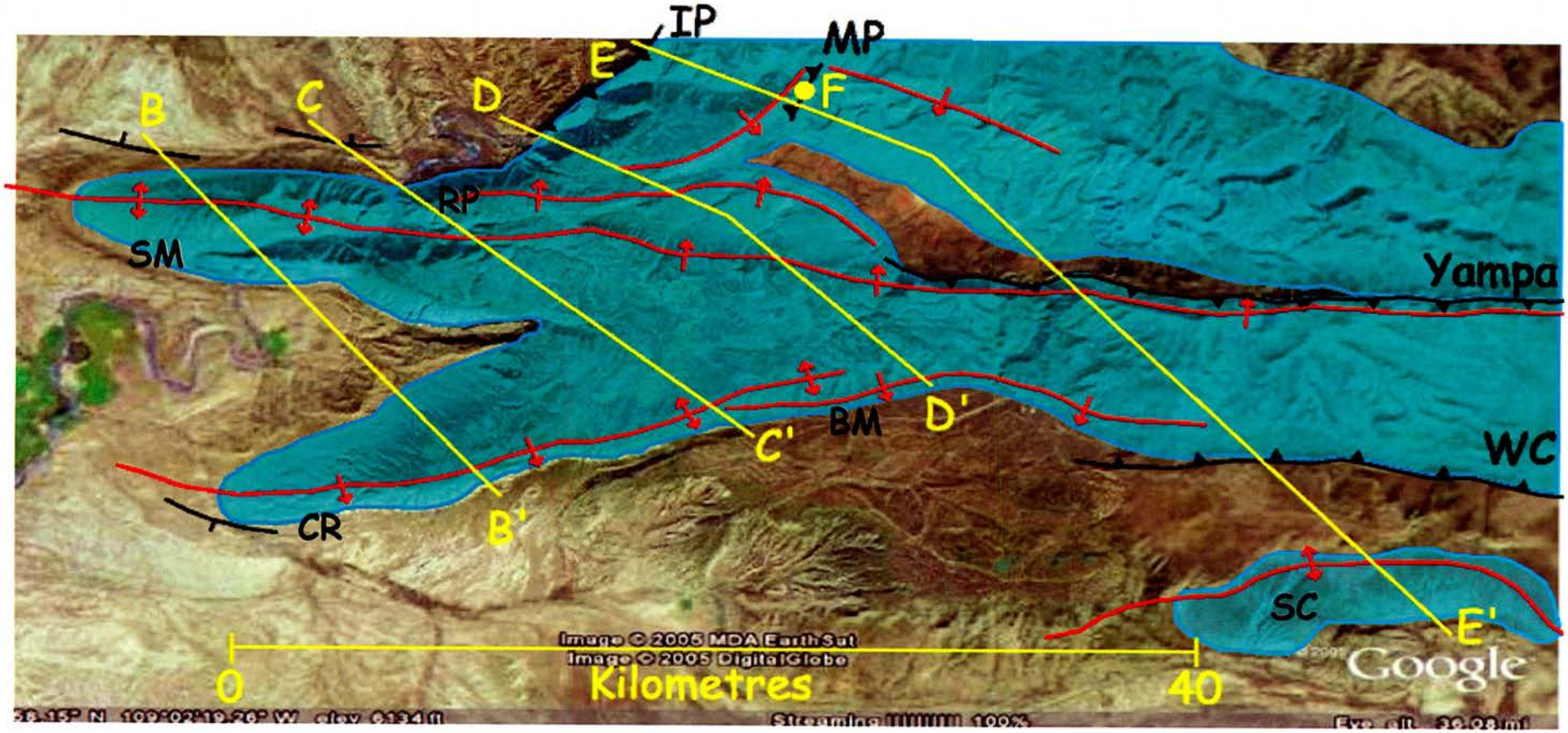

Figure 7.5: Aerial view of the southern Uintas study area (location shown in figure 7.1). The map is annotated to show the spatial extent of Palaeozoic outcrop, of which the major constituent is aeolian sandstone of the Pennsylvanian Weber Formation. SM= Split Mountain, RP= Ruple Point, IP= Island Park, MP= Mitten Park, CR= Cliff Ridge, BM= Blue Mountain, WC= Wolf Creek, and SC= Skull Creek. The fold, fault and fracture characteristics of the area were examined along the four transects labelled B-B', C-C', D-D' and E-E'.

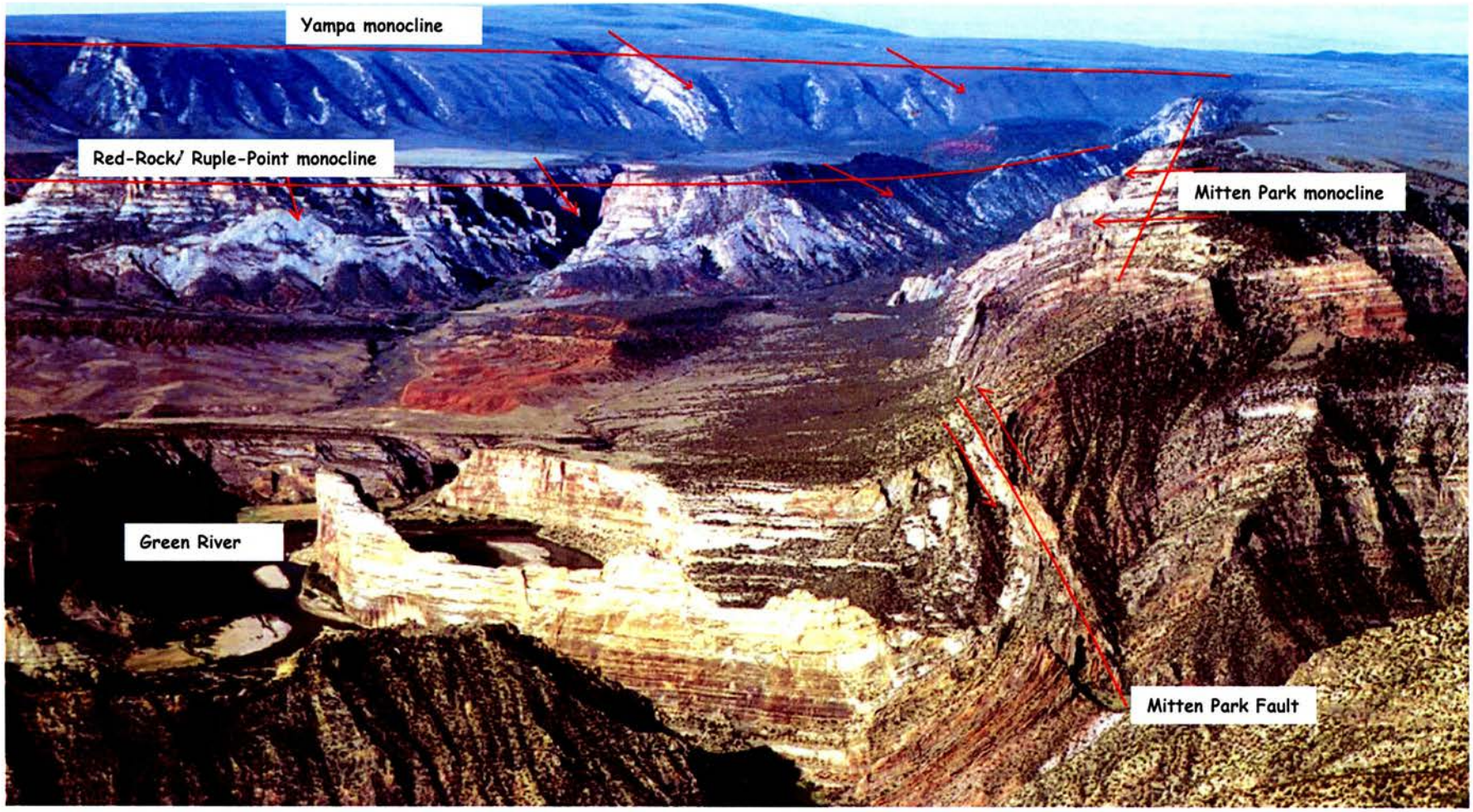

Figure 7.6 : Aerial photograph of locality F, viewed towards the southwest. The monoclinal character of folding is clearly visible. At river level, the Mitten Park fault juxtaposes Pennsylvanian Round Valley Limestone against quartzites of the Precambrian Uinta Mountain Group, but this offset passes into a monocline in the cliffs 200m above the river. *(Photograph obtained courtesy of William Mitchum)*

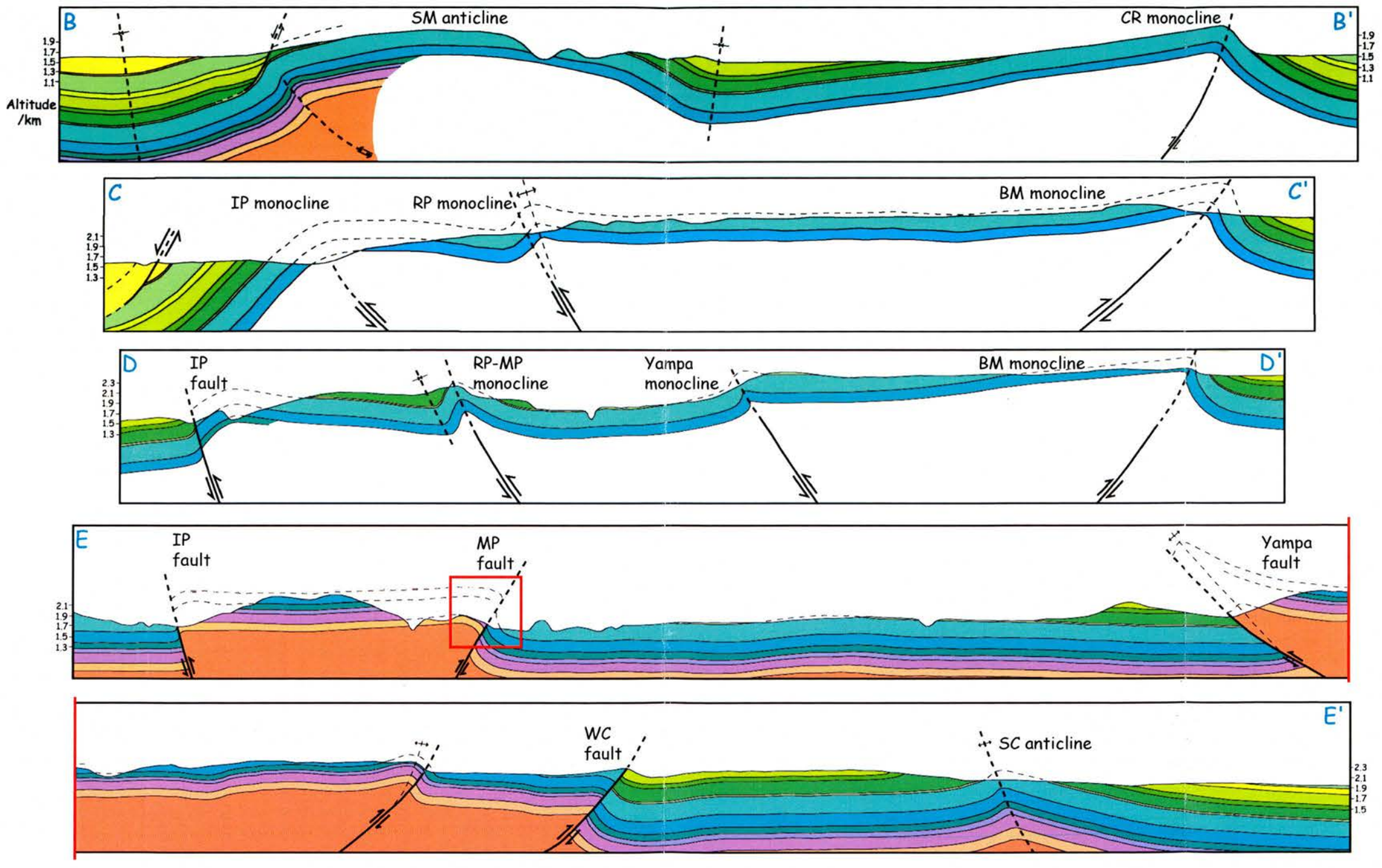

Figure 7.7: Serial cross sections through forced folds of the southern Uinta Mountains. The pronounced variability in fold amplitude and geometry is attributed to major lateral (along-strike) variations in fault throw. An outcrop photograph of the Mitten Park faulted monocline (red box in section EE') is shown in figure 7.8.

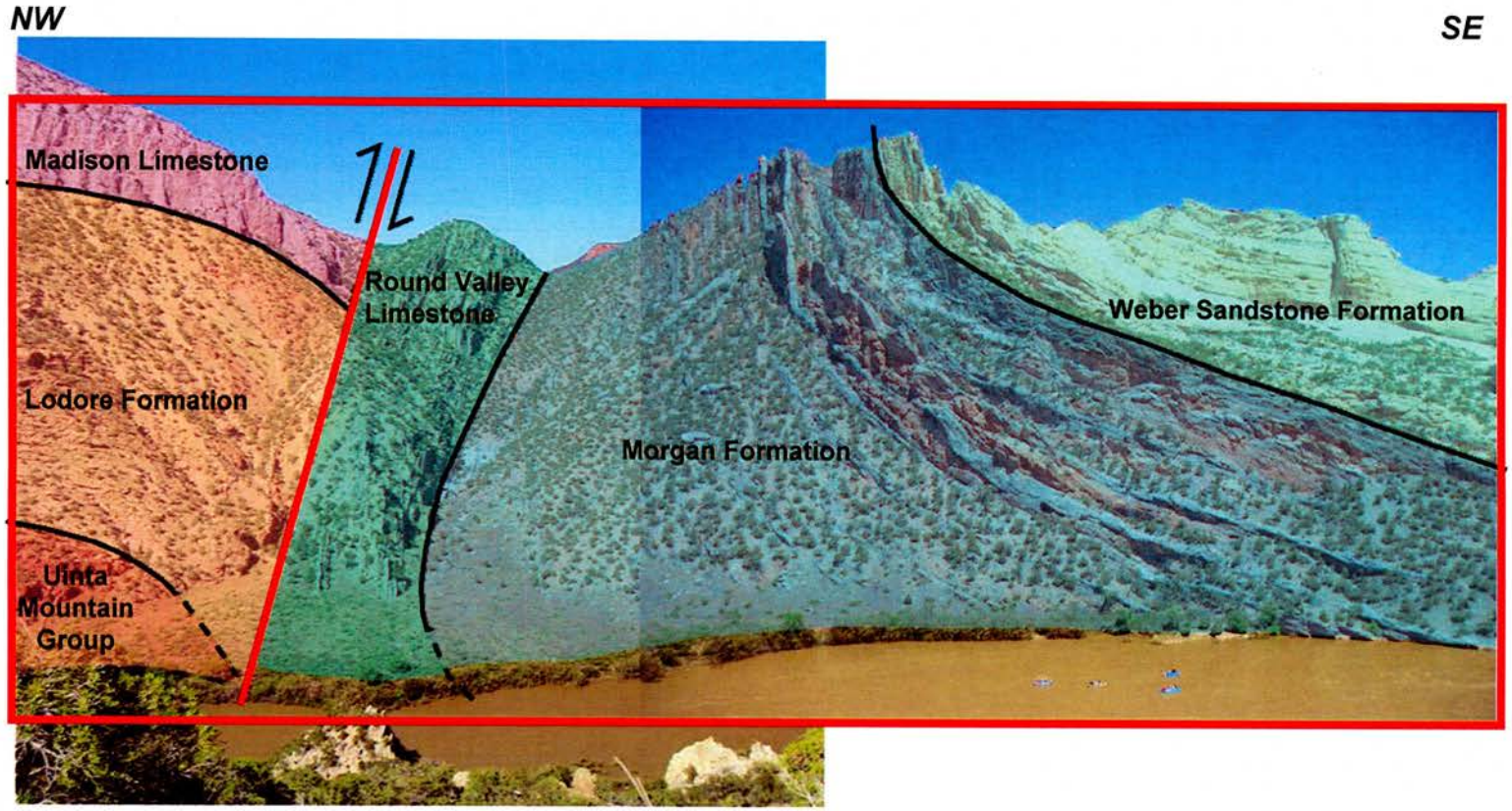

Figure 7.8: Outcrop photograph of the Mitten Park faulted monocline (locality F), viewed towards the northeast (compare with figure 7.6). See text for discussion. River rafters for scale.

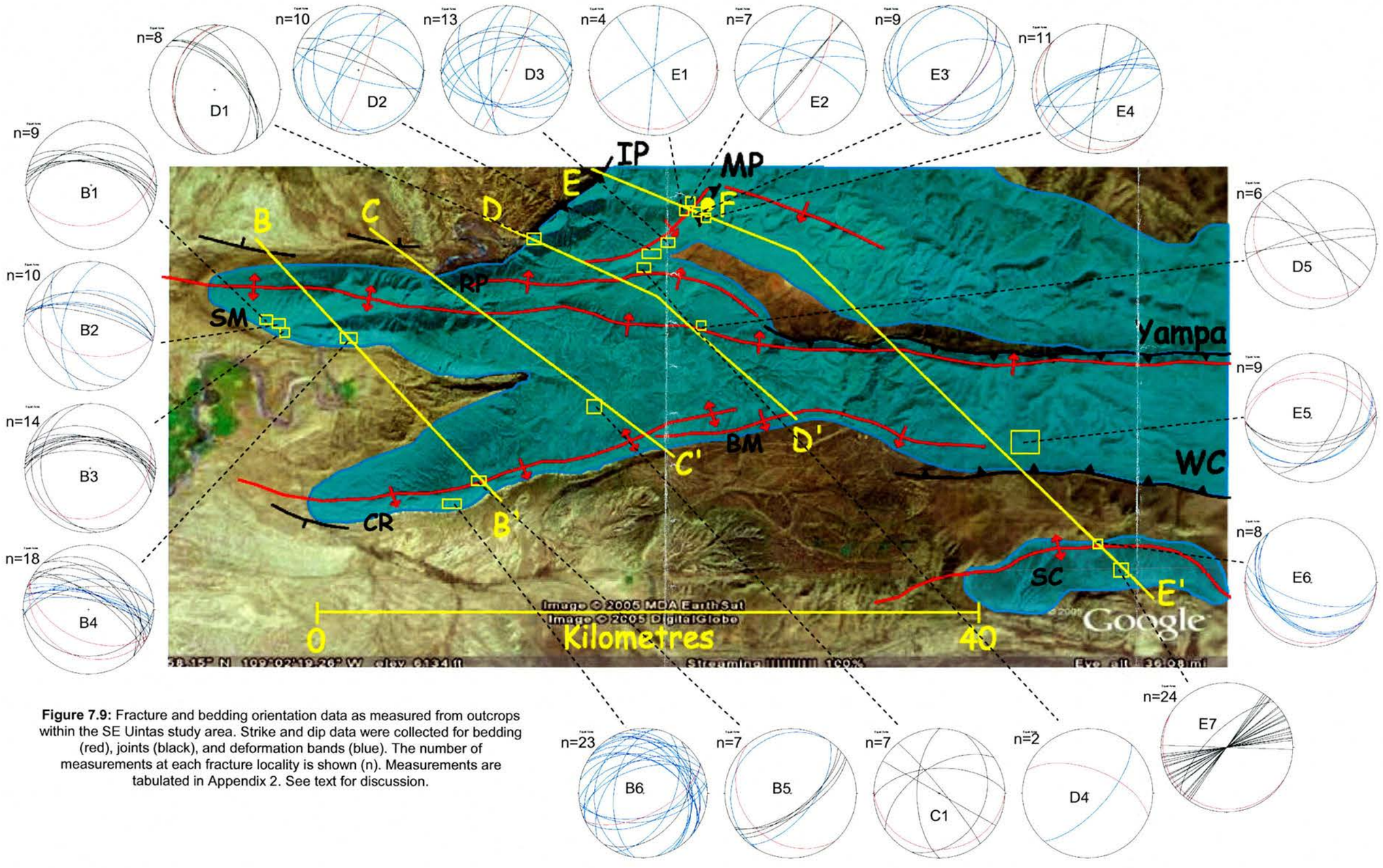

Figure 7.9: Fracture and bedding orientation data as measured from outcrops within the SE Uintas study area. Strike and dip data were collected for bedding (red), joints (black), and deformation bands (blue). The number of measurements at each fracture locality is shown (n). Measurements are tabulated in Appendix 2. See text for discussion.

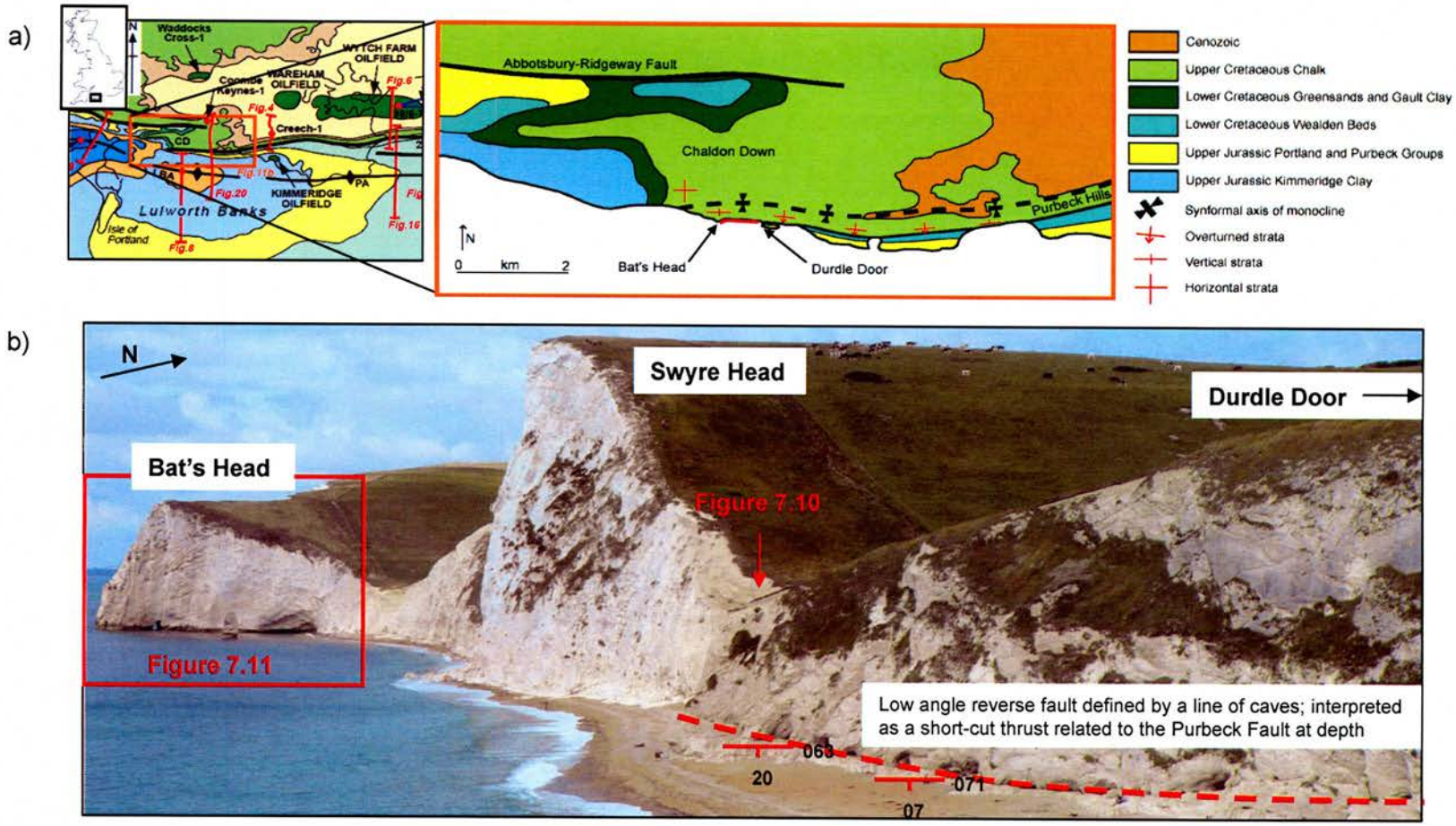

Figure 7.10: Location map and field photograph of Chalk in outcrop, South Dorset. **a)** Simplified geological map of the Chaldon Down area, showing the extent of coastal outcrop of Chalk and the location of the study area. **b)** Near-vertical dipping exposures of the Upper Chalk Group, looking West from Durdle Door.

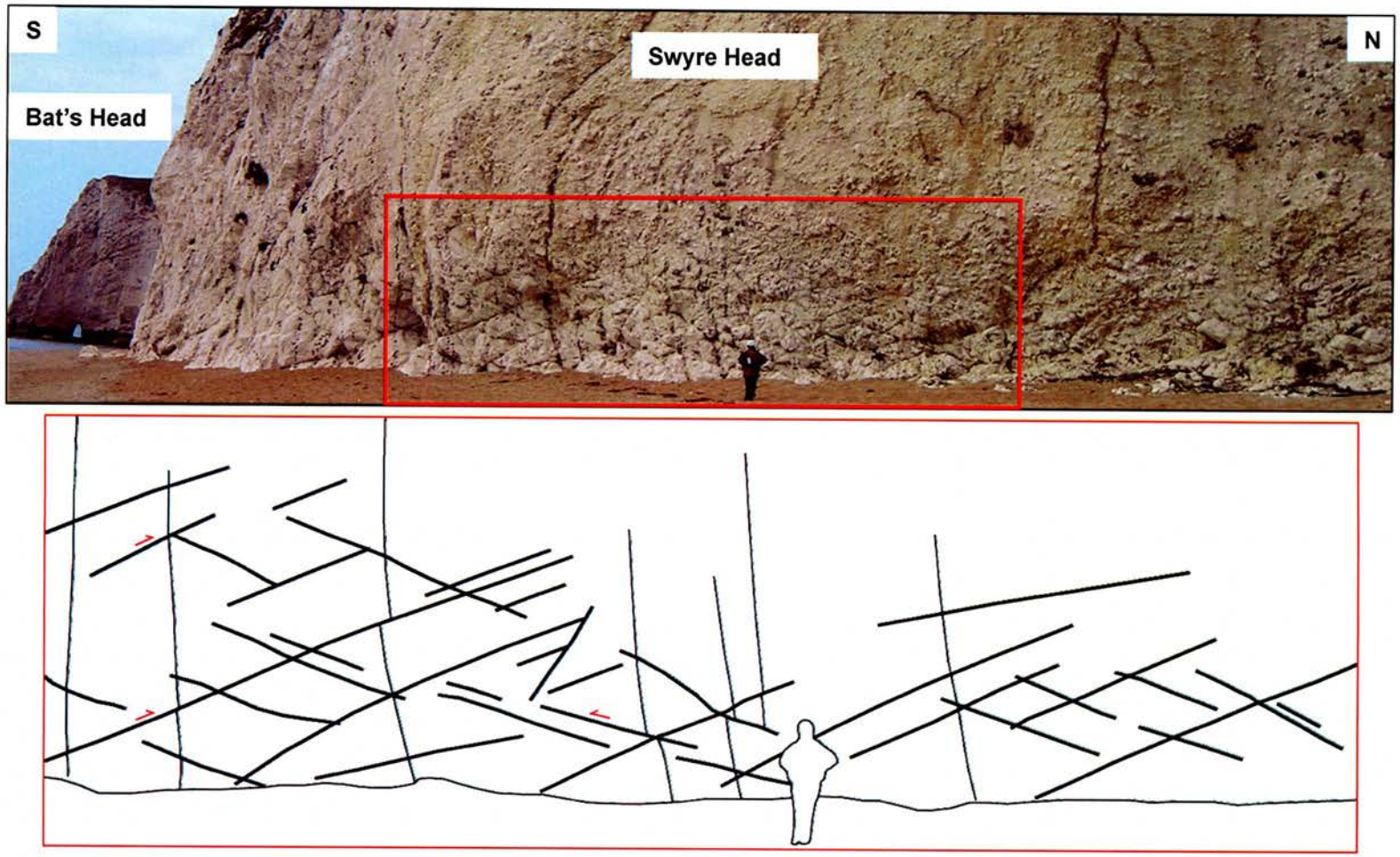

Figure 7.11: Mesoscale fracture patterns in the Chalk Group of Swyre Head, Dorset. Vertical Bedding here is defined by flints. Fractures occur as a conjugate set.

a)

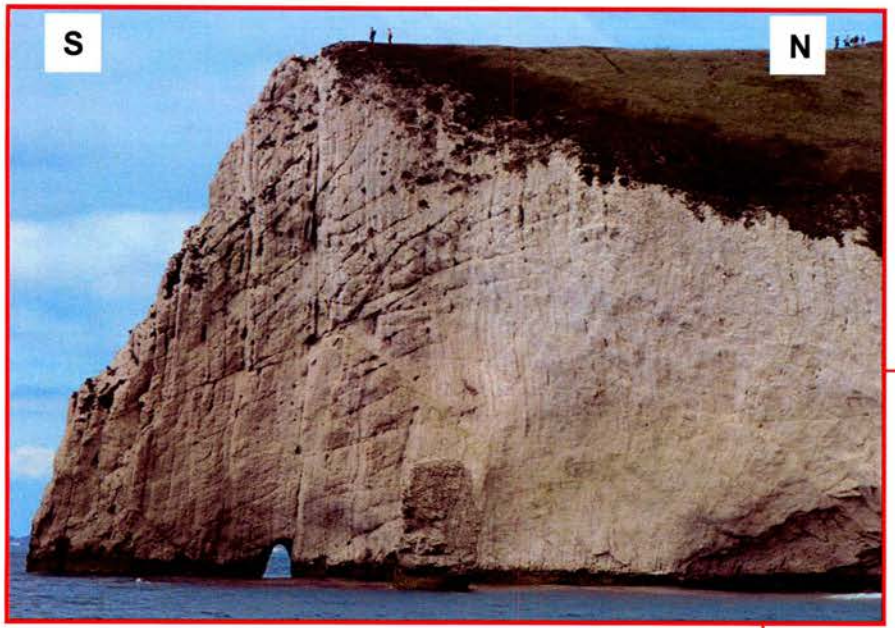

c)

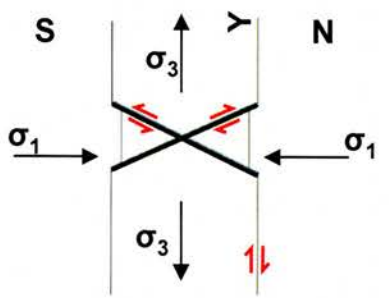

b)

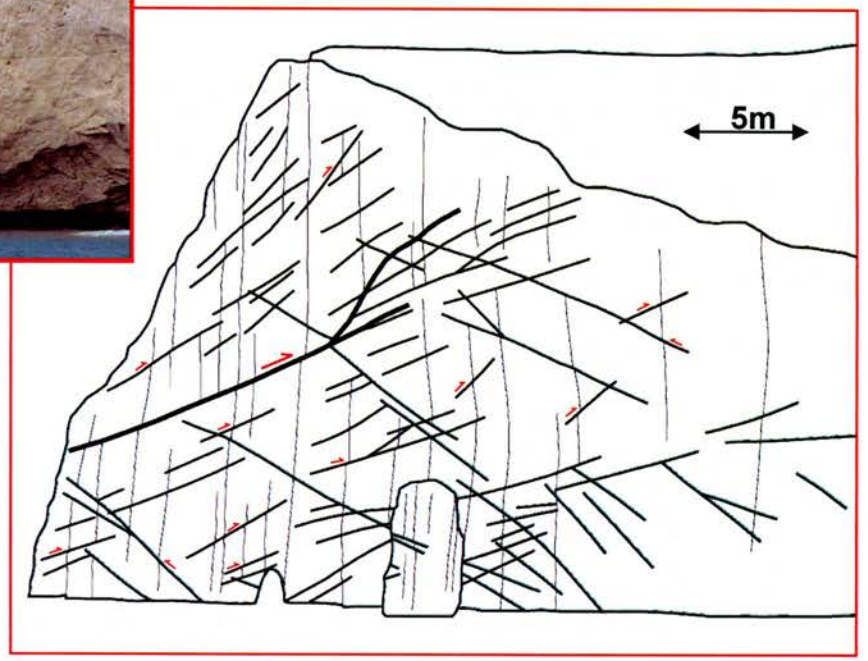

Figure 7.12: Mesoscale fracture patterns in the Chalk Group of Bat's Head, Dorset.

a) Bat's Head pictured from the East. Hikers for scale

b) Fracture interpretation *(After Bevan, 1985)*

c) Schematic illustration of the stress conditions affecting the Chalks of Swyre and Bat's Heads

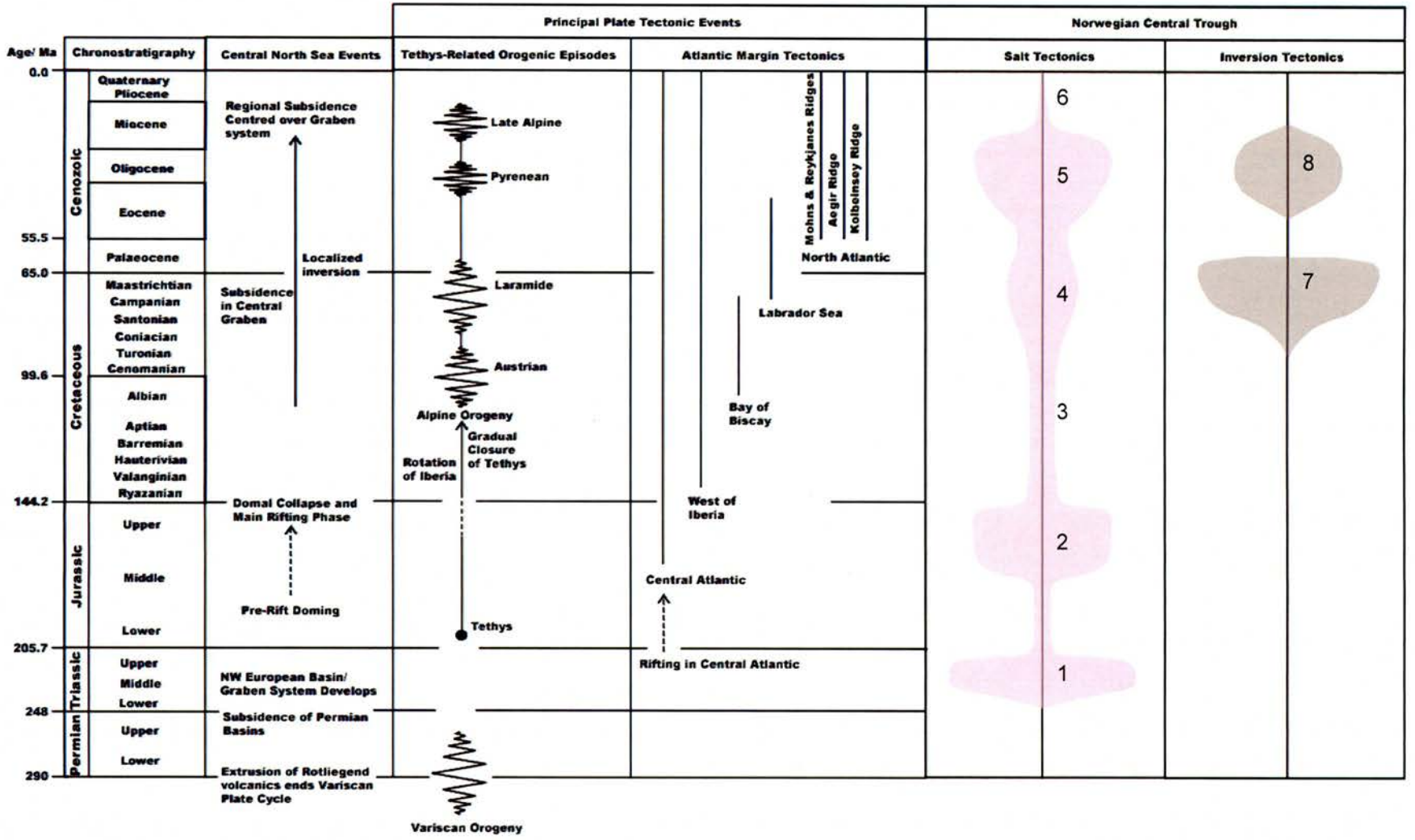

Figure 8.1: Summary illustration of the major Permian to Recent tectonic events affecting Western Europe, including timings and relative intensity of halokinesis and inversion tectonics in the Norwegian Central Trough. 1) Triassic minibasin formation 2) Active diapirism during Late Jurassic rifting 3) Continued growth of salt structures through passive downbuilding 4) Salt movements associated with Upper Cretaceous compression 5) Salt movements associated with Cenozoic compression; squeezing of diapirs 6) Sedimentation outpaces growth by passive downbuilding 7) Late Cretaceous inversion initiates during Turonian-Santonian; peaks during Maastrichtian-Earliest Palaeocene 8) Cenozoic compression

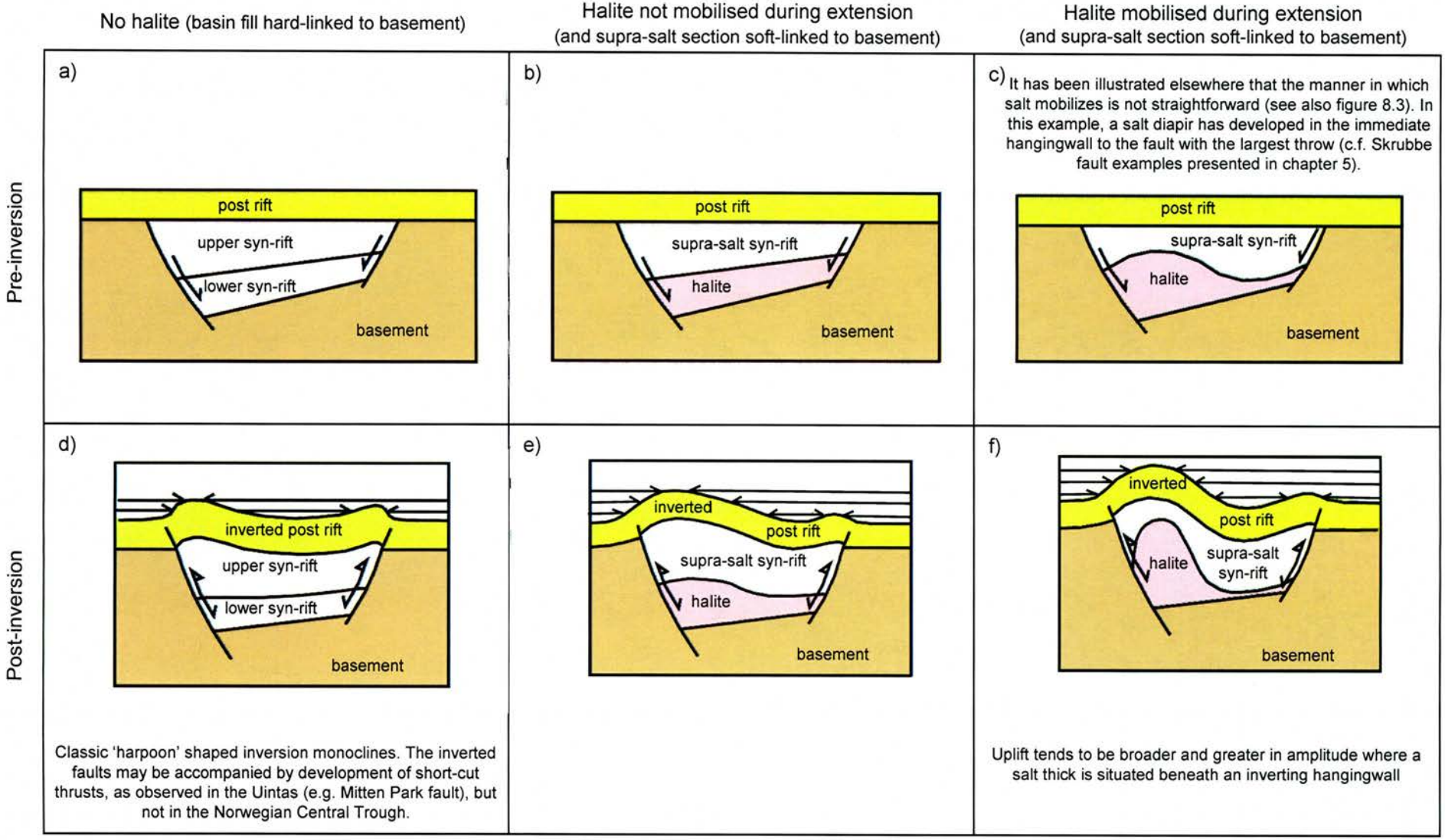

Figure 8.2: Influence of halite on tectonic inversion geometry. The presence of halite within a graben infill sequence will affect the response of that graben to subsequent compression.

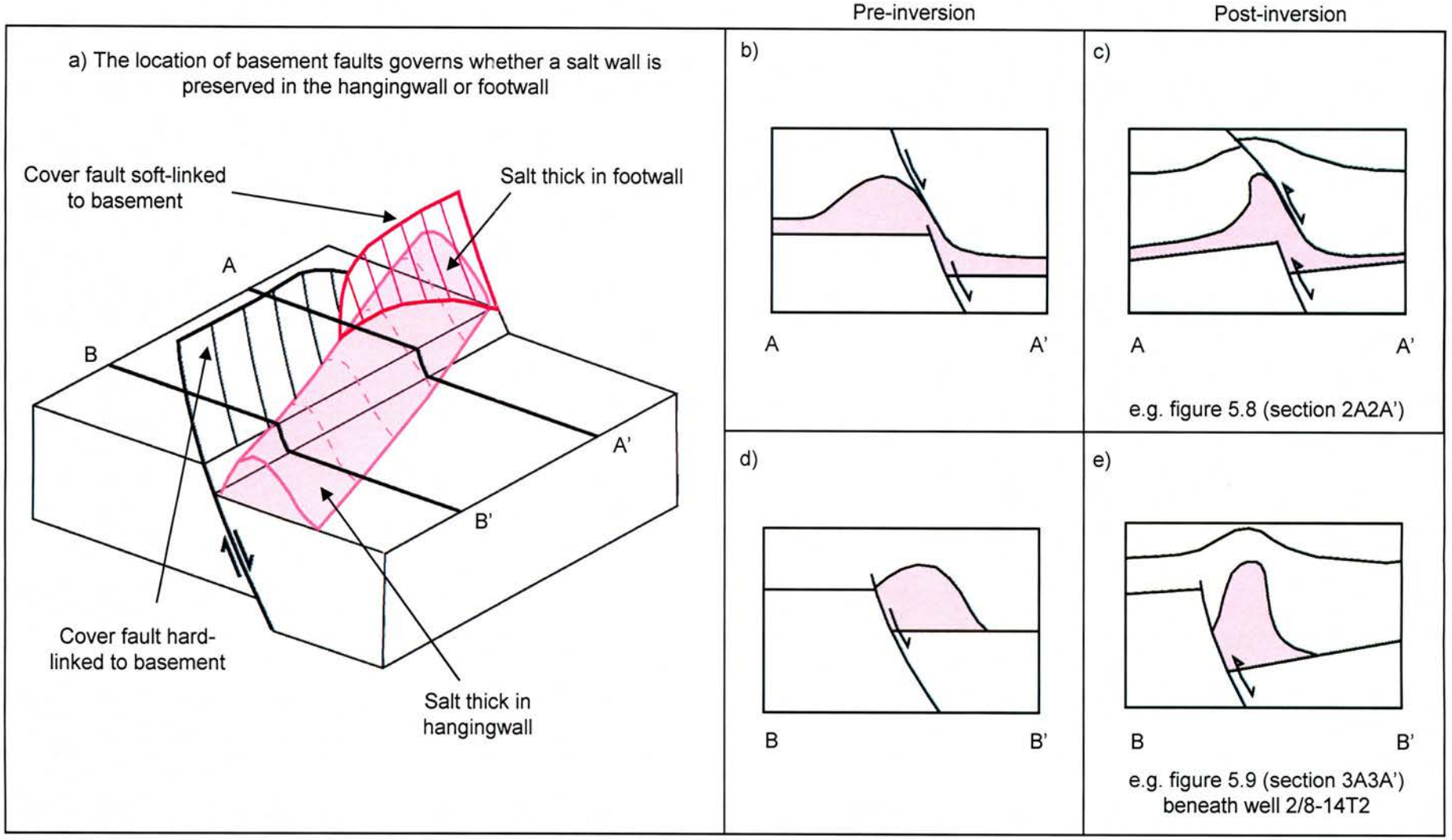

Figure 8.3: Schematic illustration of how the location of salt thicks in relation to fault lineaments influences the structural style during compression. *(Figure **a)** is modified from Stewart et al., 1996)*